Comparing machine learning and deep learning models for probabilistic post-processing of satellite precipitation-driven streamflow simulation

Yuhang Zhang[1], Aizhong Ye[1], Bita Analui[2], Phu Nguyen[2], ~~Bita Analui[2],~~ Soroosh Sorooshian[2], Kuolin Hsu[2], Yuxuan Wang[3]

[1]State Key Laboratory of Earth Surface Processes and Resource Ecology, Faculty of Geographical Science, Beijing Normal University, Beijing 100875, China
[2]Center for Hydrometeorology and Remote Sensing, Department of Civil and Environmental Engineering, University of California, Irvine, Irvine, California, CA 92697, USA
[3]College of Arts and Sciences, University of Virginia, Charlottesville, Virginia, 22903, USA

Correspondence to: Aizhong Ye (azye@bnu.edu.cn)

Abstract. Deep learning (DL) ~~models~~ and machine learning (ML) are widely used in hydrological post-processing, which plays a critical role in improving the accuracy of hydrological predictions. ~~are popular but computationally expensive, machine learning (ML) models are old-fashioned but more efficient.~~ However, the trade-off between model performance and computational cost has always been a challenge for hydrologists when selecting a suitable model, particularly for probabilistic post-processing with large ensemble members. Moreover, it is unclear whether the performance ~~Their~~ differences between DL and ML models is significant in ~~in~~ hydrological probabilistic post-processing ~~are not clear at the moment~~. Therefore, t~~T~~his study aims to systematically ~~conducts a systematic model comparison between~~compare the quantile regression forest (QRF) model and countable mixtures of asymmetric Laplacians~~probabilistic~~ long short-term memory (~~PLSTM~~CMAL-LSTM) model as hydrological probabilistic post-processors. Specifically, we ~~compare~~ evaluate ~~these two models~~their ability ~~to~~ in dealing with ~~the~~ biased streamflow simulation driven by three ~~kinds of~~ satellite precipitation products ~~in~~ across 522 sub-basins of Yalong River basin ~~of~~ in China. Model performance is comprehensively assessed ~~by~~ using a series of scoring metrics from ~~the~~ both probabilistic and deterministic perspectives~~, respectively~~. ~~In general,~~ Our results show that the QRF model and the ~~PLSTM~~CMAL-LSTM model are comparable in terms of probabilistic prediction, ~~.~~ and t~~T~~heir performance is closely related to the flow accumulation area (FAA) of the sub-basin. ~~For sub-basins with flow accumulation area less than 60,000 km^2, t~~The QRF model outperforms the ~~PLSTM~~CMAL-LSTM model in most of the sub-basins with smaller FAA~~.~~, while the ~~For sub-basins with flow accumulation area larger than 60,000 km^2, the PLSTM~~CMAL-LSTM model has an undebatable advantage in sub-basins with FAA larger than 60,000 km^2 in Yalong River basin. In terms of deterministic predictions, the ~~PLSTM~~CMAL-LSTM model ~~should be more~~is preferred ~~than the QRF model~~, especially when the raw streamflow is poorly simulated and used as an input. However, ~~But~~ if we put aside the differences in model performance, the QRF model is more efficient than the CMAL-LSTM model in computation time ~~in all cases, saving half the time~~ in all experiments~~than the PLSTM model~~. As a result, t~~T~~his study provides insights into model selection in hydrological post-processing and the trade-offs between model performance and computational efficiency. The findings highlight the importance of considering the specific application scenario, such as the catchment size and the required accuracy level, when selecting a suitable model for hydrological post-processing.~~This study can deepen our understanding of ML and DL models in hydrological post-processing and enable more appropriate model selection in practice.~~

Key words: Bias correction, long-short memory network, quantile regression forest, satellite precipitation, streamflow simulation.

1 Introduction

By generalizing the physical processes, hydrologists or modelers abstract the hydrological mechanism into a series of numerical equations, ~~which are~~ collectively ~~referred to~~known as hydrological models (Sittner et al., 1969; Clark et al., 2015; Sivapalan, 2018; Chawanda et al., 2020; Zhou et al., 2021). Hydrological models are widely used ~~in~~ for rainfall-runoff simulation, flood forecasting, drought assessment, decision making, and water resource~~s~~ management (Corzo Perez et al., 2011; Tan et al., 2020; Wu et al., 2020; Gou et al., 2020,2021; Miao et al., 2022). Depending on the complexity~~ of the model~~, hydrological models can be classified as lumped~~conceptual (or lumped)~~, semi-distributed, and distributed models (Beven, 1989; Jajarmizadeh et al., 2012; Khakbaz et al., 2012; Mai et al., 2022). Although current models simulate the hydrological processes well, they still suffer from multiple uncertainties, including input uncertainty, model structure and parameter uncertainty, and observation uncertainty (Nearing et al., 2016; Herrera et al., 2022). These uncertainties limit the accuracy of hydrological models (Honti et al., 2014; Sordo-Ward et al., 2016; Mai et al., 2022). Among ~~them~~ these various sources, input uncertainty is considered to be one of the largest sources of uncertainty. ~~.~~ Hence, p~~P~~recipitation, which is the driver of the water cycle, is the most important factor affecting streamflow simulation (Kobold and Sušelj, 2005).

Precipitation information is mainly derived from gauge observations, radar precipitation estimates, ~~and~~ satellite precipitation retrievals and reanalysis products (Sun et al., 2018). Gauge stations and radar are limited by the density of the station network ~~density~~ and the topography, especially in remote areas such as mountainous regions and high altitudes (Sun et al., 2018; Chen et al., 2020). Reanalysis requires the assimilation of observations from multiple sources and therefore cannot be obtained in real time. Satellite precipitation ~~estimation~~ estimates ~~is~~ are available in near-real-time and ~~are~~have shown valuable potentials for applications in regions where ground measurements are scarce.~~the most promising hydrological model input with high spatial and temporal resolution at present~~ (Jiang and Bauer-Gottwein, 2019; Dembélé et al., 2020). In the past decades, s~~S~~everal research institutions have developed various satellite precipitation estimation products with different data sources and algorithms, such as the Integrated Multi-satellitE Retrievals for Global Precipitation Measurement Mission (GPM IMERG) products jointly developed by the National Aeronautics and Space Administration (NASA) and the Japan Aerospace Exploration Agency (JAXA) (Hou et al., 2013; Huffman et al., 2015), the Global Satellite Mapping of Precipitation (GSMaP) products developed by JAXA (Kubota et al., 2007, 2020), and the Precipitation Estimate from Remotely Sensed Information using Artificial Neural Networks-Dynamic Infrared Rain Rate near real-time (PDIR-Now, hereafter, PDIR)~~PDIR-Now~~ product developed by the ~~Center~~Centre for Hydrometeorology and Remote Sensing (CHRS) at the University of California, Irvine (UCI) (Nguyen et al., 2020a, 2020b). However, there are still uncertainties in these products due to factors such as data sources and algorithms (Tian et al., 2009; Zhang et al., 2021a). And, the uncertainties are even amplified during the hydrological simulation (Cunha et al., 2012; Falck et al., 2015; Zhang et al., 2021b) and ~~. This greatly~~ severely limits ~~thier~~their ~~the capability of satellite precipitation~~ capability ~~products~~ for meteorological and downstream hydrological applications.

The current study addresses the uncertainty of satellite precipitation as input in hydrological ~~modeling~~modelling in two ways, namely, pre-processing and post-processing (Wang et al., 2009; Ye et al., 2015; Li et al., 2017; Dong et al., 2020; Shen et al., 2021; Zhang et al., 2022a). Here, ~~pre-processing and post-processing~~ we use the terminology of the hydrologic ensemble prediction experiment (HEPEX), where pre- and post-processing are distinguished before and after using the hydrological model (Schaake et al., 2007). That is, ~~the~~ precipitation input to the hydrological model and hydrological ~~the~~ streamflow output ~~from the hydrological model~~ are processed separately (Li et al., 2017). Hydrological pre-processing, also known as precipitation post-processing, is commonly used to obtain bias-corrected precipitation estimates by directly bias-correcting or fusing satellite precipitation estimates and gauge observations (Xu et al., 2020; Zhang et al., 2022a). ~~The p~~Pre-processing mainly reduces ~~the~~ precipitation input uncertainty. ~~The~~ H~~h~~ydrological post-processing mainly uses the observed streamflow to correct the streamflow simulation or prediction (Ye et al., 2014; Tyralis et al., 2019). Hydrological post-processing not only reduces the effect of input uncertainty, or further reduces input uncertainty after hydrological pre-processing, but also reduces uncertainty caused by hydrological model structure and model parameters (Parrish et al., 2012; Kaune et al., 2020). Both hydrological pre-processing and post-processing can be used to generate deterministic and probabilistic predictions. ~~in a deterministic or probabilistic waymanner~~. Our objective in this study is to compare and evaluate learning algorithms in p~~P~~robabilistic hydrological post-processing ~~is the objective of this study~~.

In addition to the skewed distribution and the heteroscedasticity, the streamflow time series have a strong autocorrelation (Herrera et al., 2022). According to this feature, there are two main types of methods used to perform hydrological post-processing. One is the autoregressive model based on residuals. Its main idea is to use the simulation residuals as forecast factors for the error update. Typical methods are error reduction models based on autoregression (Li et al., 2015, 2016; Zhang et al., 2018). Another way is to use the idea of model output statistics (MOS) (Wang et al., 2009; Bogner and Pappenberger, 2011; Bellier et al., 2018). That is, the simulated streamflow is used directly ~~used~~ as a forecast ~~forecasting~~ factor to establish statistical relationships between simulations and observations. A representative approach of this type is the general linear model post-processor (GLMPP) (Zhao et al., 2011).

In recent years, machine learning (ML) and deep learning (DL) algorithms have become powerful tools for hydrological ~~modeling~~modelling (Sit et al., 2020; Zounemat-Kermani et al., 2021; Shen and Lawson, 2021; Fang et al., 2022). For example, long short-term ~~Long-short~~ memory (LSTM) models have been used to simulate streamflow in ~~several~~ a number of gauged and ungauged basins in North America (Kratzert et al., 2018, 2019), the United Kingdom (Lees et al., 2021), and Europe (Nasreen et al., 2022). In addition to direct streamflow ~~modeling~~modelling, ML and DL algorithms can also be used as powerful hydrological post-processors for bias correction of streamflow simulation. For example, Frame et al. (2021) used LSTM to build a post-processor to correct the U.S. National Hydrologic Model and validated it on the CAMELS (Catchment Attributes and Meteorology for Large-sample Studies) dataset containing 531 North American watersheds. The results showed that the LSTM post-processing significantly enhanced the output of the raw national hydrological model ~~(Frame et al., 2021)~~. Shen et al. (2022) used the random forest as a hydrological post-processor to enhance the simulation performance of the large-scale hydrological model PCR-GLOBAL (PCRaster Global Water Balance) model at three hydrological stations in the Rhine basin. Compared to deterministic forecasts, probabilistic forecasts can provide more insights regarding the uncertainties~~y~~ and ~~information to~~ improve ~~our~~ the risk management strategies. In terms of probabilistic ~~modeling~~modelling, Tyralis et al. (2019) compared the usability of the statistical model (e.g., quantile regression) and the machine learning algorithm (e.g., quantile regression forests) as hydrological post-processors on the CAMELS ~~(Catchment Attributes and Meteorology for Large-sample Studies)~~ dataset. And the results showed that the quantile regression forests model outperformed the quantile regression ~~model~~. Zhu et al. (2020) investigated the applicability of LSTM for probabilistic hydrological forecasting coupled with a Gaussian process model. Similarly, Althoff et al. (2021) quantified the uncertainty of LSTM for hydrological ~~modeling~~modelling using stochastic deactivation of neurons. Li et al. (2021, 2022) quantified the uncertainty of LSTM for hydrological ~~modeling~~modelling using variational inference from a Bayesian perspective. All these individual models can quantify the uncertainty ~~information~~. More recently, Klotz et al. (2022) compared the ~~application~~ use of dropout and three Gaussian mixture distribution models for uncertainty estimation in LSTM rainfall-runoff ~~modeling~~modelling. They found that the mixture density model outperformed the random dropout model and provided~~, providing~~ more reliable probabilistic information ~~on uncertainty~~. Both ML models and DL models have been successfully practiced in hydrological probabilistic post-processing. In addition, there has been -some scholarly work in which ~~And some~~ DL models have been compared and ~~analyzed~~analysed (e.g., Klotz et al., 2022). However, to our knowledge there has not been a ~~there is no~~ comparison between ML ~~models~~ and DL models for hydrological probabilistic post-processing in the literature. DL models, ~~while although powerful~~despite their powerful predictive capabilities, are often criticized for their higher ~~requiring large~~ computational complexities and costs. ~~expenditures and time costs~~. ML models, on the other hand, are more efficient and easier to implement but may perform poorly in comparison. Notwithstanding these evidences, ~~HoweverAt present, we still do not know~~ their differences in the field of hydrological probabilistic post-processing, such as the scope of application, model performance and computational efficiency is not well studied.

Therefore, in this study, we attempt to comprehensively ~~fully~~ compare the ~~comprehensive~~ performance of the two most widely used ML and DL models for streamflow probabilistic post-processing: ~~applications. The two models chosen are~~ quantile regression forests (QRF) and countable mixtures of asymmetric Laplacians ~~probabilistic~~ LSTM (~~PLSTM~~CMAL-LSTM), ~~respectively. Our goal is~~at a sub-basin scale~~probabilistic post-processing of the~~ daily streamflow, respectively.~~We aim at sub-basin-scale daily streamflow probabilistic post-processing.~~ In particular, a full model comparison is performed in a complex basin with 522 nested sub-basins in southwest China. Three sets of global satellite precipitation products are applied to generate uncorrected streamflow simulations. The three precipitation products represent different algorithms. Also, they have been proven to have relatively good accuracy in our previous study (Zhang et al., 2021b). They are also used for single-feature and multi-feature input analysis. A variety of evaluation metrics are used to assess the performance of the proposed models~~ performance~~, including probabilistic metrics for multi-point prediction and deterministic metrics for single-point prediction. The relationship between model performance and basin size is also ~~analyzed~~analysed according to the difference in the flow accumulation area of the sub-basin. This study can deepen our understanding of ML and DL models, and enable targeted model selection in practice. The paper is organized as follows: In Sect.2, we introduce the study area and data. In Sect.3, we present the post-processing models, experimental design and evaluation metrics. Sect. 4 presents the streamflow results before and after post-processing with different experiments. In Sect. 5, we discuss the interpretation of post-processing model differences, as well as their limitations. Finally, the conclusions are summarized at the end of this article.

2 Study area and Data

2.1 Study area

The Yalong River (Fig. 1a) is a major tributary of the Jinsha River, which belongs to the upper reaches of the Yangtze River. The Yalong River basin is located between the Qinghai-Tibet Plateau and the Sichuan Basin. The Yalong River basin has a long and narrow shape (96° 52’–102° 48’ E, 26° 32’–33° 58’ N), with snow-capped mountains scattered in the upper reaches, surrounded by high mountain valleys in the middle reaches, and flowing into the Jinsha River in the lower reaches. It spans seven dimensional zones with complex climate types. The total length of the basin is about 1,570 km, and the total area is about 130,000 km^2. The mean annual precipitation of the basin is about 800 mm.~~in the upstream and downstream is about 600 mm and 1,000 mm, respectively.~~

Following the watershed division method of Du et al. (2017), ~~the whole~~ Yalong River basin is divided ~~to~~ into 522 ~~serval~~ sub-basins with ~~different~~ catchment areas ranging from 100 km^2 to 127,164 km^2 (Fig. 1b). The key to sub-basin delineation is the minimum catchment area threshold (100 km^2 in this study), which is related to the total area of the basin, the model architecture complexity, the ~~time scale and~~ step size~~,~~ and the spatial resolution of the input data. ~~Taking the above into consideration, the threshold is set to 100 km^2 in this study. As a result, the Yalong River basin is divided into 522 sub-basins (Fig. 1b).~~ Location~~The location~~, elevation, area, flow accumulation area and flow direction of each sub-basin can be found in Table S1.

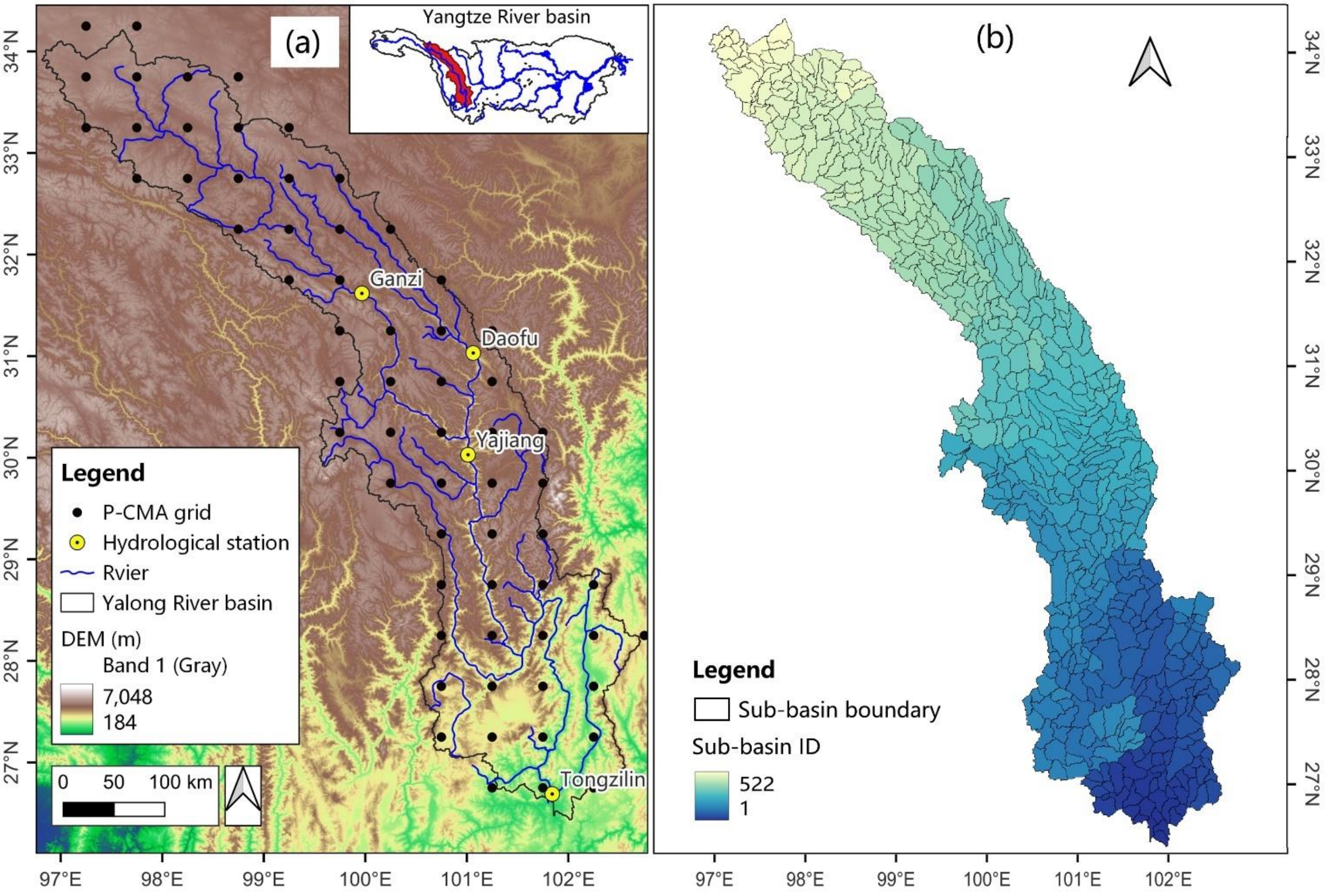
(a)
Yangtze River basin
Ganzi
Daofu
Yajiang
Tongzilin
Legend
● P-CMA grid
Hydrological station
Rvier
Yalong River basin
DEM (m)
Band 1 (Gray)
7,048
184
0 50 100 km
34°N
33°N
32°N
31°N
30°N
29°N
28°N
27°N
97°E
98°E
99°E
100°E
101°E
102°E
(b)
Legend
Sub-basin boundary
Sub-basin ID
522
1

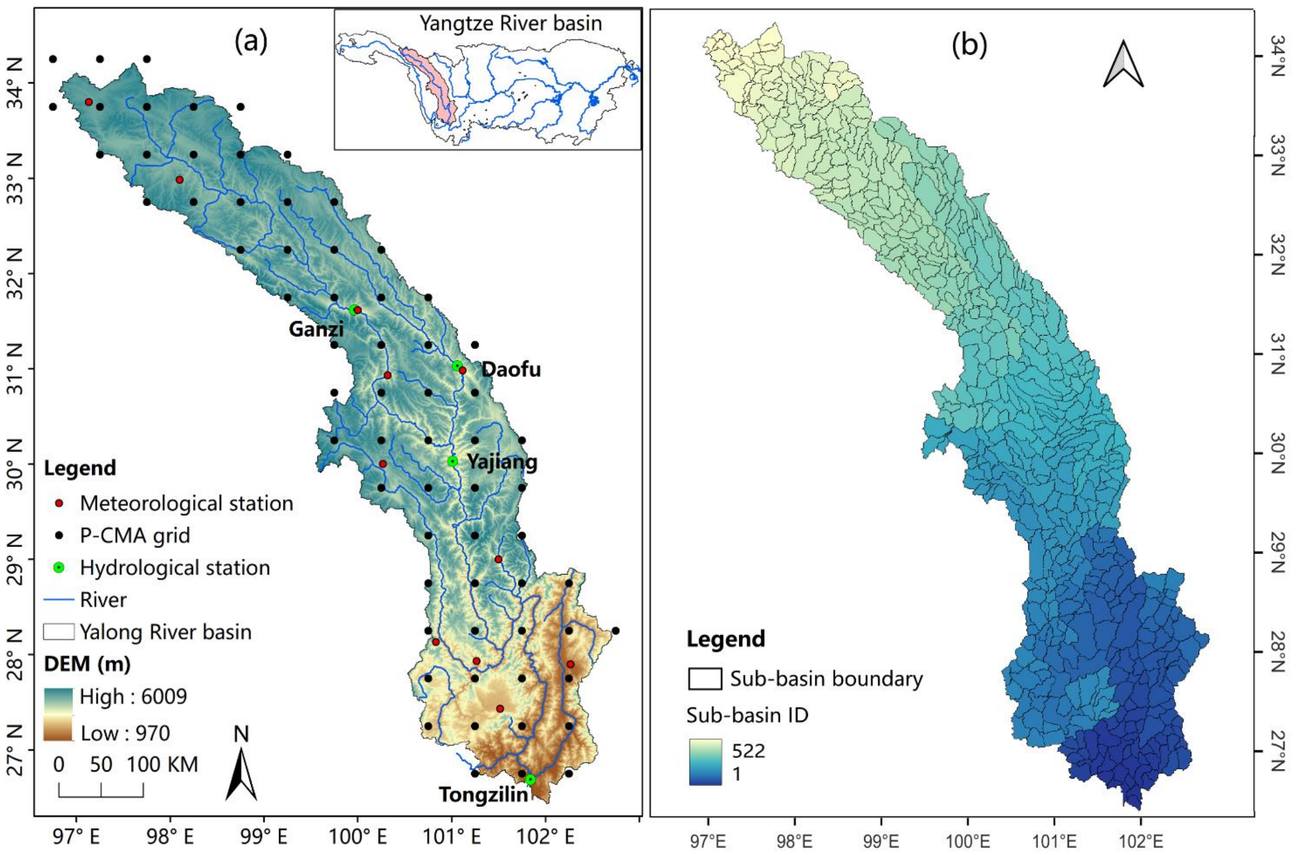

Figure 1. (a) Study area and (b) 522 sub-basins (Zhang et al., 2022a).

2.2 Data

2.2.1 Gauge precipitation observations

The 0.5-degree, daily precipitation observation data were obtained from the National Meteorological Information ~~Center~~Centre of the China Meteorological Administration (CMA-NMIC). The product was produced by interpolating gauge data from more than 2000 stations across China. This product has been ~~verified ~~proven to be highly accurate~~to have high accuracy~~ and has been widely applied to a variety of studies such as streamflow simulation, drought assessment, and water resource~~s~~ management (Gou et al., 2020, 2021; Zhang and Ye, 2021; Miao et al., 2022). In this study, the gridded precipitation observations are used as a reference for the satellite-based precipitation products. Using the inverse distance weighting (IDW) method, they are resampled ~~interpolated ~~to each sub-basin. And due to limited hydrological observatories, the streamflow of each sub-basin obtained from the calibrated hydrological model driven by this product is also used as a reference for the satellite precipitation-driven streamflow simulation. Errors caused by factors such as interpolation are ignored. The selected study period is from January 1, 2003 to December 31, 2018.

2.2.2 Global satellite precipitation estimates

Three sets of the latest quasi-global satellite precipitation ~~estimate~~ estimation products are selected. The first one is~~-~~ PDIR product~~the Precipitation Estimate from Remotely Sensed Information using Artificial Neural Networks-Dynamic Infrared Rain Rate near real-time (PDIR Now, hereafter, PDIR)~~, which solely relies on infrared data. It ~~Therefore it~~ has a very high spatiotemporal resolution (0.04 degree~~s~~ and 1 hour) and a very short delay time (1 hour)~~, and it is a near real-time product without bias correction~~. The other two products are bias-adjusted products, IMERG Final Run version 6 (hereafter, IMERG-F) (Huffman et al., 2015, 2019) and Gauge-calibrated ~~Global Satellite Mapping of Near real-time Precipitation~~GSMaP product (GSMaP_Gauge_NRT_v6, hereafter, GSMaP) (Kubota et al., 2007, 2020), with a spatial resolution of 0.1 degree~~s~~. The selected study period is also from January 1, 2003 to December 31, 2018. All these products are aggregated to the daily scale and resampled ~~interpolated~~ to each sub-basin using IDW~~ method~~. ~~The three precipitation products represent different research institutions and algorithms. Also, they have been proven to have relatively good accuracy in our previous study (Zhang et al., 2021b).~~ It should be noted that these products are selected as examples only and any other precipitation product can be used as an alternative.

2.2.3 Other data

In addition to precipitation gauge observations and satellite precipitation products, other meteorological data such as: temperature, wind speed and evaporation~~,~~ basin attributes, and streamflow observations are needed for hydrological ~~modeling~~modelling. The meteorological data ~~(including temperature, wind speed, etcand evaporation.)~~ were also obtained from the CMA-NMIC, and ~~they are~~ were used to drive the hydrological model together with precipitation. The streamflow observations (January 1, 2006 to December 31, 2015) were collected from four gauged hydrological stations in the Yalong River basin from the upstream to the downstream, namely Ganzi (GZ), Daofu (DF), Yajiang (YJ), and Tongzilin (TZL) (cf. Figure 1(a)). These data were obtained from the Hydrological Yearbook of the Bureau of Hydrology. The National Aeronautics and Space Administration Shuttle Radar Topographic Mission (NASA SRTM) digital elevation model (DEM) data with a spatial resolution of 90~~-~~m was obtained from the Geospatial Data Cloud of China. The 1 km soil data was clipped from the China Soil Database issued by the Tibetan Plateau Data ~~Center~~Centre of China. The 1km land use data was obtained from the Resource and Environment Science and Data ~~Center~~Centre provided by the Institute of Geographical Sciences and Resources, Chinese Academy of Sciences.

3 Methodology

~~3.1 Overview~~

The framework of this study is shown in Fig. 2. We adopt a two-stage streamflow post-processing approach. In the first stage (Sect. 3.1), the hydrological model is calibrated and validated by hydrological station observations~~ (Sect. 3.2.1)~~. Then, we use the observed precipitation to drive the calibrated hydrological model to generate streamflow references for each sub-basin ~~(Sect. 3.2.2)~~. And we use satellite precipitation to drive the model to generate uncorrected (raw) streamflow simulations ~~(Sect. 3.2.3)~~. In the second stage (Sect. 3.2), we perform probabilistic post-processing of the streamflow using the QRF ~~model~~ and the ~~PLSTM~~CMAL-LSTM models ~~(Sect. 3.3)~~. In the last subsection (Sect. 3.3), we describe the ~~scoring~~ evaluation metrics used in this study ~~(Sect. 3.4)~~.

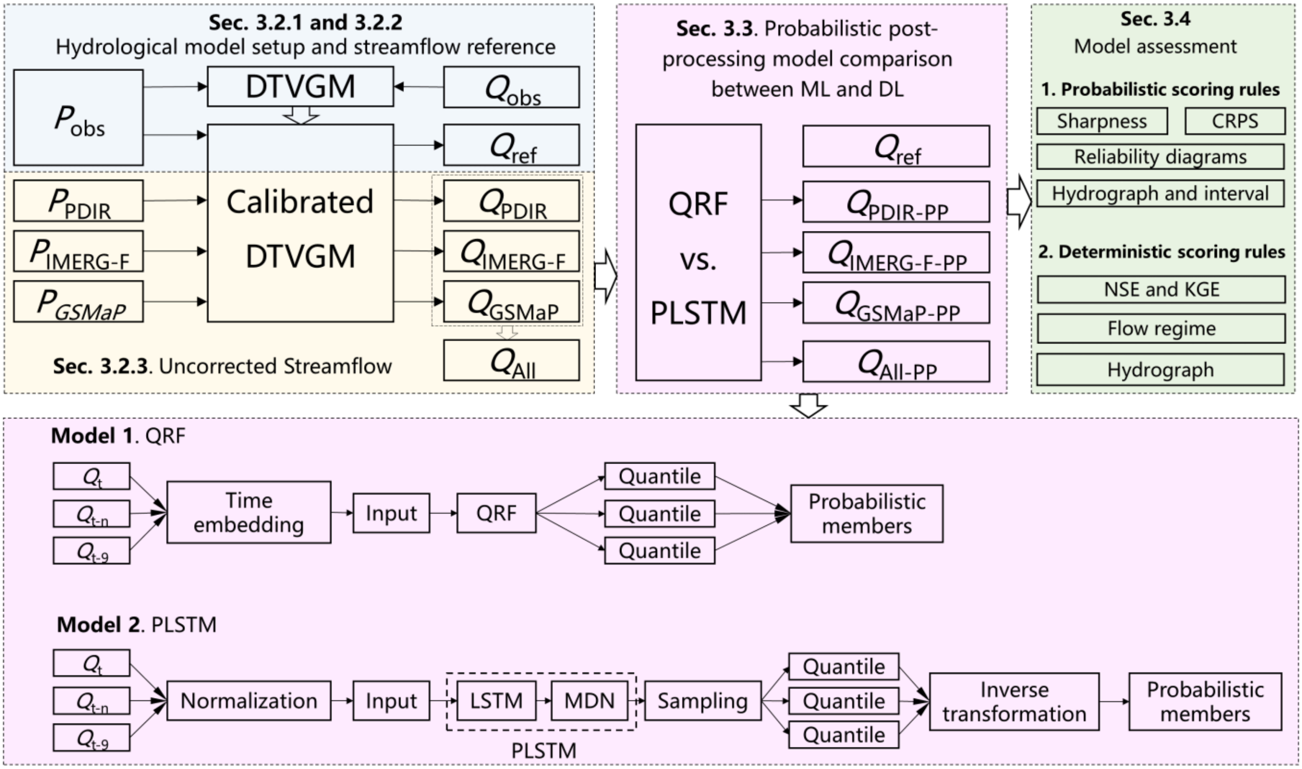
Sec. 3.2.1 and 3.2.2
Hydrological model setup and streamflow reference
P_{obs}
DTVGM
Q_{obs}
Q_{ref}
Calibrated DTVGM
P_{PDIR}
$P_{IMERG-F}$
P_{GSMaP}
Q_{PDIR}
$Q_{IMERG-F}$
Q_{GSMaP}
Q_{All}
Sec. 3.2.3. Uncorrected Streamflow
Sec. 3.3. Probabilistic post-processing model comparison between ML and DL
QRF vs. PLSTM
Q_{ref}
$Q_{PDIR-PP}$
$Q_{IMERG-F-PP}$
$Q_{GSMaP-PP}$
Q_{All-PP}
Sec. 3.4
Model assessment
1. Probabilistic scoring rules
Sharpness
CRPS
Reliability diagrams
Hydrograph and interval
2. Deterministic scoring rules
NSE and KGE
Flow regime
Hydrograph
Model 1. QRF
Q_t
Q_{t-n}
Q_{t-9}
Time embedding
Input
QRF
Quantile
Quantile
Quantile
Probabilistic members
Model 2. PLSTM
Q_t
Q_{t-n}
Q_{t-9}
Normalization
Input
LSTM
MDN
PLSTM
Sampling
Quantile
Quantile
Quantile
Inverse transformation
Probabilistic members

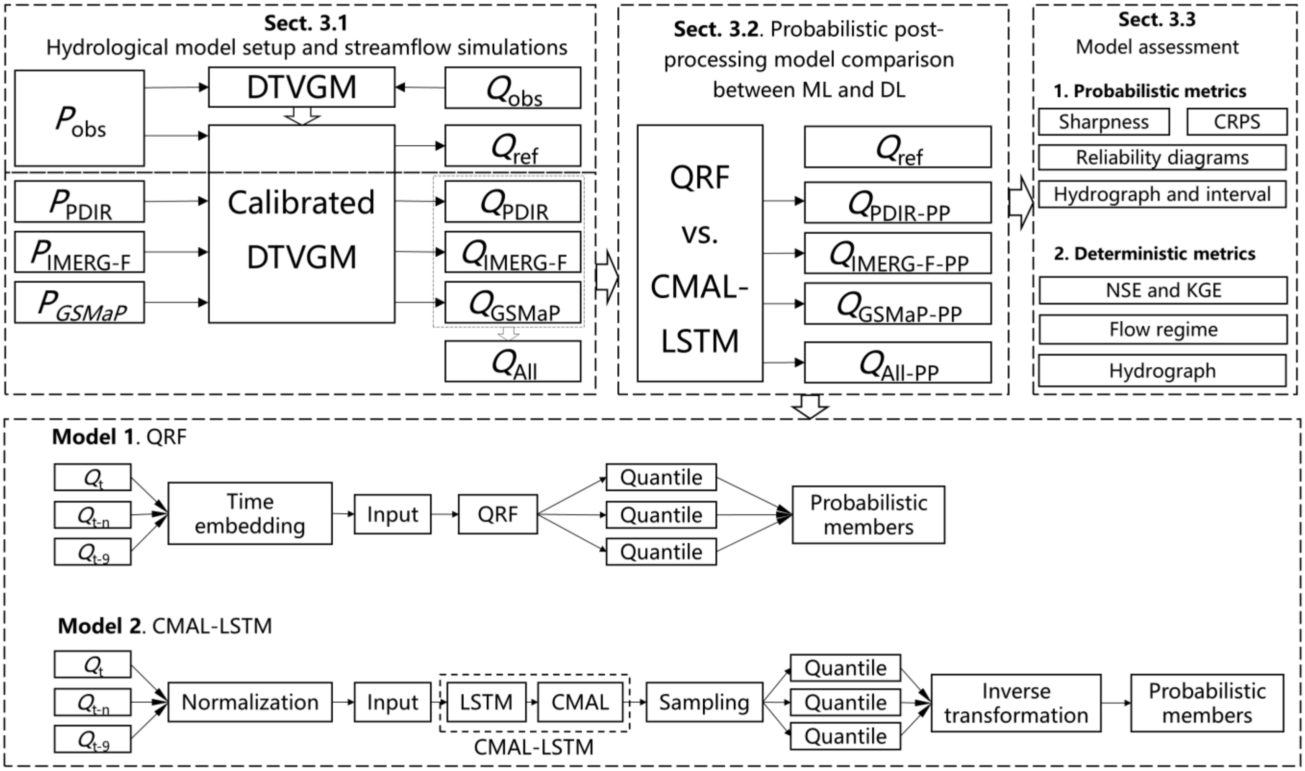

Figure 2. ~~The~~ Framework ~~framework~~ of this study.

3.1~~3.2~~ Streamflow reference and uncorrected streamflow simulations

~~3.2.1 Hydrological model setup, calibration and verification~~

The purpose of this study is to post-process the streamflow simulations for all sub-basin outlets, and therefore corresponding references are needed. Due to the limited streamflow observations, we use streamflow simulations from the hydrological model driven by observed precipitation as a reference. To ensure that the results are reliable, we first use the collected streamflow observations from four hydrological stations to setup, calibrate and validate the hydrological model.

We choose ~~a hydrological model named~~ distributed time-variant gain model (DTVGM), a process-based model that uses the rainfall-runoff nonlinear relationship (Xia, 1991; Xia et al., 2005) for ~~rainfall-runoff~~ simulation~~. The DTVGM is a distributed, process-based model that uses the rainfall-runoff nonlinear relationship (Xia, 1991; Xia et al., 2005)~~. In each sub-basin, ~~the~~ runoff is calculated according to Eq. (1).~~water balance.~~ The kinematic wave equation is used for river routing (Ye et al., 2013). The snowmelt process in the high-altitude regions of the basin is simulated by the degree-day method (Bormann et al., 2014). A detailed description of the model can be found in (Xia et al., 2005; Ye et al., 2010).

$$P_t + AW_t = AW_{t+1} + g_1\left(\frac{AW_{u,t}}{C\cdot WM_u}\right)^{g_2}\cdot P_t + K_r\cdot AW_{u,t} + K_e\cdot EP_t + K_g\cdot AW_{g,t} \qquad (1)$$

where t is the time step; P and EP are precipitation and potential evapotranspiration, respectively; AW and WM are soil moisture (mm) and field soil moisture (mm), respectively; u and g are the upper and lower soil layers, respectively; K_e, K_r and K_g are evapotranspiration, interflow and groundwater runoff coefficients, respectively; g_1 and g_2 are factors describing the non-linear rainfall-runoff relationship; and C is the land cover parameter.

Based on the length of the streamflow observation collected from hydrological stations (2006-2014~~, 9 years in total~~), we divide ~~them~~ the streamflow time series into three periods: a one-year spin-up period (2006), a four-year calibration period (2007-2010), and a four-year validation period (2011-2014). We use Nash-Sutcliffe efficiency (NSE) as the objective and regionalize the parameters from upstream to downstream using manual tuning, while ensuring that the water balance coefficient converges to 1. The model calibration and validation are shown in Fig. ~~S3~~S1 in the supplement. The NSE for the four gauged hydrological stations (GZ, DF, YJ, and TZL) are 0.89, 0.91, 0.93, 0.79, and 0.79, 0.86, 0.87, and 0.59 for ~~the~~ calibration and validation periods, respectively. In the ~~following~~remaining part of this study, the hydrological model is fixed and we mainly post-process the streamflow bias introduced by satellite precipitation, ~~ignoring~~disregarding other sources of uncertainty such as ~~(e.g.,~~model structure, DEM and other forcing data~~)~~. ~~The relatively poor performance of TZL during the validation period (2011-2014) is due to the downstream reservoir construction that changes the natural streamflow process. The used hydrological model does not include a reservoir regulation module, but we believe that the model is able to reproduce the natural runoff process well, so the model is reliable. More importantly, the observed precipitation-driven streamflow simulation is viewed as a reference. And in the post-processing stage, only the precipitation input is changed to compare the performance of the post-processing model to resolve the input uncertainty. Therefore, the errors caused by the model structure and model parameters are neglected.~~

~~3.2.2 Producing observed precipitation-driven streamflow simulation~~

After model calibration and validation, to ensure the number of data samples for data-driven post-processing methods, we use the observed precipitation from 2003 to 2018 to drive the hydrological model. A 16-year streamflow simulation reference data ~~in~~ for ~~the~~ 522 sub-basin outlets is ~~finally~~ obtained. Streamflow from different sub-basins can also reflect hydrological processes of diverse climate types and scales.

Finally, ~~3.2.3 Producing satellite precipitation-driven uncorrected streamflow simulation~~

~~The uncorrected streamflow simulations are also needed before post-processing. Here~~ we use three different satellite precipitation products PDIR, IMERG-F and GSMaP for period ~~(~~2003-2018~~)~~ to separately drive the hydrological model ~~separately~~ ~~to~~ and obtain three different streamflow simulations accordingly. ~~(PDIR, IMERG-F and GSMaP).~~ In addition, the equally weighted average of the three outputs can be ~~seen~~ viewed as a multi-product driven simulation (All) ~~multi-model (All) simulation~~. The reason for considering the multi-product simulation (All)~~, All,~~ for reference is two-fold. ~~We do this for two~~

~~considerations, ~~F~~f~~irst, the model performance of two different post-processing models can be adequately compared in three different contexts. Secondly, the ~~multi-model~~multiple inputs can be used to compare the effects of model averaging and multi-dimensional features on the post-processing models. The experimental design is described ~~below~~in the following ~~section~~Sect. 3.2~~.~~.

~~3.3~~3.2 Post-processing model and experimental design~~Hydrological post-processing procedure~~

The two post-processing models selected are the QRF model (Meinshausen and Ridgeway, 2006) and the CMAL-LSTM model (Klotz et al., 2022). The QRF model was chosen because it enables us to analyse the distribution of the entire data based on different quantiles, and it has been previously used in several studies (Taillardat et al., 2016; Evin et al., 2021; Kasraei et al., 2021; Tyralis et al., 2019; Tyralis and Papacharalampous, 2021). The CMAL-LSTM model is a combination of an LSTM model and a CMAL mixture density function, which allows it to estimate prediction uncertainty. To the best of our knowledge, these two models currently considered state-of-the-art in ML and DL for hydrological probabilistic modelling. Avid readers are highly encouraged to read the original papers for more d~~D~~etailed information about each model. ~~can be found in their original papers and will not be restated in this study.~~

~~In this section, we present the two probabilistic post-processing models compared in this study. Flowcharts of the two post-processing models can also be found in the bottom panel of Fig. 2. The principles of the two models are briefly described in Sect. 3.3.1 and Sect. 3.3.2. Model setup, including feature selection, hyperparameters and experiments are in Sect. 3.3.3. The probabilistic members are generated by the post-processing model in Sect. 3.3.4.~~

~~3.3.1 QRF~~

~~Random forests (RF) is an ensemble machine learning (ML) algorithm based on decision trees (Li et al., 1984; Breiman, 2001). Three steps are required to implement the RF model. First, we start by splitting the total samples and sampling K subsamples for K individual decision trees. Then each decision tree makes its own prediction. Finally, multiple decision trees are averaged or voted to get the final prediction. Compared to decision trees, random forests provide two additional randomness: (1) random sampling of samples, and (2) parallel integration of multiple decision trees. Therefore, the random forests can correct the inductive preferences induced by individual decision trees from falling into local optima, thus effectively preventing overfitting.~~

~~However, the prediction made using RF regression is the conditional mean of the target variable. This means that the RF model will ignore the entire conditional probability distribution. By introducing quantiles, the RF model produces a variant of quantile regression forests (QRF) (Meinshausen and Ridgeway, 2006). The QRF model considers the distribution of the entire data by selecting different quantiles, and therefore is able to generate probabilistic members. A more detailed description of RF and QRF models can be found in Zhang et al. (2022a). QRF model has been widely used in several studies (Taillardat et al., 2016; Evin et al., 2021; Kasraei et al., 2021; Tyralis et al., 2019; Tyralis and Papacharalampous, 2021).~~

~~3.3.2 PLSTM~~

~~Long short-term memory (LSTM) network is one of the most famous recurrent neural networks (RNNs), and it is a representative of sequential deep learning (DL) algorithms (Staudemeyer and Morris, 2019). RNN models are designed to effectively utilize temporal information and have a wide range of applications in speech recognition and speech translation (Hori et al., 2018). However, the original RNN model is prone to gradient vanishing as the time series grows, leading to model failure to converge. LSTM effectively solves the gradient problem by introducing gate functions. The LSTM model has been widely used in various fields such as rainfall-runoff simulation and soil moisture simulation (Fang et al., 2017, 2022; Kratzert et al., 2018, 2019; Fang and Shen, 2020). The formulas of LSTM can be found in the previous studies (Fang et al., 2017; Kratzert et al., 2018; Staudemeyer and Morris, 2019).~~

~~Similar to the RF model, the LSTM model can only make deterministic predictions and cannot provide probabilistic information. There are currently several methods in the literature to quantify the uncertainty of LSTM and thus give probabilistic predictions. In a recent study, Klotz et al. (2022) compared four different methods, including three mixture density networks (MDNs) and one Monte Carlo dropout (MCD) method. A mixture density is a probability density function created by combining multiple densities. In their studies, three forms of MDNs with different levels of complexity were adopted, namely, Gaussian mixture models (GMMs), Countable mixture of asymmetric Laplacians (CMAL) and Uncountable mixtures of asymmetric Laplacians (UMAL). MCD randomly changes the number of neurons through multiple experiments to obtain probabilistic outputs. The complexity of CMAL is between that of GMM and UMAL, and it achieved the best performance in the study of Klotze et al. (2022). Therefore, we choose CMAL as a representative of PLSTM in this study. A detailed description of CMAL can be found in Klotz et al. (2022) and will not be repeated in this study.~~

~~3.3.3 Model setup and experimental design~~

Both post-processing models require input features. Here, ~~to~~ in order to keep ~~maintain~~ the ~~low~~ complexity of the models low, ~~we select~~ only the uncorrected streamflow simulations are chosen as input features. Considering the autocorrelation skill of the streamflow (see Fig. S2 in the supplement), for the post-processing (Q_t) on day t ~~(Q_t)~~, we select the simulated streamflow for the first 9 days (Q_{t-9}^{sim}, Q_{t-8}^{sim},…, Q_{t-1}^{sim}) and the simulated streamflow of that day (Q_t^{sim}) as the inputs. In the QRF model, the input features are fed by temporal embedding. And in the CMAL-LSTM model, the seq-length is set to 9. For both models, we select the streamflow reference (Q_t^{ref}) on day t ~~(Q_t^{ref})~~ as the target. In addition, since we used three different satellite precipitation products, the experiments are divided into a single-~~model~~ product experiment and a multi-~~model~~ product experiment (All). The information ~~of~~ for each experiment is summarized in Table 1. The training period is from 1 January 2003 to 31 December 2010. The validation period is from 1 January 2011 to 31 December 2014. And the test period is from 1 January 2015 to 31 December 2018.

Table 1. Experimental design.

Streamflow simulation	Model	Input feature	~~Dimension~~	Target
PDIR	QRF	$Q_{t-9}^{sim}, Q_{t-8}^{sim},\dots, Q_{t}^{sim}$	10	Q_t^{ref}
	~~PLSTM~~CMAL-LSTM		1	
IMERG-F	QRF		10	
	CMAL-LSTM~~PLSTM~~		1	
GSMaP	QRF		10	
	CMAL-LSTM~~PLSTM~~		1	
All (PDIR, IMERG-F, GSMaP)	QRF		30	
	CMAL-LSTM~~PLSTM~~		3	

~~The training period is from 1 January 2003 to 31 December 2010. The validation period is from 1 January 2011 to 31 December 2014. And the test period is from 1 January 2015 to 31 December 2018.~~

We implemented the QRF model using *pyquantrf* package (Jnelson18, 2022). We tuned three sensitive hyperparameters in the QRF model ~~through~~ by grid search, finally setting the number of trees (K) ~~is~~ to 70, the number of non-leaf node splitting features ~~is~~ to 10, and the number of samples used for leaf node predictions (N_{leaf}) ~~is~~ to 10. ~~The~~ All other hyperparameters ~~are~~ were set to default values.

We implemented the CMAL-~~P~~LSTM model using *NeuralHydrology* package (Kratzert et al., 2022a). We followed the model architecture of Klotz et al. (2022), which contains an LSTM layer and a CMAL layer. ~~Unlike~~ In contrast to the QRF model, the input data of the CMAL-LSTM ~~PLSTM~~ model needs to be normalized. Here, by several comparisons, we used the normal quantile transform method (Fig. S3 in the supplement). The ~~model~~ hyperparameters of the model include the number of neurons in the LSTM layer (N_{LSTM}), the number of components of the mixture density function (N_{MDN}), the dropout rate, the learning rate, the epoch, and the batch size. ~~For~~ N_{MDN}, is ~~we~~ set ~~it~~ to 3, which follows ~~is the same as~~ Klotz et al. (2022). ~~We fine-tuned the~~The other hyperparameters are also fine-tuned such ~~. The~~that the final learning rate is set to 0.0001, the dropout to~~is~~ 0.4, the epoch to ~~is~~ 100, the batch size to~~is~~ 256, and the N_{LSTM} to~~is~~ 256.

For the QRF model, ~~we equally sampled~~ 100 ~~quantiles~~percentiles (0.005 to 0.995) were equally sampled for each basin and time step and ~~bring~~fed ~~them~~ directly into the model to obtain the final probabilistic (100) members. For the ~~PLSTM~~CMAL-LSTM model, ~~we~~ first ~~sample~~~~generated~~ 10,000 sample points for each basin and time step by sampling from the mixture distribution were generated~~.~~ ~~to get 10,000 sample points for each basin and time step. We~~ and ~~then take~~~~extracted~~ ~~the~~ same 100 percentiles ~~quantiles~~ (0.005 to 0.995) from these sample points were extracted and~~,~~ remapped ~~them~~ to the original streamflow space using inverse quantile normal transformation, where~~and~~ finally ~~produced~~ ~~the probabilistic~~ the probabilistic ~~(100)~~ members were produced.

Our computing platform is a workstation configured with an Intel(R) Xeon(R) Gold 6226R CPU @ 2.9GHz and an RTX3090 GPU with 24G video memory. It is ~~important to note~~worth noting that we ~~model~~modelled each sub-basin separately due to the random sampling process of ~~. This is because~~ the ~~PLSTM~~ CMAL-LSTM model ~~generates probabilistic members with random sampling~~ exceeding ~~exceeding~~ the GPU's video memory ~~(see Sect. 3.3.4 and Sect. 5.3)~~. For consistency, the QRF model ~~is~~ was also modelled locally. ~~It takes took~~ The computational time was approximately 12 hours to complete all ~~PLSTM~~CMAL-LSTM ~~experiments. It takes took about~~ and 6 hours to complete all QRF experiments.

~~3.3.4 Producing probabilistic members~~

~~For the QRF model, we equally sample 100 quantiles (0.005 to 0.995) for each basin and time step and bring them directly into the model to obtain the final probabilistic (100) members. For the PLSTM model, we first sample from the mixture distribution to get 10,000 sample points for each basin and time step. We then take the same 100 quantiles (0.005 to 0.995) from these sample points, remap them to original streamflow space using inverse quantile normal transformation, and finally produce the probabilistic (100) members.~~

~~3.4~~3.3 Performance ~~measures~~evaluation

In this section ~~We evaluate the~~ two post-processing models are evaluated from both probabilistic and deterministic perspectives. The ~~scoring~~ evaluation metrics are presented in Sect. 3.~~4~~3.1 and Sect. 3.~~4~~3.2, respectively.

~~3.4.1~~3.3.1 Probabilistic (multi-point) metrics

We followed the criterion for probabilistic predictions proposed by Gneiting et al. (2007): to maximize the sharpness of the prediction distributions subject to reliability. We both use scoring rules and diagnostic graphs to assess reliability and sharpness holistically.

The continuous rank probability score (CRPS) is a widely used proper scoring rule that assesses reliability and sharpness simultaneously (Gneiting et al., 2007). ~~The evaluation of probabilistic post-processing uses metrics that describe the accuracy, reliability, and sharpness.~~

~~1) Continuous rank probability score (CRPS)~~

~~The continuous rank probability score (CRPS) is widely used in probabilistic evaluations (Bröcker, 2012).~~ For given probabilistic members, the CRPS calculates the difference between the cumulative distribution function (CDF) of the probabilistic members and the observations. We also used a weighted version of CRPS (threshold weighted CRPS, twCPRS), which is commonly used to give more weight to extreme cases (Gneiting and Ranjan, 2011). ~~It can be used for a comprehensive assessment of the accuracy, reliability and sharpness of probabilistic forecasts (Bröcker, 2012). The CRPS is also the basic metric for evaluating the goodness of probabilistic outputs in this study. For different thresholds focused on the evaluation of extreme events, we also chose threshold weighted CRPS (hereafter twCRPS, Gneiting and Ranjan, 2011; Zhao et al., 2022).~~ These two metrics can be expressed as follows:

$$CRPS(F,x) = \int_{-\infty}^{\infty} \{F(y) - \mathbf{1}(y \geq x)\}^2 dy \qquad (2)$$

$$twCRPS(F,x) = \int_{-\infty}^{\infty} \{F(y) - \mathbf{1}(y \geq x)\}^2 \omega(y) dy \qquad (3)$$

~~$CRPS = \int_{-\infty}^{\infty} \left(F(Q_t) - O(Q_t)\right)^2 dP_t$ (1)~~

~~$twCRPS = \int_{-\infty}^{\infty} \left(F(Q_t) - O(Q_t)\right)^2 \omega(Q) dQ_t$ (2)~~

where $\omega(y)$~~$\omega(Q)$~~ is a threshold weighted function and is calculated based on the threshold q (80%, 90% and 95% ~~quantiles~~percentiles of observations in this study). When y~~Q~~ $\geq q$ (~~or~~ y ~~Q~~ $< q$), $\omega(y)$~~$\omega(Q)$~~ equals 1 (~~or~~ 0)~~ if. P_t is a streamflow reference threshold~~; $F(y)$~~$O(Q_t)$~~ is the CDF obtained from the probabilistic members for the corrected streamflow~~outputs for day t~~; $\mathbf{1}(y \geq x)$~~$F(Q_t)$~~ is the Heaviside function.~~, and it can be expressed as:~~

~~$O(Q_t) = \begin{cases} 1, & O_i > Q_t \\ 0, & O_i \leq Q_t \end{cases}$ (3)~~

~~where O_i is i^{th} probabilistic members, and Q_t is the corresponding reference.~~ The better performing model has both metrics ($CRPS$ and $twCRPS$) closer to 0.

~~We also used the~~The CRPS skill score ($CRPSS$) is also used to define the relative differences between the two post-processing models. For ~~example, for~~ QRF and ~~PLSTM~~CMAL-LSTM, the $CRPSS$ can be calculated ~~using the following Eq. (4)~~as:

$$CRPSS_{QRF/PLSTM} = \left(1 - \frac{CRPS_{QRF}}{CRPS_{PLSTM}}\right) \times 100\% \qquad (4)$$

A $CRPSS$ greater than 0 indicates that the QRF model is better than the CMAL-LSTM model, and vice versa.

~~The CRPSS is greater than 0, indicating that the QRF model is better than the PLSTM model; conversely, the PLSTM model is better than the QRF model.~~

~~2) Reliability diagram~~

The reliability diagram is used as diagnostic graph to assess the ~~conformity~~ agreement between the predicted probability and ~~its~~ the observed frequency (Jolliffe and Stephenson, 2003)~~(Hartmann et al., 2002)~~. ~~For example~~Namely, if the predicted probability of a particular event is 30%, then the observed relative frequency should also be 30%. Ultimately, perfectly reliable predictions at multiple levels of probability result in a distribution along the diagonal line corresponding to the same levels of observed frequency. ~~A perfectly reliable prediction will match the diagonal line (1:1). A forecast point above (or below) the diagonal line indicates an underestimation (or overestimation).~~A point above (below) the diagonal line in the reliability diagram indicates that the observed relative frequency is higher (lower) than the predicted probability and that there is an underprediction (overprediction) ~~of the predictions~~phenomenon. Here again, three thresholds (80%, 90%~~,~~ and 95%) are chosen to better evaluate the reliability of ~~heavy flood~~extreme ~~events~~ cases (Yang et al., 2021).

~~3) Sharpness~~

Sharpness is a fundamental characteristic of predictive distributions. A sharp probabilistic output corresponds to a low degree of variability in the predictive distribution. To evaluate the sharpness of probabilistic predictions, prediction intervals are commonly employed~~Predict intervals are often used to describe the sharpness of probabilistic~~ ~~forecasts~~ (Gneiting et al., 2007). For this study, t~~T~~he 50% and 90% ~~quantile~~ percentile intervals were chosen~~ in this study~~. ~~In addition~~Furthermore, to establish the relationships between predictive distributions and observations, we ~~calculated~~ assessed the coverage of the prediction intervals over the observations. ~~We adopted the~~The average Euclidean distance of the 25% and 75% probabilistic members is adopted as the sharpness metric (DIS$_{25\text{-}75}$) for the 50% prediction interval, and~~ likewise,~~ the 5% and 95% probabilistic members were used to compute the sharpness metric (DIS$_{5\text{-}95}$) for the 90% prediction intervals. The ratio of the number of observations in the prediction intervals to the total number of observations was used as the coverage of observations (CO$_{25\text{-}75}$ and CO$_{5\text{-}95}$). ~~And~~ In addition, ~~we also selectedemployed serval~~ three additional metrics used in a previous study (Klotz et al., 2022) are also employed to calculate the sharpness metric for the full probabilistic members, including ~~Mean~~ mean absolute deviation (MAD), ~~Standard~~ standard deviation (STD) and ~~Variance~~ variance (VAR).

3.4.2 Deterministic (single-point) metrics

The widely used ~~and standard scoring metrics (e.g.,~~ Nash-Sutcliffe efficiency~~,~~ (NSE) (Nash and Sutcliffe, 1970) and Kling-Gupta efficiency~~,~~ (KGE) (Gupta et al., 2009) ~~–~~are applied for assessing ~~deterministic hydrological modeling~~the deterministic model performance~~ (Nash and Sutcliffe, 1970; Kling et al., 2012)~~. In addition, t~~T~~wo components of NSE, namely ~~(~~Pearson correlation coefficient~~,~~ (PCC) and relative bias~~,~~ (RB) ~~of NSE~~ are ~~also~~ calculated to ~~describe~~ assess the temporal consistency and systematic bias of the difference between simulations and observations, respectively.

~~In addition~~Furthermore, ~~due~~ to account for the seasonality of the flow regime, four metrics are selected to ~~describe~~ characterize the different ~~flow~~ aspects of flow regimes~~regimes~~, including the peak flow bias (FHV, Eq. (A3) in Yilmaz et al., 2008)~~ (Yilmaz et al., 2008)~~, ~~the~~ low-flow bias (FLV, Eq. (A4) in Yilmaz et al., 2008), ~~the~~ flow duration curve bias (FMS, Eq. (A2) in Yilmaz et al., 2008), and mean peak time lag bias (in days) (PT, Appendix D in Kratzert et al., 2021). These metrics provide a comprehensive assessment of model performance across different flow conditions and facilitate a more accurate evaluation of ~~the~~ model ability to reproduce the hydrological processes.

4 Results

4.1 Uncorrected streamflow simulations

Figure 3 shows the spatial ~~performance~~ distribution of NSE ~~(NSE) of the~~for streamflow simulations in 522 sub-basins, driven by ~~the~~ three different satellite precipitation products and multi-~~model~~ product outputs using equal-weighting averaging (All). Among the three satellite precipitation products, the IMERG-F achieves the best model performance, followed by PDIR and GSMaP. PDIR performs poorly in the upstream and outlet regions of the basin. GSMaP ~~differs~~ exhibits significant deviations ~~significantly~~ from the streamflow reference in almost all sub-basins. The precipitation product quality plays a crucial role in streamflow performance with the same hydrological model configuration. The high precipitation bias in GSMaP (Fig. S4f in the supplement) leads to high biases in streamflow simulations (Fig. 8b), resulting in the lowest NSE values (Fig. 3c and Fig.8c) ~~of the~~among the three products. The performance of PDIR-driven streamflow is mainly influenced by the poor temporal variability (PCC) against observations (Fig. S4a in the supplement and Fig. 8a). Equal-weighting averaging (All) ~~Direct simple model averaging (SMA)~~that~~,~~ ~~which introduces~~incorporates biased information ~~of~~ from PDIR and GSMaP~~, does~~ has little impact ~~to~~ on improvinge model performance.

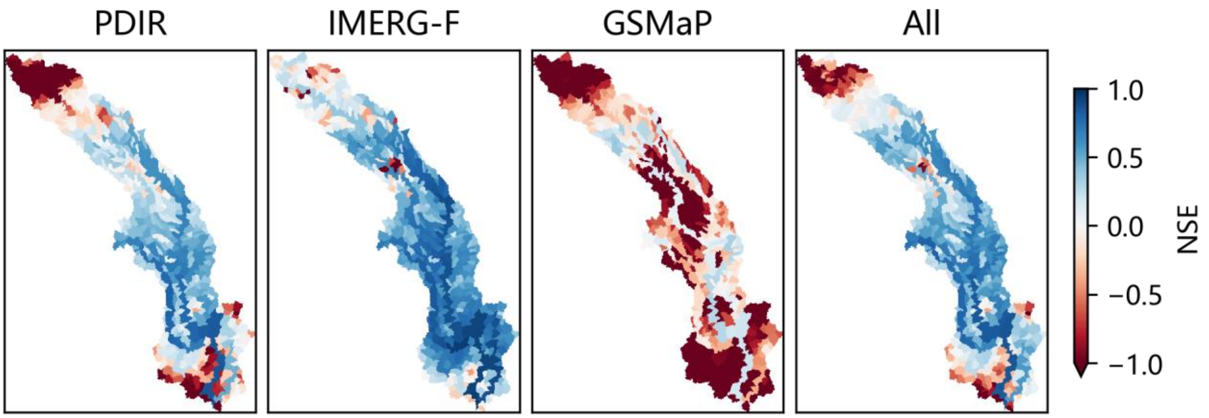

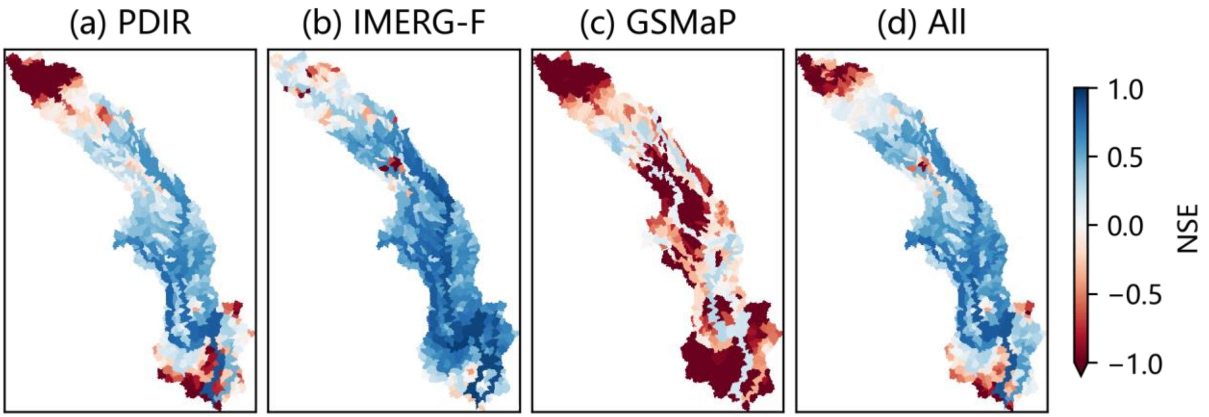

Figure 3. The ~~performance (Nash-Sutcliffe efficiency, NSE)~~NSE of uncorrected~~ (raw)~~ streamflow simulation for the 522 sub-basins.~~ The closer the NSE is to 1, the better the model performs. PDIR is a near real-time product; IMERG-F and GSMAP are bias-adjusted products.~~

4.2 Probabilistic (multi-point) assessment

The flow magnitudes in different sub-basins vary widely. Therefore, ~~when we~~in the presented ~~the~~ results ~~for all sub-basins, we normalize~~ for each sub-basin the results ~~-~~are normalized ~~for each sub-basin~~ separately according to the probabilistic membership of all experiments. By doing so, the probabilistic members of all sub-basins are ~~unified~~ mapped to the range ~~of 0 to 1.~~between 0 and 1.

4.2.1 CRPS ~~and twCRPS~~ overall performance

Overall, the QRF and CMAL-LSTM models demonstrate similar performance in terms of CRPS and twCRPS ~~In general, the performance (CRPS and twCRPS) of the QRF and PLSTM models is similar for~~across all threshold conditions (as shown in Fig. 4 and Fig. S5). However, it is ~~worth noting~~noteworthy that the QRF model ~~has~~ exhibits more outliers compared~~in contrast~~ ~~to~~ with the CMAL-LSTM ~~PLSTM~~ model, indicating that the latter is more stable across sub-basins. When it comes to different precipitation-driven streamflow inputs, the IMERG-F-QRF and IMERG-F-CMAL-LSTM experiments have median CRPS values of 0.0197 and 0.0199, respectively, for 522 sub-basins; the GSM~~A~~aP-QRF and GSM~~A~~aP-CMAL-LSTM experiments have median CRPS values of 0.024 and 0.0241, respectively; the PDIR-QRF and PDIR-CMAL-LSTM experiments have median CRPS values of 0.0287 and 0.0292, respectively. The results show that IMERG-F performs better than GSMaP, and both bias-corrected products outperform the near real-time product PDIR in post-processing performance. ~~.~~ ~~For different precipitation-driven streamflow inputs, the post-processing performance of the bias-corrected product (e.g., IMERG-F) is better than that of the near-real-time product (e.g., PDIR). In the category of bias-corrected products, IMERG-F gives better results than GSMaP. This indicates the value of bias correction of precipitation products as a pre-processing tool for hydrological simulations. At the same time, high-quality precipitation forcing is helpful for both streamflow simulation as well as probabilistic post-processing. The multi-model results (All) are similar to the best-performing single-model results (IMERG-F). However, they are slightly worse than IMERG-F above the 90% threshold This suggests that the input of multiple models, especially when the single model performs poorly, may have a negative effect on the post-processing.~~The results of the multi-product approach (All) are close to those of IMERG-F, but better than those of PDIR and GSMaP. As the threshold conditions increase, the performance of the multi-product approach is slightly worse than that of IMERG-F (Fig. S5). This suggests that introducing features that perform well in a model, such as IMERG-F driven raw streamflow, can improve the performance of post-processing models, but introducing features that perform poorly, such as GSMaP and PDIR driven raw streamflow, can ~~lower~~worsen the performance of post-processing model. The results indicate that the QRF and CMAL-LSTM models can automatically perform feature filtration, but cannot completely avoid learning from disruptive information. Using IMERG-F driven raw streamflow as input, the post-processing models perform better than when driven by the other two products as input features, which is related to the quality of IMERG-F features. In terms of temporal correlation and bias, IMERG-F is the optimal product. The raw streamflow simulation of GSMaP performs worse than PDIR, but the post-processing model performs better than PDIR, because the raw streamflow of GSMaP has higher temporal correlation and better autocorrelation skill as input features compared to PDIR. This leads to PDIR being the worst-performing post-processing experiment among the selected datasets.

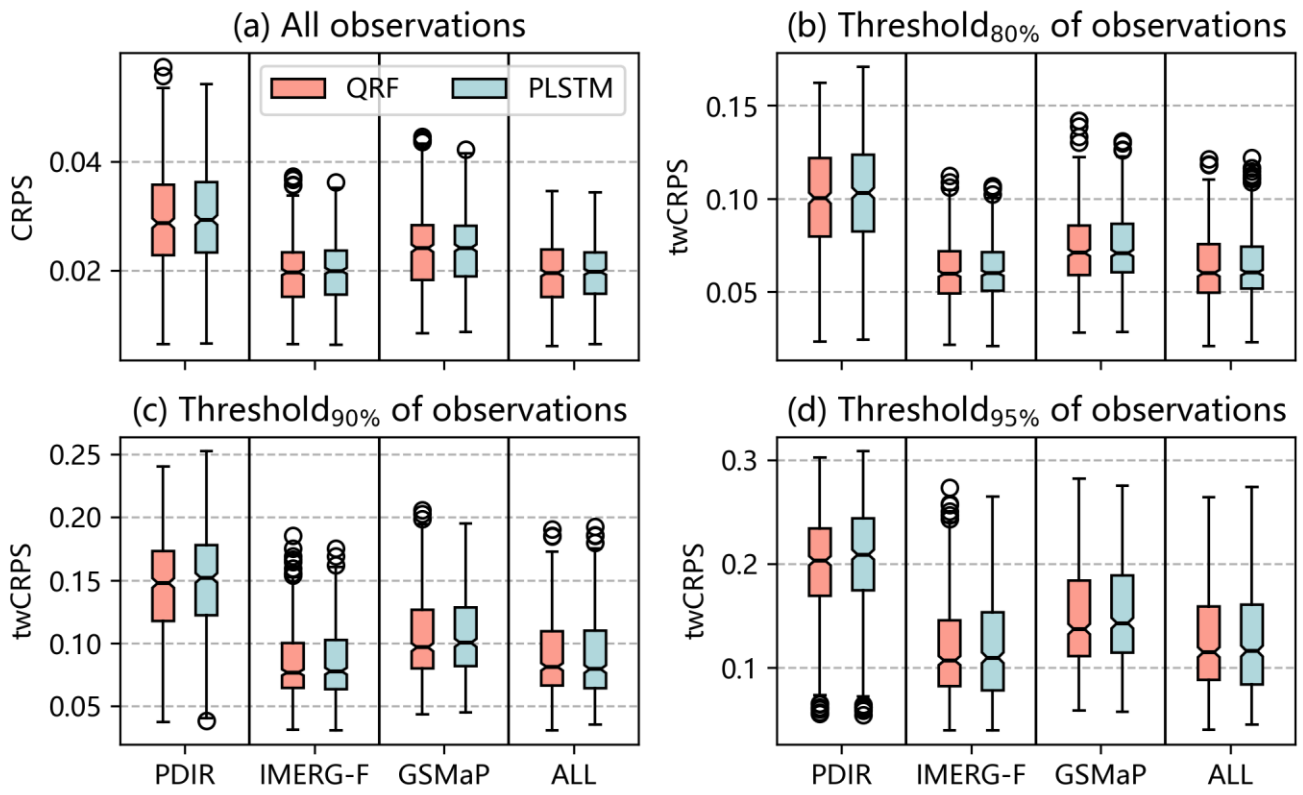

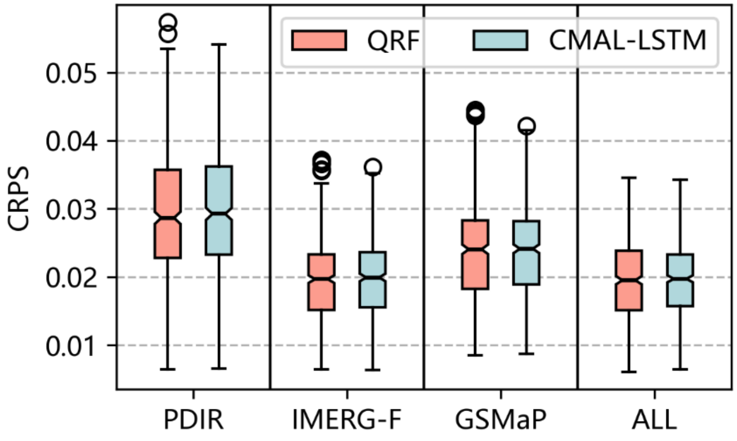

Figure 4. The boxplot of CPRS for different post-processing experiments. ~~continuous rank probability score (CRPS) and twCRPS overall performance. The better performing model has both metrics closer to 0. PDIR is a near real-time product; IMERG-F and GSMAP are bias-adjusted products.~~

~~4.2.2 CRPS spatial distribution~~

In addition to their overall performance (Fig. 4), the QRF and ~~PLSTM~~CMAL-LSTM models exhibit similar spatial ~~distributions~~ performance as it is reported in ~~(~~Fig. 5~~)~~. Compared to PDIR and GSMaP, IMERG-F and multi-~~model~~ product results achieve relatively good performance in most of the 522 sub-basins. PDIR performs the worst, which inherently is ~~still~~ attributed to its poorer input features, such as ~~the~~ low autocorrelation skill of streamflow.~~PDIR performs poorly in the middle and lower reaches of the basin.~~ The third row in ~~of~~ the Fig.~~figure~~5 (i.e., ~~(~~Fig. 5i–l)~~)~~ shows that the differences between QRF and ~~PLSTM~~CMAL-LSTM ~~is~~ are mostly within 10%. However, the introduction of multi-product features~~ple models~~ increased~~s~~ the gap between them, indicating that CMAL-LSTM has an advantage over the QRF model in processing multi-dimensional features. In the PDIR experiment, the QRF model demonstrates superior performance in 68.2% of the sub-basins (356 out of 522), while the CMAL-LSTM model performs better in the remaining 31.8% of sub-basins. Regarding the experiments conducted on IMERG-F, GSM~~A~~aP, and multi-product (All), the proportions of QRF and CMAL-LSTM models are 65.5% and 34.5%, 54.2% and 45.8%, and 64.6% and 35.4% respectively.~~.~~

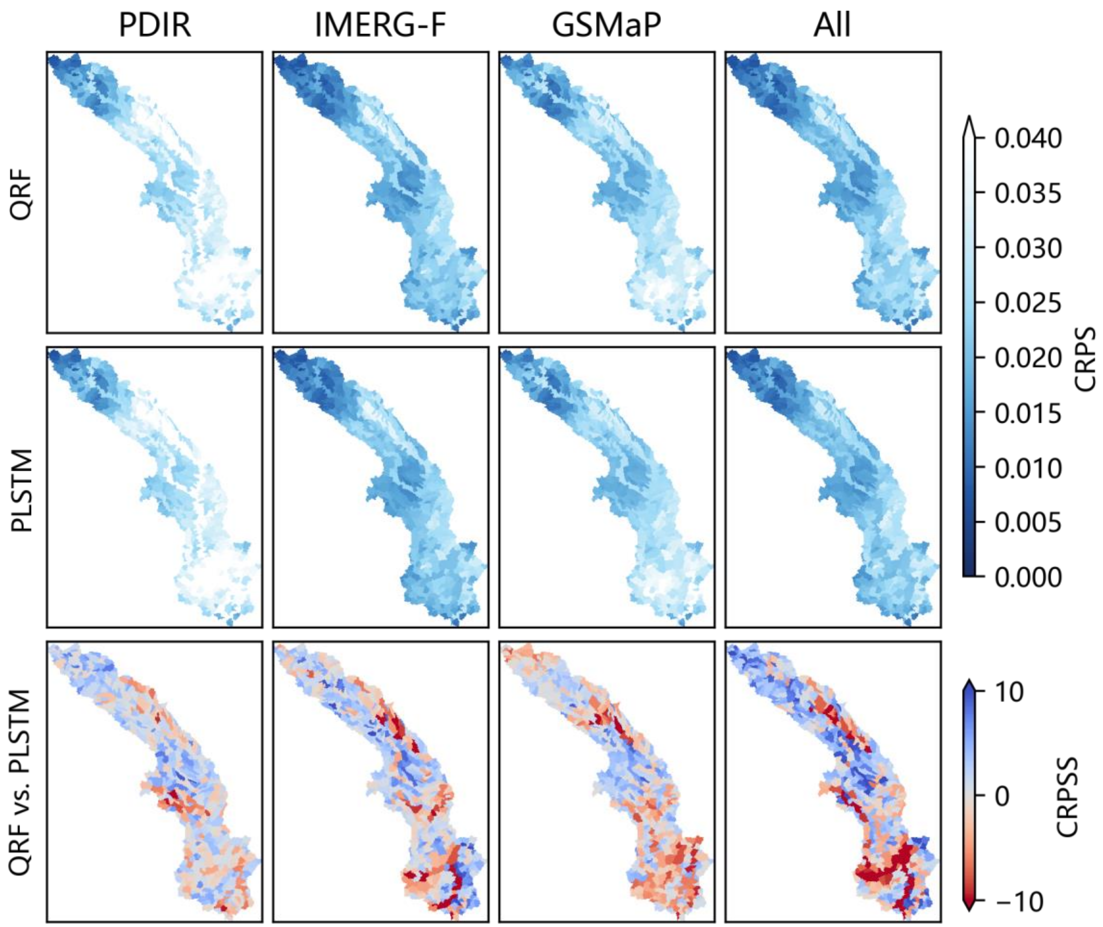
PDIR
IMERG-F
GSMaP
All
QRF
PLSTM
QRF vs. PLSTM
0.040
0.035
0.030
0.025
0.020
0.015
0.010
0.005
0.000
CRPS
10
0
−10
CRPSS

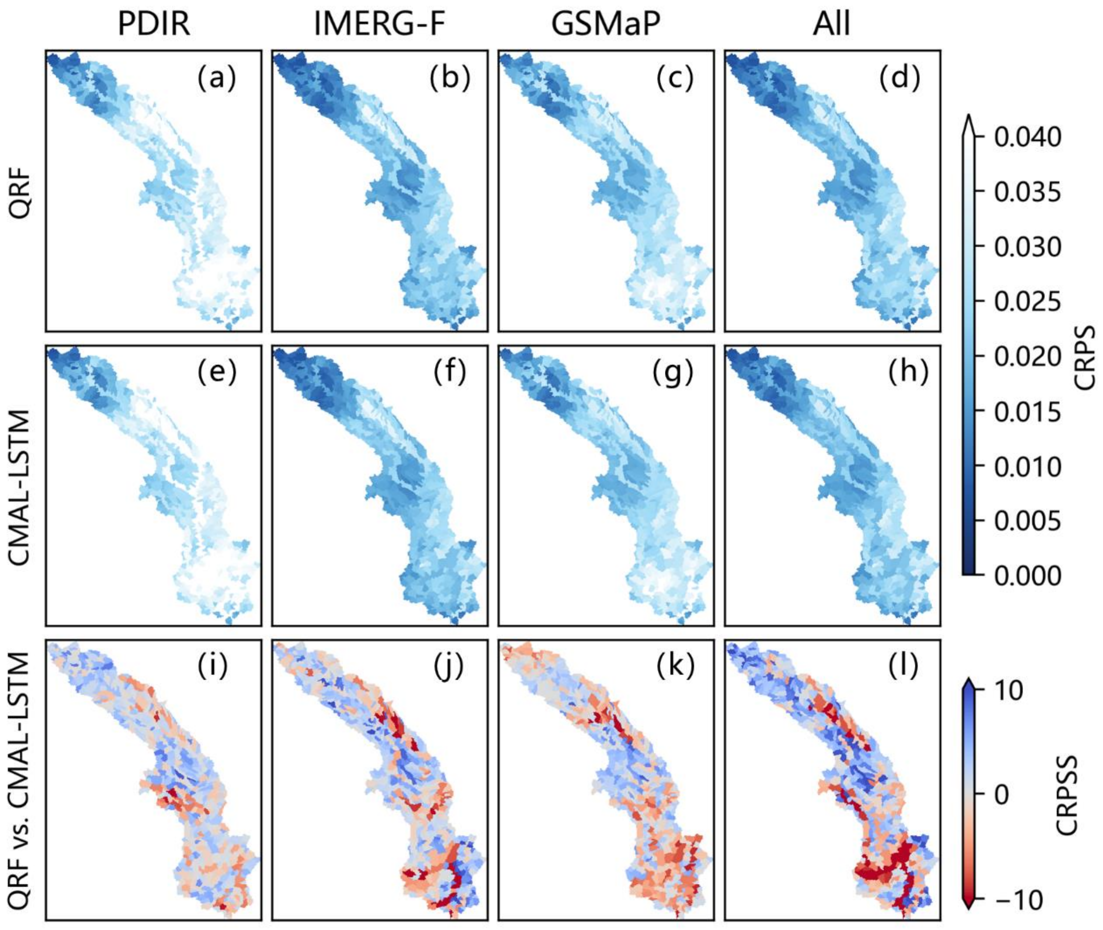

Figure 5. ~~The continuous rank probability score (CRPS) and CRPS score (CRPSS) spatial distributions. The closer the CRPS is to 0, the better the model performs. The CRPSS is greater than 0, indicating that the QRF model performs better than PLSTM; conversely, the PLSTM model performs better than QRF. PDIR is a near real-time product; IMERG-F and GSMAP are bias-adjusted products.~~The spatial distribution of CRPS and CRPSS for different post-processing experiments.

4.2.~~3~~ 2 The relationship between model performance and flow accumulation area (FAA)

To further investigate the differences between the two post-processing models, ~~we plot~~ the relationship between the CRPS/CPRSS metrics and the FAA of sub-basins are presented in ~~(~~Fig. 6~~)~~. Overall~~In general~~, the CRPS values of both post-processing models increases with increasing FAA, which is related to the streamflow amplitude of different sub-basins. Therefore, ~~we focus on~~ the relationship between the CRPSS score and the FAA as reported in Fig. 6e–h is of interest in order to compare the differences between the two post-processing models~~ (Fig. 6e–h)~~. ~~It can be seen~~It is observed that when the FAA is small, the QRF model ~~performs better than~~performance is superior to the CMAL-LSTM model. However, as the FAA increases, the post-processing skill of the CMAL-LSTM model surpasses that of the QRF model. Additionally, the ~~we divide~~

~~the~~ sub-basins are categorised, based on their size, into five intervals: less than 20,000 km^2, 20,000–40,000 km^2, 40,000–60,000 km^2, 60,000–100,000 km^2, and greater than 100,000 km^2. The corresponding number of sub-basins for each of the five intervals are 476, 15, 4, 13 and 14, respectively. The statistics of model performance in different FAA intervals are summarized in Table 2. In sub-basins with FAA less than 20,000 km^2, the QRF model shows a better performance. In the PDIR experiment, the QRF model has a higher CRPS value in 69.5% of sub-basins. In the IMERG-F, GSMaP, and multi-product experiments, the percentage of sub-basins where the QRF model outperforms the CMAL-LSTM model are 69.7%, 57.4%, and 67.2%, respectively. In sub-basins with FAA greater than 60,000 km^2, the CMAL-LSTM model shows an absolute advantage. In the PIDR experiment, the CMAL-LSTM model has a higher CRPS value in 16 sub-basins. In the IMERG-F, GSMaP, and multi-product experiments, the number of sub-basins where the CMAL-LSTM model has a higher CRPS value are 24, 27, and 25, respectively.

~~The spatial variation of CRPS and CRPSS seems to be irregularly and scattered distributed. To further investigate the model difference, we analyze the relationship between CRPS, CRPSS and the flow accumulation area (FAA) of the sub-basin. The results are presented in Fig. 6. We can observe the interesting phenomenon that there is a scale effect in the performance of different models. In the sub-basins with flow accumulation area (FAA) less than 20,000 km^2, the performance of QRF and PLSTM is disorderly scattered, with high and low CRPS values (Fig. 6a). But, as the flow accumulation area (FAA) of the sub-basin increases, the value of CRPS stabilizes when the FAA is greater than 20,000 km^2.~~

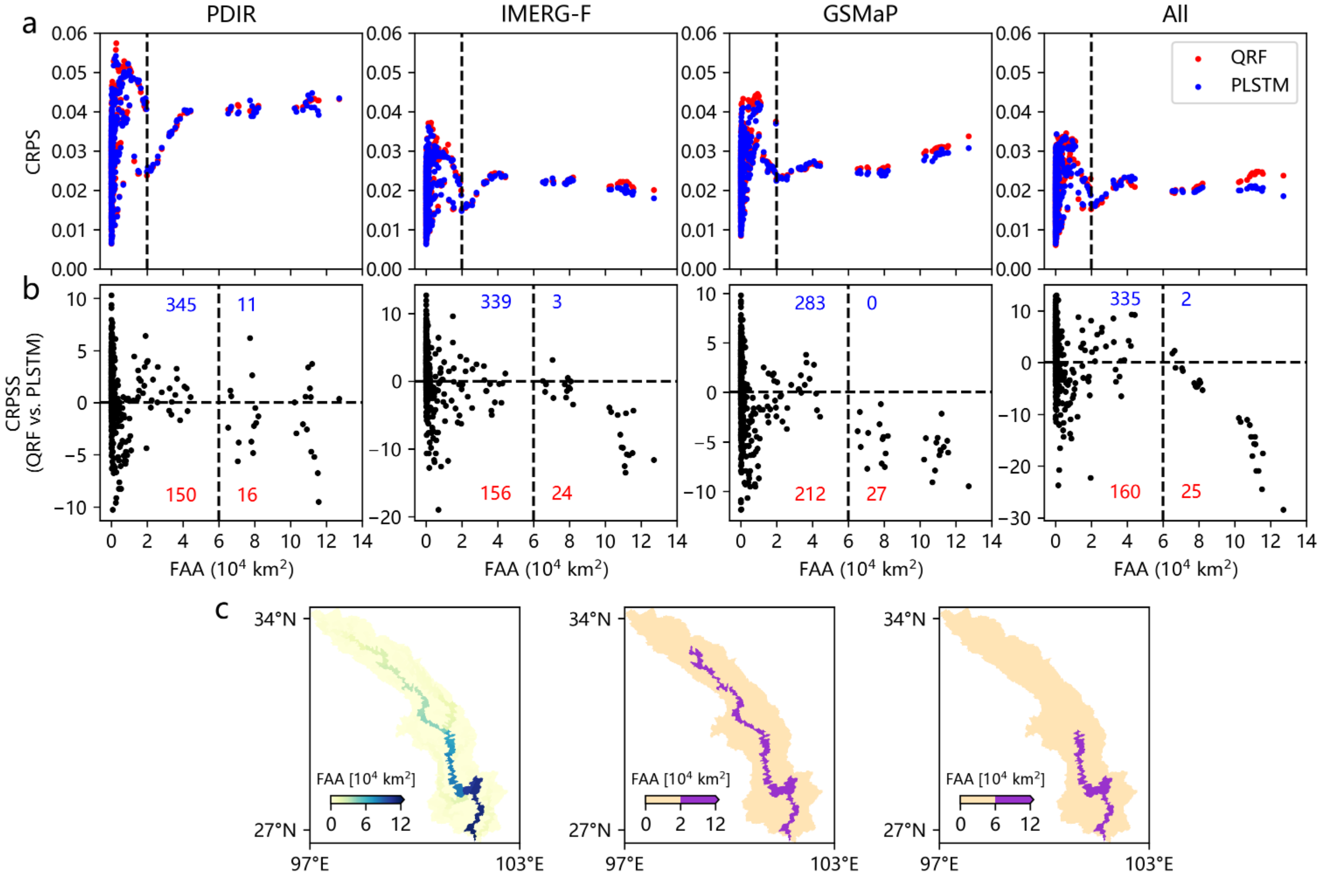
a
PDIR
IMERG-F
GSMaP
All
CRPS
0.06
0.05
0.04
0.03
0.02
0.01
0.00
QRF
PLSTM
b
CRPSS
(QRF vs. PLSTM)
345
11
150
16
339
3
156
24
283
0
212
27
335
2
160
25
10
5
0
−5
−10
−20
−30
0 2 4 6 8 10 12 14
FAA (10^4 km^2)
c
34°N
27°N
97°E
103°E
FAA [10^4 km^2]
0 6 12
0 2 12
0 6 12

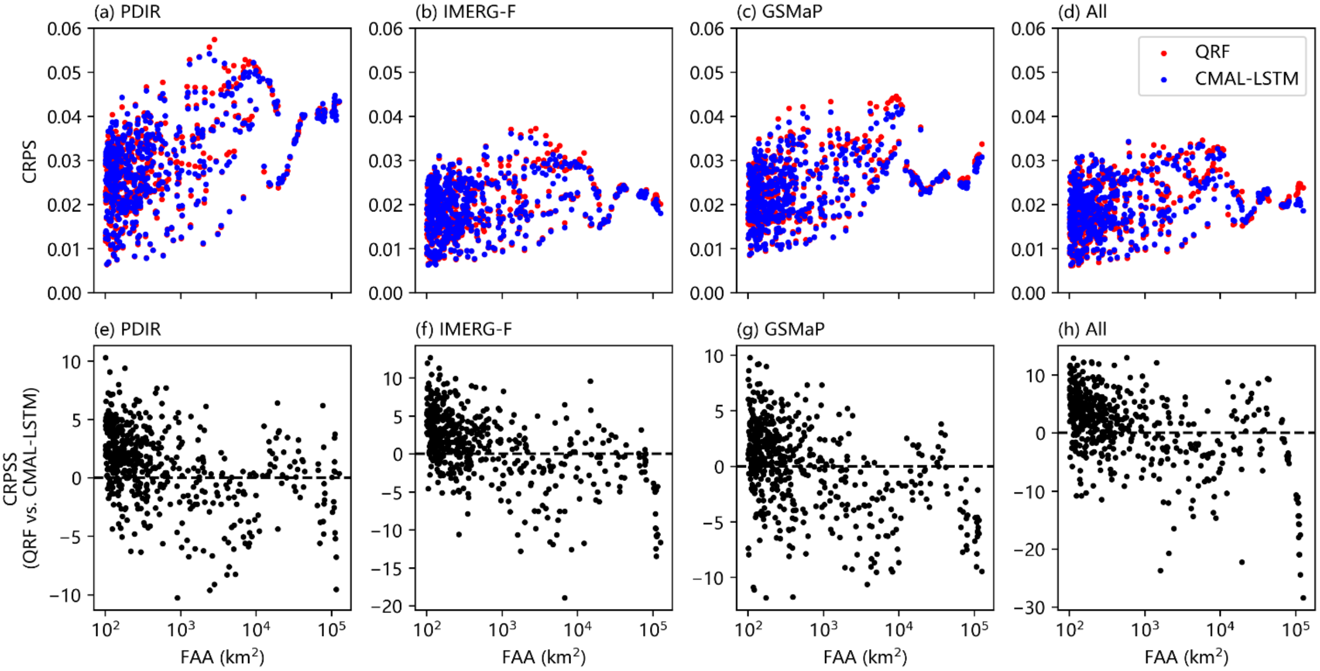

Figure 6. The relationships between (a–d) ~~continuous rank probability score (~~CRPS~~)~~, (e–h~~b~~) ~~CRPS score (~~CRPSS~~)~~ and ~~(c) flow accumulation area (~~FAA~~)~~. ~~The closer the CRPS is to 0, the better the model performs. The CRPSS is greater than 0, indicating that the QRF model is better than the PLSTM model; conversely, the PLSTM model is better than the QRF model. PDIR is a near real-time product; IMERG-F and GSMAP are bias-adjusted products.~~

Table 2. The probabilistic performance of two post-processing models for different FAA intervals. The bold numbers indicate better performance in each group.

FAA (10^4 km)	Number of sub-basins	PDIR		I~~EMRG~~MERG-F		GSMa~~A~~P		ALL	
		QRF	CMAL-LSTM	QRF	CMAL-LSTM	QRF	CMAL-LSTM	QRF	CMAL-LSTM
< 2	476	**331**	145	**332**	144	**273**	203	**320**	156
2–4	15	**11**	4	6	**9**	**9**	6	**11**	4
4–6	4	**3**	1	1	**3**	1	**3**	**4**	0
6–10	13	4	**9**	3	**10**	0	**13**	2	**11**
> 10	14	7	7	0	**14**	0	**14**	0	**14**

~~In addition, there is also a very clear dividing line between the performance of the QRF and LSTM models (Fig. 6b). If we divide this scatter plot into four quadrants, quadrants 1,2 represent the QRF model better than the PLSTM model (blue number), and quadrants 3,4 represent the QRF model worse than the PLSTM model (red number). When the flow accumulation area (FAA) of the sub-basin is less than 60,000 km², the QRF model is a little more dominant than the PLSTM model. But in sub-basins with flow accumulation area (FAA) greater than 60,000 km², the PLSTM model shows overwhelming performance. This feature is most pronounced in the GSMaP-driven streamflow post-processing, followed by multi-model (All), IMERG-F and PDIR.~~

4.2.~~4~~ 3 Reliability ~~diagrams~~and sharpness

~~We further use the~~The reliability diagram is further used to diagnose the difference in post-processing model performance in terms of reliability. To distinguish the differences in model performance ~~between~~ of the ~~PLSTM~~CMAL-LSTM ~~model~~ and ~~the~~ QRF models ~~as the flow accumulation area (FAA)~~with the change of FAAs, ~~we split~~ ~~divide~~ the calculation of the reliability diagram is divided into two parts~~)~~. On part is for ~~the calculation of the reliability diagrams into two parts, one for the~~ FAA less than 60,000 km^2 as shown in ~~(~~Fig. 7a–c~~)~~, which is obtained by combing all the streamflow prediction of 495 sub-basins. The ~~other~~second part is for ~~and one for the~~ FAA greater than 60,000 km^2 as shown in ~~(~~Fig. 7d–f~~8)~~, which is obtained by combing all the streamflow prediction of 27 sub-basins. Overall, when the FAA is less than 60,000 km^2, the performance of the two post-processing models is similar. The QRF model is slightly better than the CMAL-LSTM model. Except for the PDIR experiments, all experiments have a high reliability. As the threshold increases, all experiments show an increasing deviation from the diagonal line and a decrease in reliability. ~~When~~Moreover, when the FAA of sub-basin exceeds 60,000 km^2, the reliability of the post-processing experiments declines and ~~.~~t~~T~~he CMAL-LSTM model performs slightly better than the QRF model, with more points distributed along the diagonal line. As the threshold increases, the curve becomes more oscillatory, resulting in a significant decrease in reliability. Especially under extreme conditions and as is shown in ~~(~~Fig. 7f~~)~~, the difference between the two post-processing models is large, with the CMAL-LSTM performing relatively better.

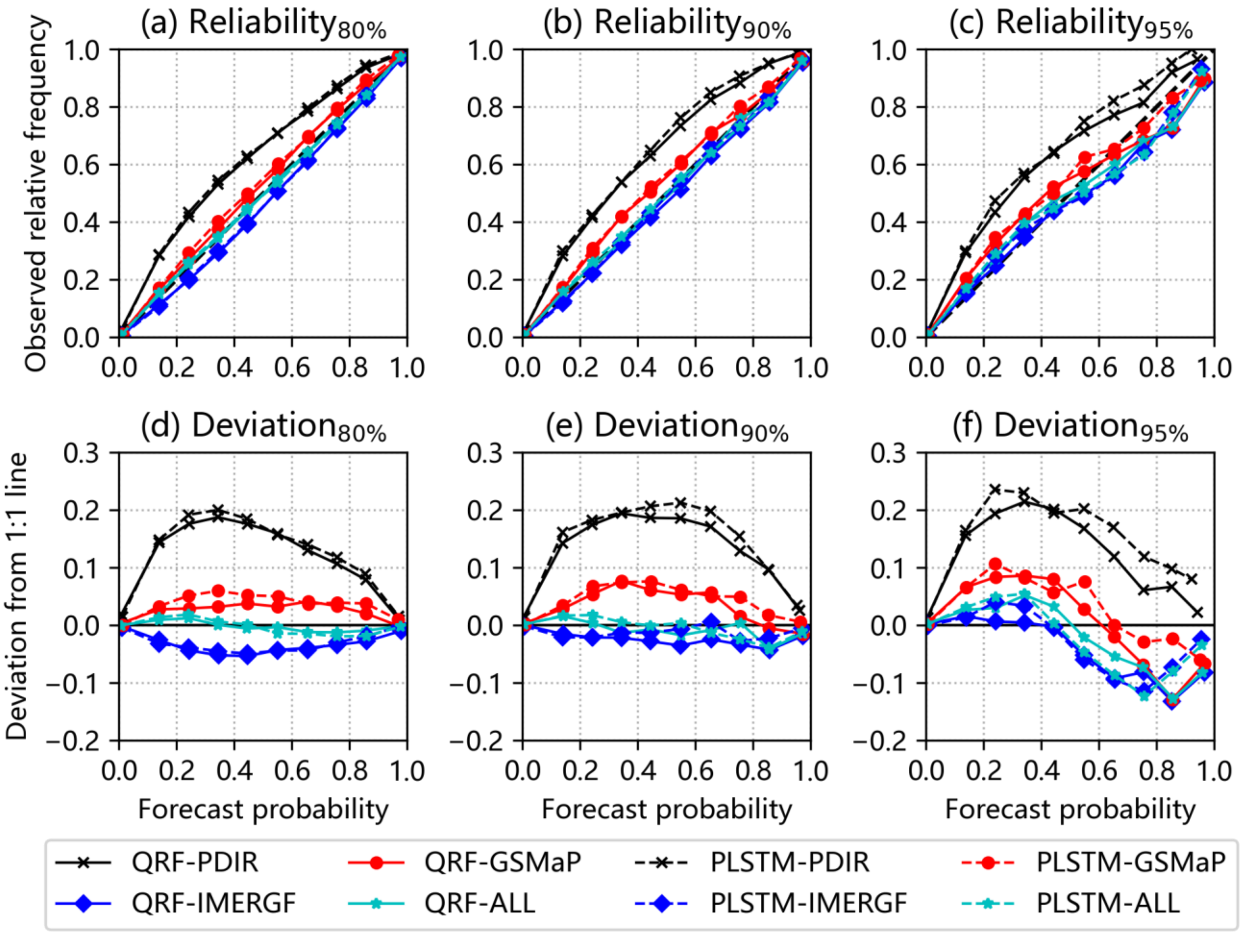
(a) Reliability$_{80\%}$
(b) Reliability$_{90\%}$
(c) Reliability$_{95\%}$
Observed relative frequency
1.0
0.8
0.6
0.4
0.2
0.0
0.0
0.2
0.4
0.6
0.8
1.0
(d) Deviation$_{80\%}$
(e) Deviation$_{90\%}$
(f) Deviation$_{95\%}$
Deviation from 1:1 line
0.3
0.2
0.1
0.0
−0.1
−0.2
Forecast probability
QRF-PDIR
QRF-GSMaP
PLSTM-PDIR
PLSTM-GSMaP
QRF-IMERGF
QRF-ALL
PLSTM-IMERGF
PLSTM-ALL

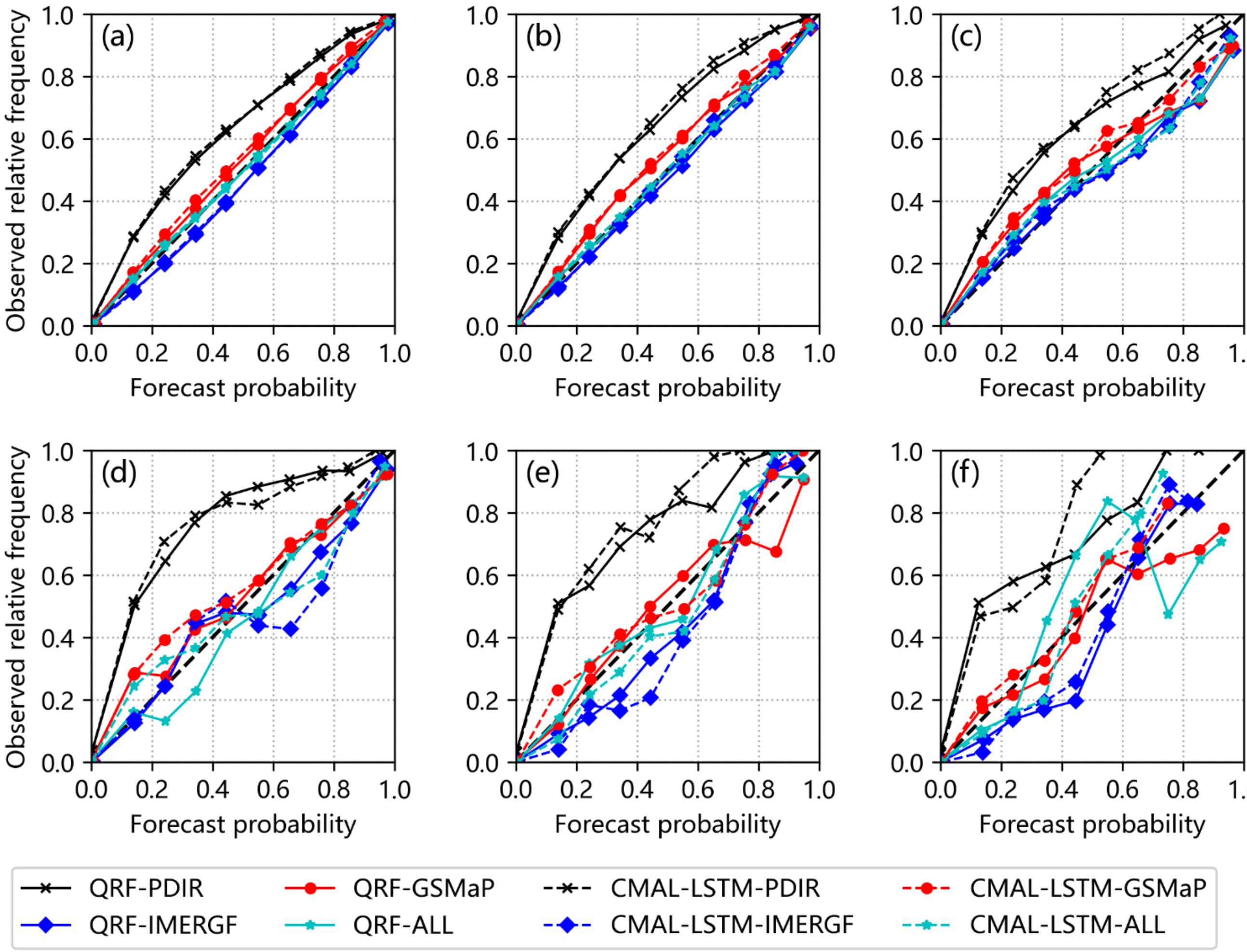

Figure 7. Reliability diagrams. (a) 80%, (b) 90% and (c) 95% ~~quantiles~~percentiles of observations for the sub-basins with FAA less than 60,000 km^2 and (d) 80%, (e) 90% and (f) 95% ~~quantiles~~percentiles of observations for the sub-basins with FAA greater than 60,000 km^2. ~~(a-c) and deviation (d-f) from 1:1 line between different models for sub-basins with flow accumulation area (FAA) less than 60,000 km^2. PDIR is a near real-time product; IMERG-F and GSMAP are bias-adjusted products.~~

~~Figure 7 shows the reliability plots of different models for sub-basins with flow accumulation area (FAA) less than 60,000 km^2 and their deviations from the diagonal (1:1 line). Also, we selected 80%, 90% and 95% quartiles of the observation as the threshold conditions, respectively. And the reliability plots are calculated by combing all streamflow simulations from 495 sub-basins with FAA less than 60,000 km^2. In general, the two post-processing methods perform close to each other. The QRF model (solid line) is slightly better than PLSTM (dashed line), with a relatively smaller deviation from the diagonal (1:1 line). All experiments have high reliability except for the one with PDIR-driven streamflow simulation as input. As the threshold increases, the deviation of all experiments from the diagonal increases and the reliability level decreases. Among the different experiments, IMERG-F is the best. Multi-model (All) is close to IMERG-F but slightly worse. But they both show some degree~~

~~of underestimation. The GSMaP is the second best and the PDIR the worst. The GSMaP and PDIR show some degree of overestimation. These results can also explain the differences in CRPS of different models.~~

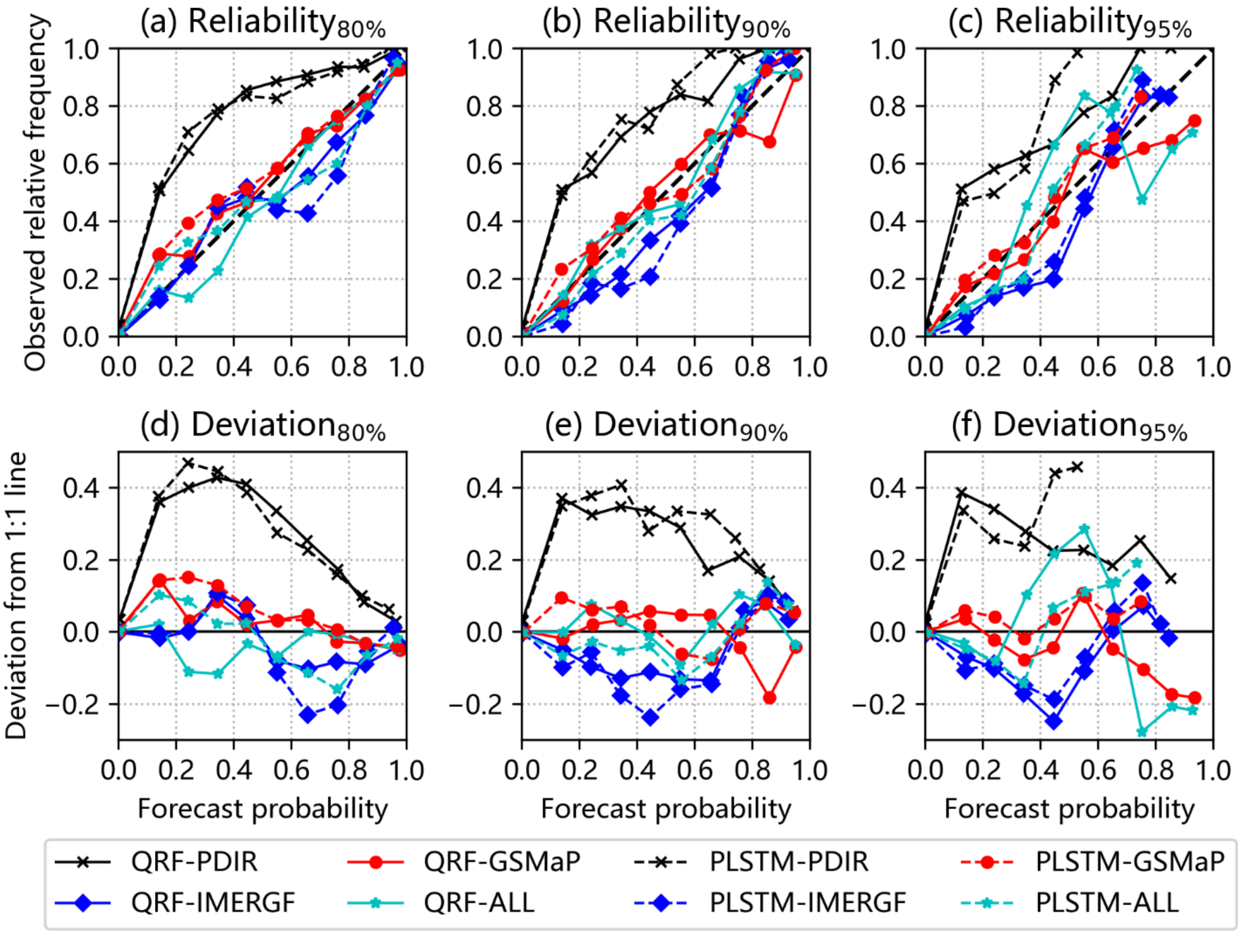

~~Figure 8.~~ ~~Same with Fig. 7, but for sub-basins with flow accumulation area (FAA) larger than 60,000 km^2. PDIR is a near real-time product; IMERG-F and GSMAP are bias-adjusted products.~~

~~Figure 8 shows the reliability plots of different models for sub-basins with flow accumulation area (FAA) larger than 60,000 km^2 and their deviations from the diagonal (1:1 line). Also, we selected 80%, 90% and 95% quartiles of the observation as the threshold conditions, respectively. And the reliability plots are calculated by combing all streamflow simulations from 27 sub-basins with FAA greater than 60,000 km^2. In general, the two post-processing methods show distinguishable differences in this case. The PLSTM (dashed line) is slightly better than QRF (solid line), possessing more points distributed around the diagonal (1:1 line). However, both models exhibit greater uncertainty in this case relative to the FAA of sub-basins smaller than 60,000 km^2 (Fig. 7). As the threshold increases, the deviation of all experiments from the diagonal increases, the curve becomes more oscillatory, and the reliability level is greatly reduced, especially in extreme cases (Fig. 8f, 95% quantile threshold). Similar to Fig. 7, among the different experiments, IMERG-F is still the best and Multi-model (All) is close to~~

~~IMERG-F, but slightly worse. They all show more underestimation. The GSMaP is the second best and PDIR the worst. Except a few points, they show more overestimation.~~

~~4.2.5 Sharpness~~

Sharpness describes the variability properties of predictive distribution and can be used to assess the differences between post-processing models from ~~an~~the uncertainty estimation perspective. To eliminate the influence of different flow regimes, all data are divided into high-flow seasons (May to October) and low-flow seasons (November to April). Sharpness metrics are calculated separately for each sub-basin. The average values of the metrics for ~~the~~all 522 sub-basins are listed in Table 3. The results show that, on average across all 522 sub-basins, the QRF model produces narrower prediction intervals than the CMAL-LSTM model during both high and low--flow seasons, indicating higher sharpness of the QRF model compared to CMAL-LSTM. This partially explains why the QRF model has higher CRPS values in most sub-basins. It is worth noting that the QRF model shows high coverage of the observations as well as narrower prediction intervals during high flow seasons. The average coverage of observations for the 25th to 75th quantiles (CO_{25-75}) is 1.5% higher for the QRF model than for the CMAL-LSTM model. However, the wider prediction interval of the CMAL-LSTM model results in higher coverage of observations during low flow seasons. The average coverage of observations for the 25th to 75th ~~percentiles~~quantiles (CO_{25-75}) is 2% higher for the CMAL-LSTM model than for the QRF model. Interestingly, the 90% prediction intervals obtained by both post-processing methods contain 100% of the observations, based on the average values across 522 sub-basins during both high and low--flow seasons.

~~In order to compare the model performance of PLSTM and QRF more comprehensively, this section further calculates the sharpness metrics for different experiments. The selected sharpness metrics include: mean absolute deviation (MAD), standard deviation (STD), variance (VAR), distance from 25% to 75% quantile (DIS25-75), distance from 5% to 95% quantile (DIS5-95), coverage of observations by 25% to 75% quantile (CO25-75), and coverage of observations by 5% to 95% quantile (CO5-95). In addition, to remove the effect of different flow regimes, all data are divided into a high flow season (May to October) and a low flow season (November to April). Sharpness metrics are calculated separately for each sub-basin. The mean results for all 522 sub-basins are presented in Table 2.~~

Table ~~2~~3. Sharpness metrics. ~~(Mean absolute deviation, MAD; Standard deviation, STD; Variance, VAR; Distance between the 0.25 and 0.75 quantiles, DIS_{25-75}; Distance between the 0.05 and 0.95 quantiles, DIS_{5-95}; Coverage of observations between the 0.25 and 0.75 quantiles, CO_{25-75}; Coverage of observations between the 0.05 and 0.95 quantiles, CO_{5-95}) for different models.~~ The bold numbers indicate better performance in each group.

Flow seasons	Metric	PDIR		~~IEMRG~~IMERG-F		GSMaP		All	
		QRF	~~PLSTM~~CMAL-LSTM	QRF	~~PLSTM~~CMAL-LSTM	QRF	~~PLSTM~~CMAL-LSTM	QRF	~~PLSTM~~CMAL-LSTM
High-flow (May–Oct.)	MAD	**0.046**	0.048	**0.047**	0.052	**0.050**	0.054	**0.045**	0.047
	STD	**0.109**	0.112	**0.133**	0.139	**0.129**	0.133	**0.129**	0.134
	VAR	**0.013**	0.014	**0.020**	0.021	**0.018**	0.019	**0.018**	0.020

	DIS$_{25-75}$	0.0714	**0.0703**	**0.0753**	0.0757	**0.0781**	0.0785	0.0710	**0.0687**
	DIS$_{5-95}$	**0.184**	0.194	**0.192**	0.215	**0.206**	0.223	**0.184**	0.195
	CO$_{25-75}$ (%)	**51.5**	50.1	**76.9**	76.0	**64.2**	62.8	**73.3**	71.4
	CO$_{5-95}$ (%)	100	100	100	100	100	100	100	100
Low-flow (Nov.–Apr.)	MAD	**0.0085**	0.0100	**0.0073**	0.0094	**0.0088**	0.0104	**0.0064**	0.0069
	STD	**0.0264**	0.0284	**0.0280**	0.0301	**0.0305**	0.0323	**0.0258**	0.0262
	VAR	**8.32**	9.48	**9.10**	10.47	**10.40**	11.52	**7.71**	7.86
	DIS$_{25-75}$	**0.0121**	0.0124	**0.0099**	0.0112	**0.0121**	0.0122	0.0086	**0.0086**
	DIS$_{5-95}$	**0.033**	0.039	**0.029**	0.037	**0.036**	0.042	**0.026**	0.027
	CO$_{25-75}$ (%)	72.2	**75.1**	88.8	**90.2**	69.1	**73.9**	**79.6**	79.2
	CO$_{5-95}$ (%)	100	100	100	100	100	100	100	100

~~As can be found in Table 2, the QRF model obtained narrower quantile intervals for both high and low flows in the average of all 522 sub-basins, representing a higher sharpness of the QRF model. It is noteworthy that the QRF model performs both a narrower quantile interval and coverage of observations in the high-flow season. For the coverage of observations from the 25th to the 75th percentile (CO25-75), the QRF model is on average 1.5% higher than the PLSTM. However, the wider quantile interval of PLSTM yields higher coverage of observations in the low-flow season. For the 25% to 75% quantile coverage of observations (CO25-75), the PLSTM is on average 2% higher than the QRF model. Surprisingly, the 5%-95% quantile interval obtained by the two post-processing methods contains 100% of the observations for both high and low flows in the average of all 522 sub-basins.~~

~~4.2.6 Hydrograph and predict interval of two typical sub-basins~~

~~Table 2 shows the average sharpness performance of all sub-basins. In this section, two typical sub-basins are selected as individual examples to explain in detail the performance differences between PLSTM and QRF models. Sub-basin No.10 and No.250 are from quadrant 4 and quadrant 2 of Fig. 6, respectively. The overall performance (CRPS) of the PLSTM model in sub-basin No.10 is better than that of the QRF, but it is worse than the QRF in sub-basin No.250.~~

~~Figure 9 shows the hydrographs and two different quantile intervals for different experiments. Corresponding to Fig. 9, Table 3 shows a statistical summary of the indicators of quantile intervals and their coverage of observations. Similarly, in both cases, the QRF and PLSTM models exhibit smaller prediction uncertainty and present narrower quantile intervals in the low-flow season (Nov. to Apr.). While in the high-flow season (May to Oct.), the prediction uncertainty is larger. Moreover, the narrower uncertainty intervals in the low-flow season yielded higher coverage of observations. The difference is that in sub-basin No.10, the PLSTM model obtains a higher coverage of observations at the expense of some sharpness. It strikes a balance between the prediction interval and the coverage of observations, which results in a higher CRPS. In contrast, the QRF model suffers from systematic errors despite its narrower prediction interval. For example, the systematic underestimation of QRF-IMERG-F in the high-flow season results in lower CRPS relative to PLSTM. For sub-basin No.250 with a smaller flow accumulation area (FAA), its concentration time is short, the flow variation is more fluctuating and complicated, and the observation points are more scattered. Little precipitation events may also cause high pulse flow, which is also the main feature~~

~~of flash flood disasters. Interestingly, in this case, the QRF wraps more observations with a narrower quantile interval, which results in higher CRPS for them.~~

~~**Table 3.** Sharpness metrics (Distance between the 0.25 and 0.75 quantiles, DIS$_{25\text{-}75}$; Distance between the 0.05 and 0.95 quantiles, DIS$_{5\text{-}95}$; Coverage of observations between the 0.25 and 0.75 quantiles, CO$_{25\text{-}75}$; Coverage of observations between the 0.05 and 0.95 quantiles, CO$_{5\text{-}95}$) for different models in two typical sub-basins. The bold numbers indicate better performance in each group.~~

~~ID~~	~~Input~~	~~Model~~	~~High flow seasons (May–Oct.)~~				~~Low flow seasons (Nov.–Apr.)~~			
			~~DIS$_{25\text{-}75}$ (m^3/s)~~	~~DIS$_{5\text{-}95}$ (m^3/s)~~	~~CO$_{25\text{-}75}$ (%)~~	~~CO$_{5\text{-}95}$ (%)~~	~~DIS$_{25\text{-}75}$ (m^3/s)~~	~~DIS$_{5\text{-}95}$ (m^3/s)~~	~~CO$_{25\text{-}75}$ (%)~~	~~CO$_{5\text{-}95}$ (%)~~
~~10~~	~~PDIR~~	~~QRF~~	**~~596.8~~**	**~~1491.5~~**	~~28.8~~	~~60.9~~	**~~113.4~~**	**~~232.6~~**	~~40.0~~	~~76.1~~
		~~PLSTM~~	~~676.4~~	~~1765.9~~	**~~33.0~~**	**~~68.6~~**	~~124.7~~	~~345.1~~	**~~56.4~~**	**~~97.0~~**
	~~IEMRG-F~~	~~QRF~~	**~~634.5~~**	**~~1576.2~~**	~~40.5~~	~~82.7~~	**~~72.6~~**	**~~186.1~~**	~~41.9~~	~~78.5~~
		~~PLSTM~~	~~670.7~~	~~1879.5~~	**~~53.8~~**	**~~92.5~~**	~~139.0~~	~~327.5~~	**~~57.8~~**	**~~94.5~~**
	~~GSMaP~~	~~QRF~~	**~~825.5~~**	**~~1755.8~~**	**~~39.3~~**	~~71.3~~	**~~125.1~~**	**~~275.8~~**	~~41.8~~	~~68.0~~
		~~PLSTM~~	~~762.5~~	~~1921.5~~	~~33.4~~	**~~81.9~~**	~~130.0~~	~~398.4~~	**~~46.3~~**	**~~82.8~~**
	~~All~~	~~QRF~~	**~~669.6~~**	**~~1542.7~~**	~~41.2~~	~~79.2~~	**~~73.4~~**	**~~191.2~~**	~~39.9~~	~~78.5~~
		~~PLSTM~~	~~558.7~~	~~1444.1~~	**~~46.1~~**	**~~83.3~~**	~~84.3~~	~~214.2~~	**~~59.4~~**	**~~84.0~~**
~~250~~	~~PDIR~~	~~QRF~~	~~0.88~~	~~2.53~~	**~~38.32~~**	**~~80.57~~**	**~~0.12~~**	**~~0.43~~**	~~82.21~~	**~~97.24~~**
		~~PLSTM~~	**~~0.73~~**	**~~2.34~~**	~~32.47~~	~~75.68~~	~~0.14~~	~~0.50~~	**~~86.76~~**	~~96.28~~
	~~IEMRG-F~~	~~QRF~~	**~~1.20~~**	**~~3.13~~**	**~~65.08~~**	**~~94.84~~**	~~0.10~~	**~~0.35~~**	**~~82.21~~**	~~93.93~~
		~~PLSTM~~	~~1.24~~	~~3.71~~	~~62.77~~	~~94.29~~	**~~0.09~~**	~~0.48~~	~~79.86~~	**~~94.07~~**
	~~GSMaP~~	~~QRF~~	**~~1.20~~**	**~~3.12~~**	~~57.07~~	**~~92.93~~**	**~~0.13~~**	**~~0.47~~**	~~79.86~~	**~~98.62~~**
		~~PLSTM~~	~~1.26~~	~~3.35~~	**~~58.29~~**	~~92.26~~	~~0.13~~	~~0.49~~	**~~85.38~~**	~~97.79~~
	~~All~~	~~QRF~~	~~1.11~~	**~~2.88~~**	**~~60.87~~**	**~~93.89~~**	~~0.09~~	**~~0.33~~**	~~80.14~~	~~97.38~~
		~~PLSTM~~	**~~1.00~~**	~~3.22~~	~~55.30~~	~~92.53~~	**~~0.08~~**	~~0.42~~	**~~81.52~~**	**~~97.93~~**

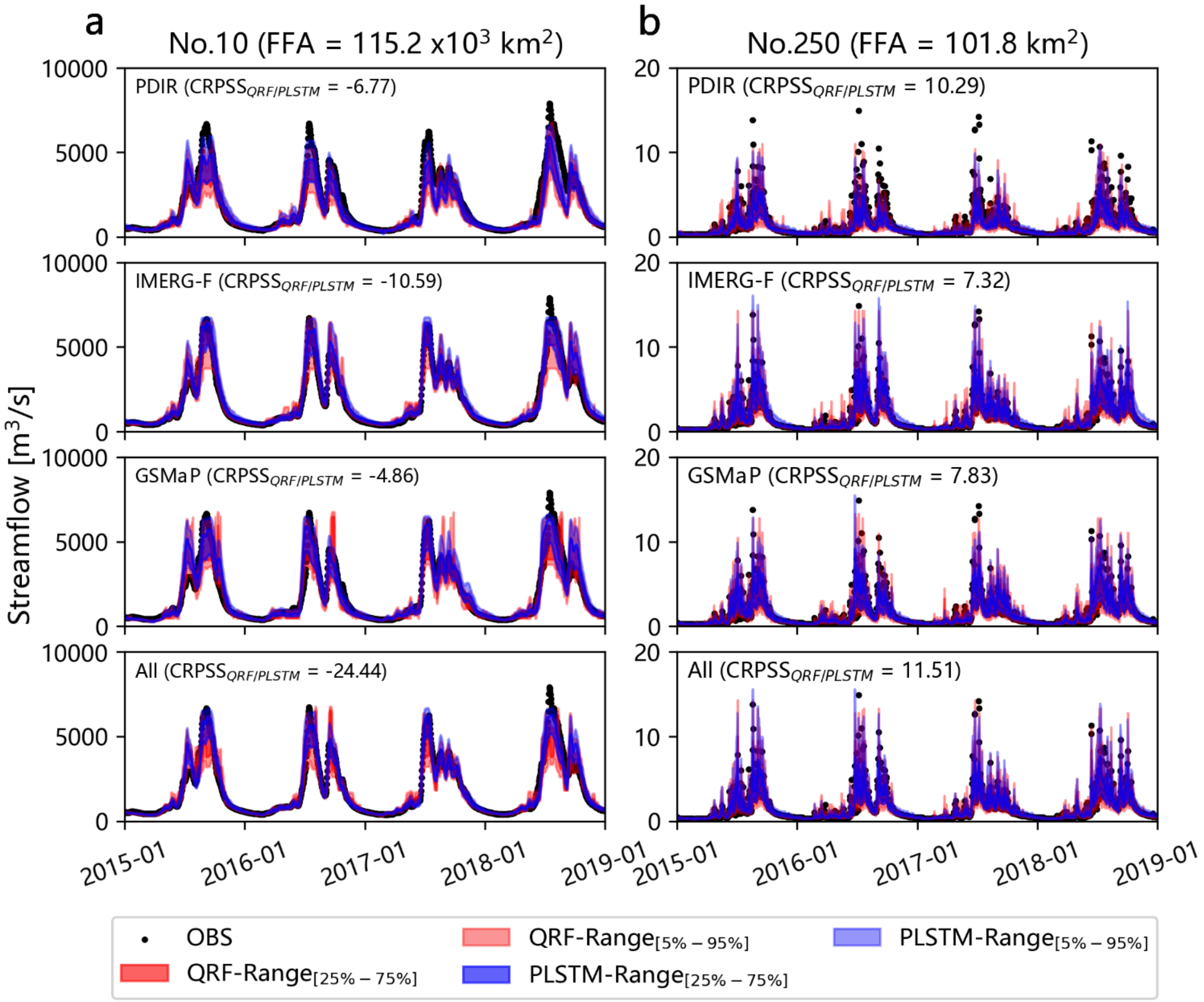

~~**Figure 9.** Hydrographs and prediction intervals for two typical sub-basins. The CRPSS is greater than 0, indicating that the QRF model is better than the PLSTM model; conversely, the PLSTM model is better than the QRF model. OBS in figure indicates streamflow reference. PDIR is a near real-time product; IMERG-F and GSMAP are bias-adjusted products.~~

4.3 Deterministic (single-point) assessment

Although the post-processing model proposed in this study is probabilistic, decision-makers tend to prefer deterministic (single-point) prediction. Therefore, ~~we utilize~~ the average of the probability members ~~are~~is utilized ~~–~~as deterministic predictions to further compare the prediction accuracy of the models. Also, it can be viewed as a p~~P~~ost hoc model examination.

4.3.1 Overall model performance

Figure ~~10~~ 8 shows the ~~model~~ performance evaluation of the streamflow simulations before (RAW) and after post-processing ~~(RAW), and after~~using the QRF and ~~PLSTM~~CMAL-LSTM ~~post-processing~~models for ~~the~~ 522 sub-basins. ~~The metrics shown here include Pearson correlation coefficients (PCC), relative bias (RB), and Nash efficiency coefficients (NSE). Each sub-basin is calculated separately.~~PCC, RB and NSE are used as performance metrics, with each sub-basin being evaluated separately. T~~Also, t~~he ~~means and~~ median~~s~~ and mean of each metric across all 522 sub-basins ~~are~~ are computed and reported ~~displayed~~ in the first three columns ~~(metric) in~~of Table 4. ~~It can be seen~~The results indicate that both post-processing models significantly improved the simulation performance over the uncorrected streamflow. However, the CMAL-LSTM model consistently outperforms the QRF model across the precipitation products and the sub-basins.~~QRF and PLSTM are better than RAW, indicating the value of the proposed two post-processing models (Fig.10). For two post-processing models, PLSTM performs better than the QRF model across the board.~~

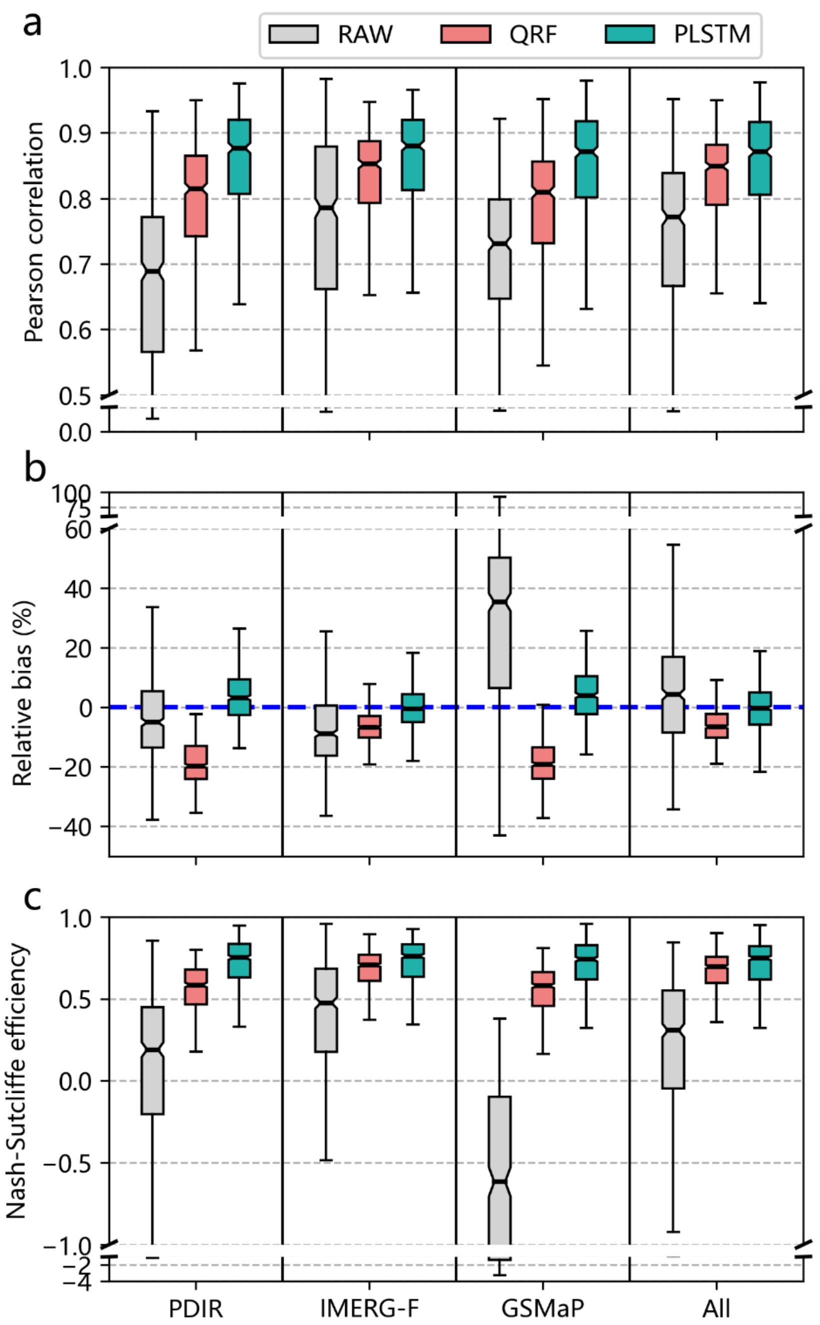
a
RAW
QRF
PLSTM
Pearson correlation
1.0
0.9
0.8
0.7
0.6
0.5
0.0
b
Relative bias (%)
100
75
60
40
20
0
−20
−40
c
Nash-Sutcliffe efficiency
1.0
0.5
0.0
−0.5
−1.0
−2
−4
PDIR
IMERG-F
GSMaP
All

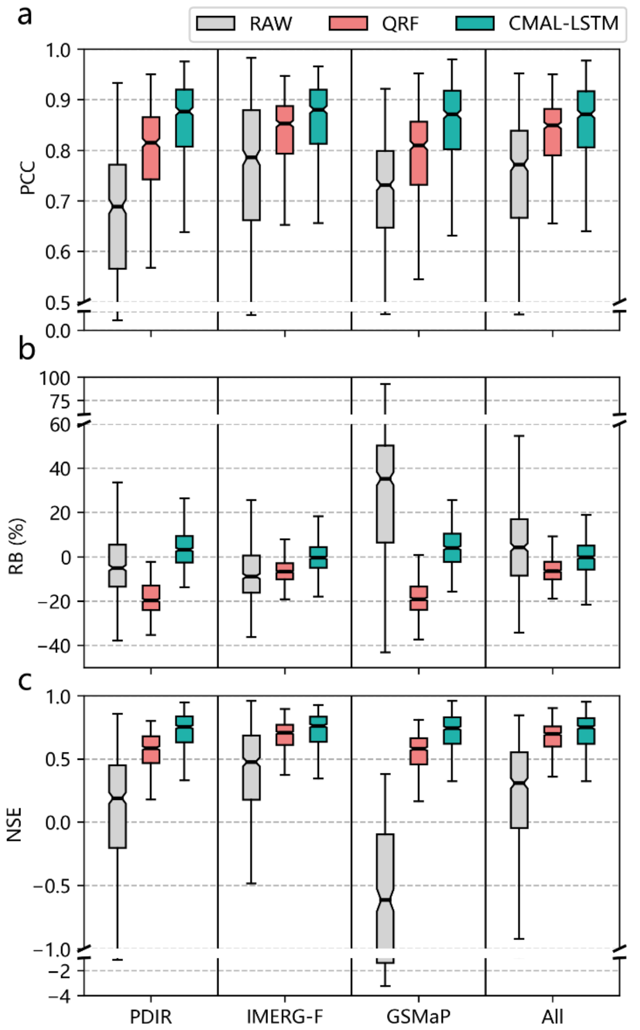

Figure 8~~10~~. Boxplots of different model performance in 522 sub-basins. (a) ~~Pearson correlation coefficient (~~PCC~~)~~; (b) ~~Relative bias (~~RB~~)~~; and (c) ~~Nash-Sutcliffe efficiency (~~NSE~~)~~. ~~The closer the NSE (PCC) is to 1, the better the model performs. The closer RB is to 0, the better the model performs. Note: PDIR is a near real-time product; IMERG-F and GSMAP are bias-adjusted products.~~

~~4.3.2 Spatial distribution of model performance~~

Figure ~~11~~ 9 illustrates ~~shows~~ the spatial characteristics of the ~~Nash-Sutcliffe efficiency (~~NSE~~)~~ improvement ~~for~~ in streamflow simulations~~s~~ obtained through ~~by~~ model comparison. Compared to the raw simulations (RAW), both QRF and ~~PLSTM~~CMAL-LSTM models exhibit significant improvements ~~show large enhancements~~ in almost all sub-basins. Among all ~~precipitation-driven streamflow~~ post-processing experiments, ~~PLSTM~~ GSMaP-CMAL-LSTM and ~~QRF~~ GSMaP-QRF provide the most significant improvement in accuracy due to the poorer performance of the raw GSMaP-driven streamflow simulations. Conversely~~On the contrary~~, the absolute NSE improvement brought by post-processing models are relatively small for the IMERG-F-driven streamflow simulations, and even a slight performance decline in 14.8% of sub-basins is observed in the IMERG-F-QRF experiment (Fig 9b). ~~bring a smaller improvement in NSE values due to the better performance of the raw IMERG-F-driven streamflow simulations. Even, there is a slight regression in model performance in some sporadic sub-basins.~~ Compared to ~~PLSTM~~CMAL-LSTM, the QRF model does not show its advantage of deterministic (single-point) estimation ~~and is inferior to the PLSTM model~~ in almost all sub-basins. The maximum ~~largest~~ difference in model performance appears ~~occurs~~ in GSMaP experiments, followed by PDIR, IMERG-F and multi-~~model~~ product (All) experiments~~(All)~~. This indicates that the deterministic (single-point) estimation ability ~~capability~~ of the QRF model differs significantly ~~more~~ from the ~~PLSTM~~CMAL-LSTM model for streamflow with poor raw simulation.

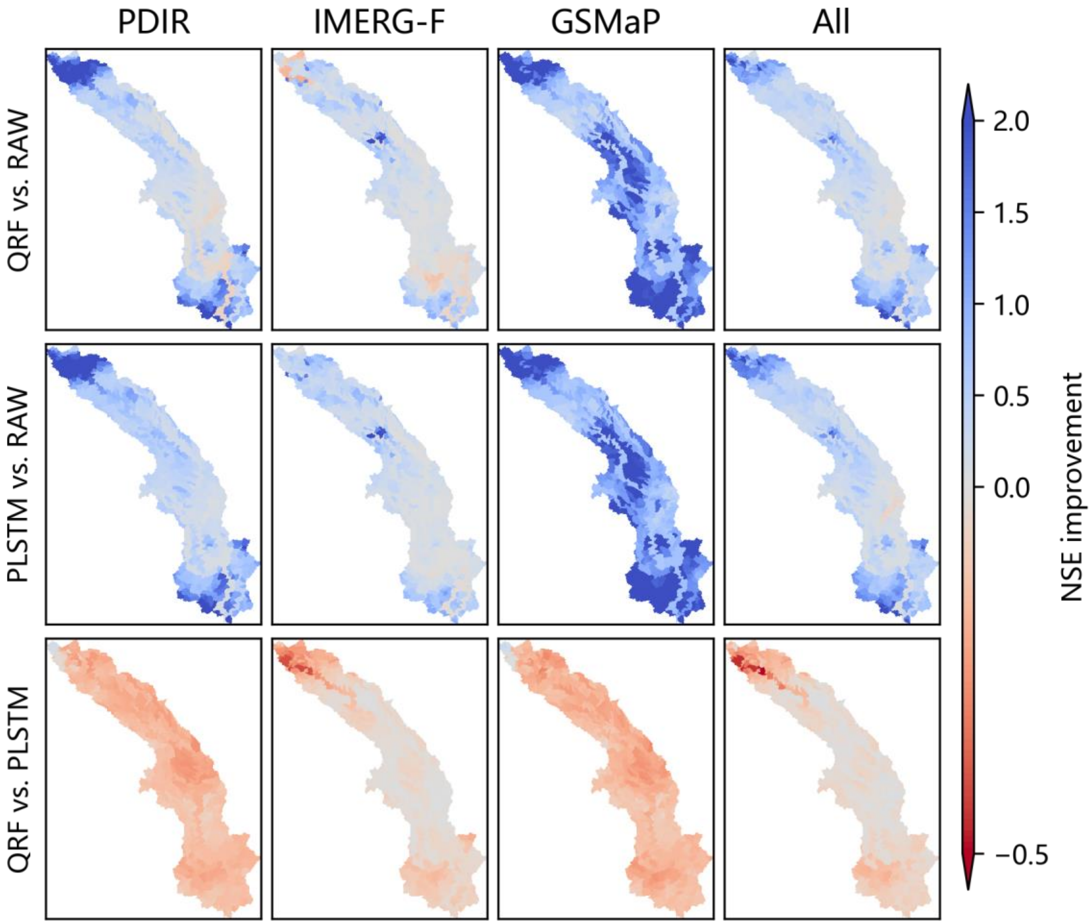
PDIR
IMERG-F
GSMaP
All
QRF vs. RAW
PLSTM vs. RAW
QRF vs. PLSTM
2.0
1.5
1.0
0.5
0.0
−0.5
NSE improvement

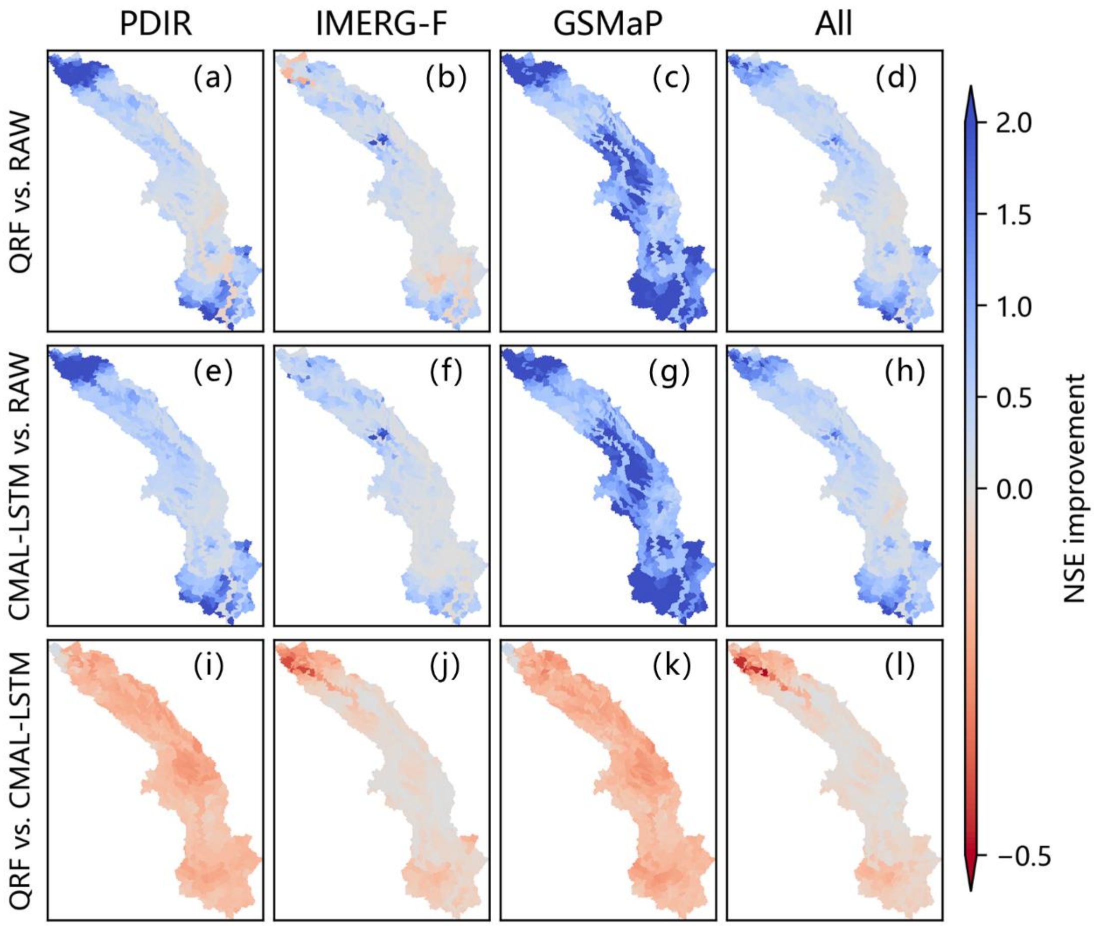

Figure 9~~11~~. ~~Individual sub-basin~~The spatial distribution of ~~Nash-Sutcliffe efficiency (~~NSE~~)~~ improvement $(NSE_{PP} - NSE_{raw})$ between (a–d) QRF and RAW, (e–h~~b~~) ~~PLSTM~~CMAL-LSTM and RAW and (~~e~~i–l) QRF and ~~PLSTM~~CMAL-LSTM in 522 sub-basins. ~~Blue indicates sub-basins where the former model is better than the latter one, and red indicates sub-basins where the former model is worse than the latter one. The darker the color, the greater the difference. is a near real-time product; IMERG-F and GSMAP are bias-adjusted products.~~

4.3.~~3~~ 2 ~~Model difference between FFAs~~The relationship between model performance and flow accumulation area

Based on the spatial distribution shown in Fig.9, ~~we further investigate~~ the relationship between model performance and the flow accumulation area (FAA) of the sub-basin is further investigated, following a similar analysis approach as in Sect. 4.2.2 and Fig. 6. The findings, presented in Fig. 10, show that the performance of the model improves as the FAA of sub-basin increases. Moreover, the CMAL-LSTM model outperforms the QRF model in all experiments (see statistics in Table S2). However, as the FAA of sub-basin increase, the gap between the CMAL-LSTM model and QRF model narrows to some extent. This trend is particularly evident the IMERG-F~~f~~ driven experiment. Nonetheless, in experiments such as PDIR, GSMaP and multi-product (All), and the increase in FAA has little effect on the difference between the CMAL-LSTM and QRF models.

This suggests that highly biased information from raw streamflow simulation has a greater impact on the QRF than on the CMAL-LSTM model.

~~Similar to the analysis route in Fig. 6, based on the spatial distribution (Fig. 11), we further explore the relationship between the model performance and the flow accumulation area (FAA) of the sub-basin, and the results are shown in Fig. 12. As the flow accumulation area (FAA) of the sub-basin increases, the model performance also improves. From Fig. 12a, the same conclusion as Fig. 11 can be drawn, PLSTM is better than QRF. Especially when the flow accumulation area (FAA) of the sub-basin is more than 20,000 km^2. The blue points (PLSTM) are distributed on top of the red points (QRF), and the red points are distributed on top of the black points (RAW). It can be seen from Fig. 12b that 20,000 km^2 is also a threshold condition. When the flow accumulation area (FAA) of the sub-basin is larger than the threshold, the gap between PLSTM and QRF is narrowing as the FAA increases. This is most evident in IMERG-F-driven experiments. But for GSMaP, the increase of FAA has little effect on the gap between PLSTM and QRF. This suggests that highly biased information from raw streamflow simulation has a greater impact on the QRF than on the PLSTM model.~~

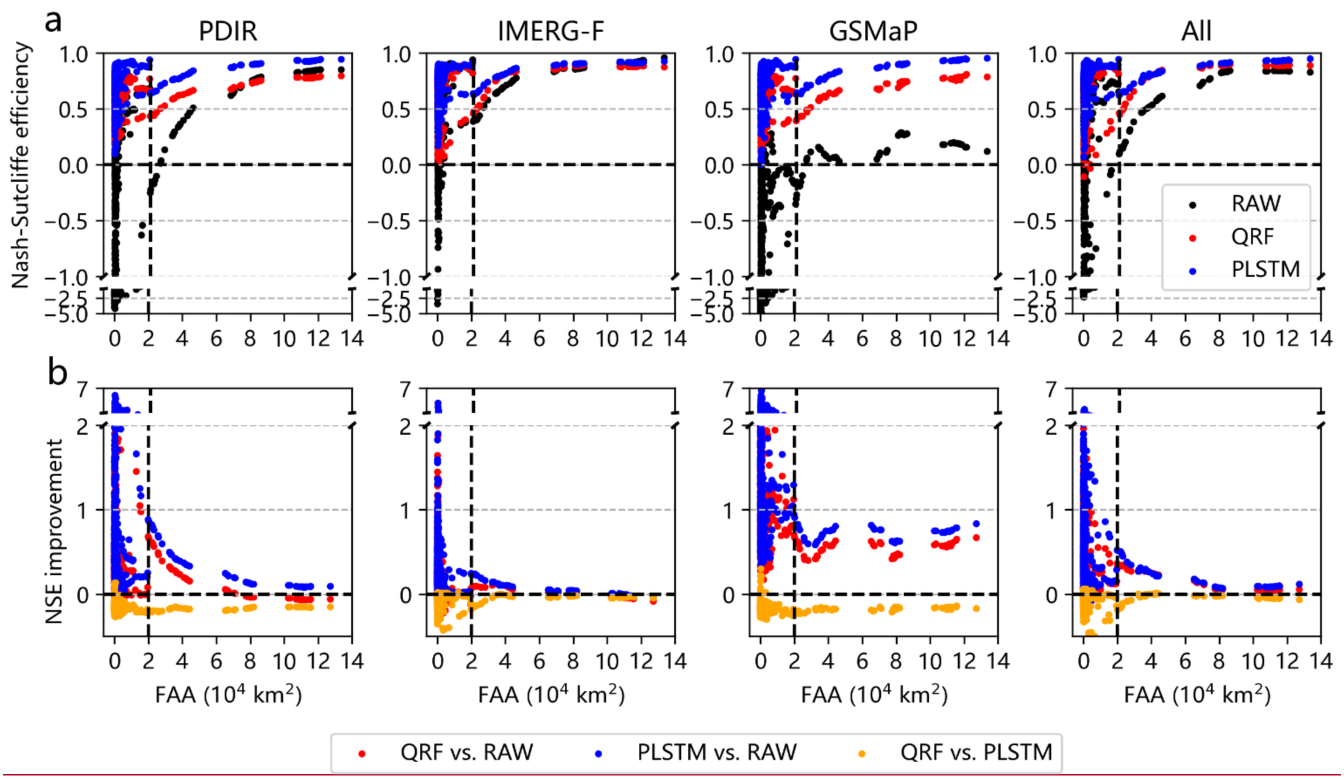
a
b
PDIR
IMERG-F
GSMaP
All
Nash-Sutcliffe efficiency
1.0
0.5
0.0
−0.5
−1.0
−2.5
−5.0
0 2 4 6 8 10 12 14
RAW
QRF
PLSTM
NSE improvement
7
2
1
0
FAA (10^4 km^2)
QRF vs. RAW
PLSTM vs. RAW
QRF vs. PLSTM

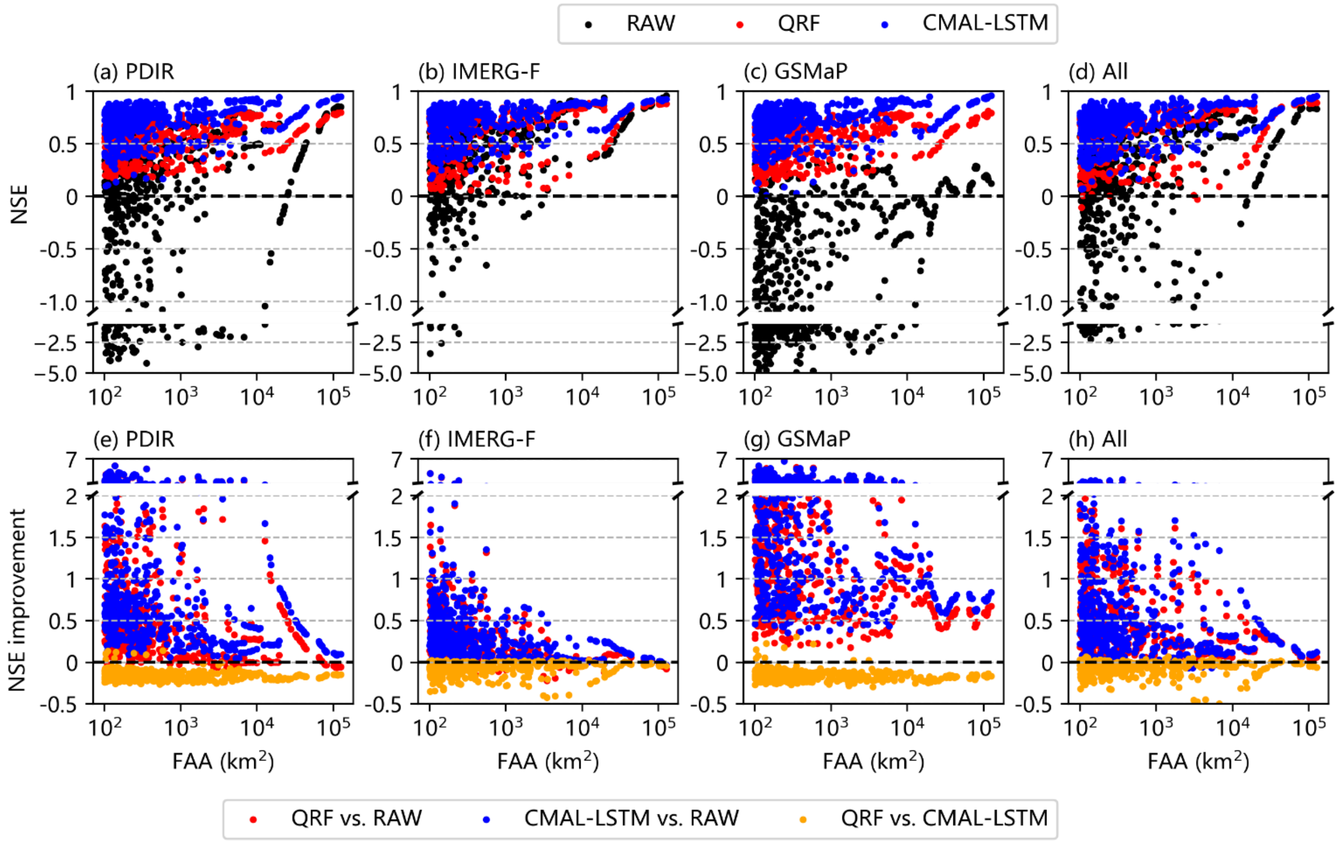

Figure ~~12~~10. The relationships between (a–d) ~~Nash-Sutcliffe efficiency (~~NSE~~)~~, (b–h) NSE improvement ($NSE_{PP} - NSE_{raw}$) and ~~flow accumulation area (~~FAA~~)~~. ~~The closer the NSE is to 1, the better the model performs. The NSE improvement larger than 0 indicates the former model is better than the latter one, conversely, the former model is worse than the latter one. PDIR is a near real-time product; IMERG-F and GSMAP are bias-adjusted products.~~

4.3.~~4~~ 3 High-flow, low-flow, and peak timing

Table 4 summarizes the means and medians of integrated metrics and flow regime indicators ~~of different models in~~ for the 522 sub-basins in different experiments. The first three columns of the table are the same as the metrics used in Fig. ~~10~~8. ~~Pearson correlation coefficient (~~PCC ~~)~~ and ~~Relative bias (~~RB~~)~~ ~~can also be regarded as~~are the components of Nash-Sutcliffe efficiency (NSE). In order to guarantee the consensus ~~robustness~~ of the results, ~~we also calculated~~ another integrated indicator KGE is also calculated. The KGE ~~performed~~ performs identical to~~ly to~~ NSE, confirming the superiority of the ~~PLSTM~~CMAL-LSTM model. The last four columns of the table are flow-related indicators. Overall, the CMAL-LSTM model remains the best, except for the low-flow bias (FLV), where the QRF model is more effective. However, as indicated by the high-flow bias (FHV), both post-processing models have limitations in handling flood peaks. Regardless of the precipitation product used to drive the streamflow simulations, the bias of the flood peak changes from an overestimation (RAW) to an underestimation (p~~P~~ost-processing). In addition, there is a certain degree of deviation in the simulations of peak time. Flood peaks have always posed a challenging problem in hydrological simulation, which highlights the necessity of probabilistic post-processing.

Table 4. Summary of integrated metrics and flow regime indicators of different models in 522 sub-basins. The bold numbers indicate better performance in each group.

Input	Aggregation	Model	Metric							
			PCC	RB	NSE	KGE	FHV	FMS	FLV	PT
PDIR	Mean	RAW	0.656	**-0.02**	-0.1	0.521	33.11	-5.3	-17.3	1.68
		QRF	0.785	-0.19	0.558	0.621	-43.4	-9.85	**3.143**	1.441
		~~PLSTM~~CMAL-LSTM	**0.851**	0.032	**0.712**	**0.755**	**-28.8**	**1.201**	15.24	**1.328**
	Median	RAW	0.689	-0.05	0.19	0.572	**24.77**	-7.63	-12.5	1.692
		QRF	0.815	-0.2	0.584	0.645	-44.6	-10.5	**9.833**	1.417
		~~PLSTM~~CMAL-LSTM	**0.877**	**0.032**	**0.752**	**0.778**	-29.6	**0.978**	19.13	**1.273**
IMERG-F	Mean	RAW	0.759	-0.06	0.389	0.664	**10.92**	-4.04	-14.3	1.459
		QRF	0.808	-0.06	0.648	0.718	-35.3	4.268	**-4.29**	1.394
		~~PLSTM~~CMAL-LSTM	**0.852**	**-0.01**	**0.715**	**0.765**	-30.4	**2.409**	-5.05	**1.282**
	Median	RAW	0.785	-0.09	0.475	0.672	**9.555**	-6.35	-4.14	1.417
		QRF	0.852	-0.07	0.706	0.739	-37.6	**2.068**	5.878	1.333
		~~PLSTM~~CMAL-LSTM	**0.88**	**-0.01**	**0.761**	**0.788**	-32.1	2.159	**2.467**	**1.231**
GSMaP	Mean	RAW	0.687	0.286	-0.92	0.308	88.82	8.465	-45.1	1.519
		QRF	0.778	-0.19	0.545	0.61	-45.4	-11.2	**15.94**	1.703
		~~PLSTM~~CMAL-LSTM	**0.848**	**0.043**	**0.703**	**0.741**	**-31.2**	**0.708**	23.71	**1.44**
	Median	RAW	0.731	0.352	-0.62	0.393	82.86	12.08	-34.1	1.5
		QRF	0.809	-0.19	0.579	0.633	-48	-11.1	**23.73**	1.696
		~~PLSTM~~CMAL-LSTM	**0.871**	**0.04**	**0.742**	**0.762**	**-32.3**	**1.037**	26.36	**1.417**
All	Mean	RAW	0.733	0.059	0.154	0.603	34.38	**2.332**	-15.5	1.456
		QRF	0.803	-0.06	0.637	0.704	-38.8	3.494	**8.635**	1.532
		~~PLSTM~~CMAL-LSTM	**0.846**	**-0.01**	**0.703**	**0.76**	**-32.3**	4.855	10.27	**1.44**
	Median	RAW	0.771	0.042	0.306	0.664	**30.53**	2.228	**-4.74**	1.417
		QRF	0.849	-0.07	0.695	0.727	-42.3	**1.317**	14.96	1.542
		~~PLSTM~~CMAL-LSTM	**0.871**	**-0.003**	**0.749**	**0.781**	-33.8	4.436	13.83	**1.417**

~~The last four columns are flow-related indicators. Overall, the PLSTM model is still the best, except for the low-flow bias (FLV). The QRF model is the best model for simulating low flow. Nonetheless, as can be seen from the high-flow bias (FHV), both the two post-processing models are limited in their ability to handle flood peaks. Regardless of the streamflow simulations driven by either precipitation product, the bias of the flood peak changes from an overestimation (RAW) to an underestimation (Post-processing). In addition, there is a certain degree of deviation in the simulations of peak time. Flood peaks have always been a challenging problem in hydrological simulation, which also confirms the necessity of probabilistic post-processing.~~

~~4.3.5 Hydrograph of two typical sub-basins~~

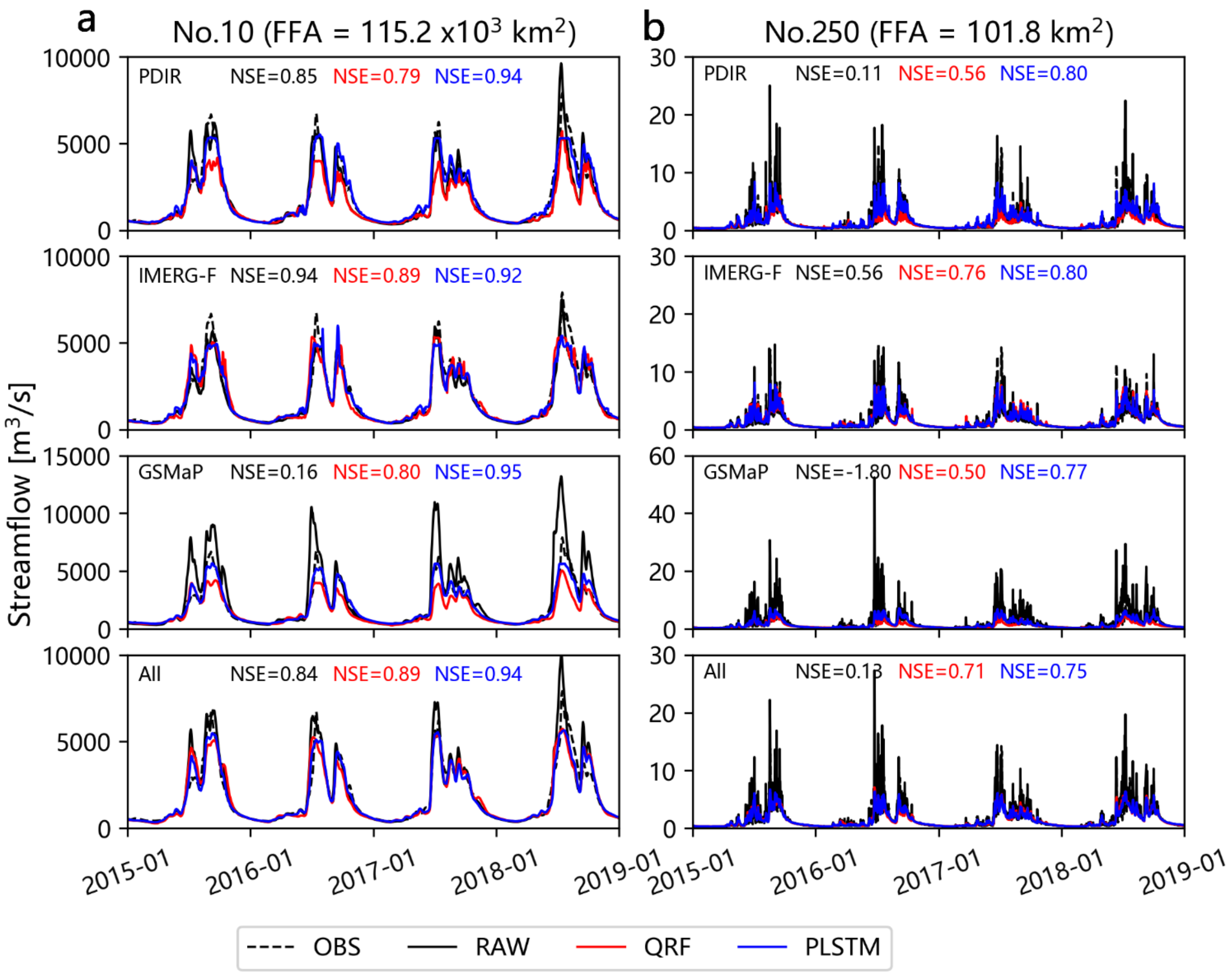

~~**Figure 13.** Hydrographs simulated by different models for two typical sub-basins. OBS in figure indicates the streamflow reference. PDIR is a near real-time product; IMERG-F and GSMAP are bias-adjusted products.~~

~~Same as Fig. 9, we still selected the same two typical sub-basins to compare the deterministic post-processing ability of different models (Fig. 13). For the uncorrected runoff simulations (RAW), except for the performance of the IMERG-F product in sub-basin No.10, the other precipitation-driven simulations present overestimation in both sub-basins, which also contributed to the poor NSE values. After QRF and PLSTM post-processing, the streamflow simulation performance is significantly improved. But it also causes an underestimation of the flood peak. Compared with PLSTM, the QRF model underestimates the flood peak more severely. This is also the main reason why the QRF model is inferior to the PLSTM model. It is also consistent with the high flow simulation bias in Table 4.~~

5 Discussion

5.1 Model comparison ~~in this study~~

Previous studies have demonstrated that the quantile regression forests (QRF) approach outperforms other quantile-based models, such as quantile regression and quantile neural networks (Taillardat et al., 2016; Tyralis et al., 2019; Tyralis and Papacharalampous, 2021). Additionally, recent research has indicated the effectiveness of mixture density networks based on the countable mixtures of asymmetric Laplacians models and long short-term memory networks (CMAL-LSTM) for hydrological probabilistic modelling (Klotz et al., 2022). In terms of reliability and sharpness evaluation for probabilistic prediction, CMAL-LSTM has been proven to achieve~~d~~ the best results compared to other models such as LSTM coupled with Gaussian mixture models, uncountable mixtures of asymmetric Laplacians models, and Monte Carlo dropout. These findings suggest that currently, QRF and CMAL-LSTM may be the most effective machine learning and deep learning model for hydrological probabilistic modelling. In this study, we conducted a comprehensive evaluation of the performance of these two advanced data-driven models in the context of streamflow probabilistic post-processing.

Our findings suggest that the QRF model outperformed the CMAL-LSTM model in terms of probability prediction in most sub-basins. And the performance difference between the two models was found to be associated with the catchment area of the sub-basins. The QRF model was superior in sub-basins with smaller catchment area, while the CMAL-LSTM model demonstrated better performance in larger sub-basins. However, when evaluated from a deterministic standpoint, the CMAL-LSTM model achieved higher NSE scores than the QRF model across nearly all sub-basins. The authors~~We~~ believe that the primary reason for the disparity in model performance is due to the differences in their respective model structure. As illustrated in Fig 2, the QRF model and the CMAL-LSTM model have dissimilar probabilistic procedure.

First, the QRF model and the CMAL-LSTM model differ in their treatment of input features. Specifically, the QRF model utilizes time embedding to flatten time-series features as input for the model. In contrast, the CMAL-LSTM model is capable of better learning the temporal autocorrelation of input features due to the inherent time-series learning capabilities of LSTM. As a result, the CMAL-LSTM model is more responsive to the autocorrelation of uncorrected streamflow features compared to the QRF model. The results depicted in Fig. S6 in the supplement provide evidence to support the interpretation that the performance difference between the QRF model and the CMAL-LSTM model is related to the autocorrelation of input features. The CMAL-LSTM model performs better in the sub-basin No. 250, where streamflow feature autocorrelations are more ~~skillful~~skillful, than in sub-basin No. 10, where streamflow feature autocorrelation skills are lacking.

Second, the QRF model and CMAL-LSTM differ in how they generate probabilistic members. The QRF model calculates the final probabilistic members by grouping them based on a predetermined number of quantiles (100 in this study). In contrast, the CMAL-LSTM model first specifies the form of the probabilistic distribution, then learns the parameters of the distribution using neural networks, and finally obtains the final probabilistic members by sampling. The QRF model produces an approximate and implicit probabilistic distribution, while the CMAL-LSTM model produces an accurate and explicit probabilistic distribution. Moreover, the predicted distribution from the CMAL-LSTM model using the mixture density function is more flexible. As a result, the QRF model produces narrower prediction intervals compared to the CMAL-LSTM model as is reported in ~~(~~Table 3~~)~~. This is especially true when the sub-basin catchment area is smaller, and the streamflow amplitude is lower. This also explains ~~why~~the reason that the QRF model has higher sharpness in these cases compared to the CMAL-LSTM model. Figure. S7 presents the hydrograph and prediction intervals in two randomly selected sub-basins as an example. In sub-basin No.10, the CMAL-LSTM model achieves a balance between the width of the prediction interval and the observation coverage, which is more important for high-flow predictions and also explains why the CMAL-LSTM model has a higher CRPS value in the sub-basin with larger catchment area. In contrast, although the prediction interval of the QRF model is narrower, it is affected by systematic bias. For example, IMERG-F-QRF underestimates the peak flow in the high-flow season, leading to its smaller CRPS value compared to the CMAL-LSTM model. For sub-basin No.250 with a smaller catchment area, its rainfall-runoff response is faster, and the fluctuation of streamflow is greater. Localized precipitation events can also cause large pulse flow, which is the main feature of flash floods. Therefore, there are relatively more extreme samples. In this case, the QRF model learns and captures more observations with narrower prediction intervals, resulting in a better CRPS value.

Third, the QRF model and CMAL-LSTM model differ in their inference process. The QRF model utilizes a decision tree model as its base learner, which is a classification algorithm based on historical searches. ~~In contrast~~Whereas, the CMAL-LSTM model uses a neural network with LSTM layer as its base learner, which is a more powerful fitting model. Due to the differences in model structure, the two models have different abilities to handle extreme events. When extreme event samples are limited, the QRF model tends to underestimate predictions due to its historical search-based approach. On the other hand, the CMAL-LSTM uses the mixture density function for extrapolation. However, both post-processing models still underestimates streamflow extreme events. The QRF model exhibits a higher degree of underestimation in sub-basins with larger catchment areas, resulting in unsatisfactory performance compared to the CMAL-LSTM model in these regions. These discrepancies also lead to lower NSE scores for the QRF model across all sub-basins, as the squared term in the NSE metric increases the sensitivity to high-flow processes which is reported in ~~(~~Fig. S8 in the supplement~~)~~.

Furthermore, besides examining the differences in model performance, we ~~conducted an investigation into~~investigated the effects of different input features on the post-processing model by using three different satellite precipitation products in this study. We observed a cascading impact on model performance in the rainfall-runoff and post-processing process. Given a fixed hydrological model, in areas with a small catchment area, the response of streamflow to precipitation is quicker, and the quality of satellite precipitation products directly influences the quality of streamflow prediction through the rainfall-runoff process. The temporal correlation of satellite precipitation determines the temporal correlation of streamflow prediction. Deviations in satellite precipitation ~~lead~~led to the biased streamflow prediction, which have a more significant effect on the NSE score of streamflow prediction. This ~~elucidates~~explains the reason that~~why~~ IMERG-F is optimal and PDIR is ~~better than~~superior to GSMaP. During the transfer process from raw streamflow to post-processed streamflow, the autocorrelation skill of the raw runoff dictates the performance of the streamflow post-processing model. This clarifies why IMERG-F is still optimal, but GSMaP is superior ~~than~~to PDIR. Based on the results of the multi-product experiment, we ~~learned~~observed that the post-processing model can learn better features to a larger extent, ~~but~~however, it cannot completely filter out the information that affects the model accuracy. ~~However, r~~Regrading information filtering, the CMAL-LSTM model surpasses the QRF model. These findings suggest that although streamflow post-processing can enhance model performance, opting for the best quality product is still a prudent decision when multiple precipitation products are available, and it can also save more computing resources. Another strategy is to execute precipitation post-processing before the hydrological model, which can assist the model to ~~learn~~ better learn the features and ultimately improve model performance.

5.~~1~~ 2 ~~Simulated and observed streamflow reference~~Limitations and future work

This study provides a systematic evaluation of QRF and CMAL-LSTM models in probabilistic streamflow post-processing, yielding valuable insights and practical experience on model selection. However, there are still some deficiencies that need to be addressed in future research, which ~~we~~are summarized as follows.

First, we used simulated streamflow driven by observed precipitation as a proxy for true streamflow. This study diverges from previous research by focusing on sub-basin scale streamflow post-processing in a nested basin comprised of 522 sub-basins exhibiting varying flow accumulation areas, ranging from 100 km^2 to 127,164 km^2. To achieve the streamflow post-processing for these 522 sub-basins, corresponding streamflow observations are ~~requisite~~required, but such data are not ~~currently~~readily available. As an alternative, we employed streamflow simulations generated by a calibrated hydrological model driven by observed precipitation. This approach yields a post-processing model performance that closely approximates the given reference; however, it is not an exact representation of actual streamflow post-processing. Despite this limitation, the reference generated was used to evaluate the performance of various post-processing models. Future studies could conduct a more in-depth comparison of different post-processing models in basins with more streamflow records. Nonetheless, our dataset remains scarce in the current community, and we have made it available along with this study to enable other researchers to evaluate and compare different methods against the benchmark presented in this study (Zhang et al., 2022b).

Second, there exists data imbalance among the studied sub-basins ~~studied~~. Among the selected 522 sub-basins, it can be observed that model performance is related to the catchment size. However, the number of sub-basins corresponding to each of the five intervals (100–20,000 km^2, 20,000–40,000 km^2, 40,000–60,000 km^2, 60,000–100,000 km^2, and greater than 100,000 km^2) are 476, 15, 4, 13 and 14, respectively. Only 5.2% of the sub-basins have a catchment area larger than 60,000 km^2. This could potentially affect the generality of conclusions drawn. To address this limitation, more extensive and balanced datasets (such as Caravan, Kratzert et al., 2022b) can be utilized to achieve further validation of the research findings and a better understanding of different post-processing models.

Third, the selection of input features and hydrological models could be extended. In order to maintain model complexity and keep computational costs low, this study only used one variable, uncorrected streamflow, as the predictor. However, there are more variables that can be used as predictors, including other meteorological variables such as temperature and wind speed (Frame et al., 2021). In addition, basin-related attributes can provide us with local information, which is particularly helpful for the prediction in ungauged areas. In previous studies, all of these variables have been shown to have varying degrees of contributions~~help~~ to the model (Jiang et al., 2022). For post-processing, there are also studies that use model state variables and other output variables as predictors (Frame et al., 2021), which can provide us with information about the hydrological processes and increase the physical interpretability of the post-processing framework (Razavi, 2021; Tsai et al., 2021). However, state variables and outputs generated by hydrological models tend to be biased due to inherent bias in the satellite precipitation. It is unclear whether this is helpful for streamflow post-processing and requires further exploration. In terms of hydrological model selection, only the distributed time-variant gain model (DTVGM) was used to simulate streamflow from three different satellite precipitation products to increase the diversity of post-processing experiments. By doing so, the other two sources of uncertainty, namely, model structure and parameters, were eliminated, since ~~. And~~ the focus of this study was on comparing post-processing model with input uncertainty. It is worthing noting that in addition to input uncertainty, hydrological model structure and parameter uncertainty are also significant sources of uncertainty, as highlighted by Herrera et al. (2022) and Mai et al. (2022). For future post-processing model comparisons, we suggest to ~~may~~ adopt the approach of using multiple hydrological models to analyse the uncertainty of model structure and parameters (Ghiggi et al., 2021; Troin et al., 2021; Mai et al., 2022).

Fourth, the post-processing models have limitations in handling streamflow extreme events, as observed through comparative analysis and visualization as reported in ~~(~~Table 4 and Fig. S8 in the supplement~~)~~. The QRF model is based on a historical analogy search, wherein the model finds a group of similar samples and averages them ~~of~~at the leaf nodes to obtain the final prediction (Li and Martin, 2017). As a result, the limited number of samples, particularly for extreme events, hinders its ability to predict such events. However, this limitation can be ~~adressed~~addressed by introducing additional parameter mixing methods, such as combining QRF and extreme value distribution. Previous attempts, such as combining QRF and extended generalized Pareto distribution, have~~n~~ shown promising results~~e~~ (Taillardat et al., 2019). Nonetheless, these mixing methods add complexity to the model and require additional calibration of hyperparameters. The CMAL-LSTM model is also constrained by the number of extreme event samples, but its performance in these extreme events exceeds that of the QRF model. Additionally, the CMAL-LSTM model chosen in this study is a mixture density network and the corresponding~~. Their~~ parameters are directly learned through neural network optimization algorithms like gradient descent. ~~We~~The authors believe that collecting more data samples and introducing additional predictors and distribution functions for extreme events can lead to further improvements.

Finally, it is important to constantly enhance and update the model comparison iteratively. The CMAL-LSTM model was selected based on its superior performance as proposed by Klotz et al. (2022). They also evaluated two other hybrid density networks and a probabilistic method using Monte Carlo dropout. Additionally, there are other probabilistic prediction methods such as the variational inference (Li et al., 2021) and generative adversarial networks (Pan et al., 2021). In a rapidly evolving community, new methods can be applied and tested to further improve the performance of streamflow post-processing in future research.

~~Unlike previous studies, the post-processing in this study is for subbasin-scale streamflow from 522 sub-basins in a nested basin. Their flow accumulation areas (FAAs) range from 100 km^2 to 120,000 km^2. In order to perform the streamflow post-~~

~~processing for the 522 sub-basins, the corresponding streamflow observation should be obtained. However such data are not available. Therefore we use the streamflow simulations from the calibrated hydrological model driven by observed precipitation. In fact, by doing so, the best post-processing model performance can only be infinitely close to the given reference. So, the post-processing we do is an imitation of the streamflow reference. This is not exactly consistent with the post-processing of the real streamflow. However, what we have done is use the generated reference to test the performance of post-processing models. Thus doing so also accomplished our goal. In future studies, the performance of the different post-processing models can be fully compared in more informative basins. However, we believe that our dataset is also very rare in the current community, so we make it open along with this study to allow other researchers to test different algorithms using the same dataset and compare it to the benchmark of this study (Zhang et al., 2022b).~~

~~5.2 Model comparison in this study~~

~~In this study, we compared two probabilistic post-processing models, the PLSTM and the QRF models. The QRF model is representative of traditional machine learning algorithms based on decision trees and ensemble learning. The PLSTM model was chosen based on the CMAL-LSTM model, proposed by Klotz et al. (2022). In their study, the CMAL-LSTM model achieved the best model performance, which is why we chose it. They also selected two other mixture density networks and a Monte Carlo dropout-based probabilistic method. Besides, there are some other probabilistic forecasting methods, such as variational inference methods (Li et al., 2021), and GANs methods (Pan et al., 2021). It is unrealistic to compare all methods in one study. In a growing community, new methods can be incorporated to brainstorm and continuously improve the performance of post-processing models in future studies.~~

~~Another thing that may affect the robustness of the results is the imbalance in the number of sub-basins. A flow accumulation area (FAA) of 60,000 km^2 is a threshold condition in the 522 sub-basins we studied. Above and below 60,000 km^2, there is a large difference in model performance between the two probabilistic post-processing models. However, among the 522 sub-basins selected, only 27 sub-basins (5.2%) have a flow accumulation area (FAA) greater than 60,000 km^2, while all other sub-basins (94.8%) have a flow accumulation area (FAA) less than 60,000 km^2. This may affect the robustness of the results, such as more discrete scatters in the reliability diagrams (Fig. 5). The comparison of the PLSTM and QRF models in a larger number and more balanced basins can further increase the robustness of our results as well as improve our understanding of the different post-processing models (Kratzert et al., 2022b).~~

~~5.3 Global model and local model~~

~~In previous studies using the LSTM model, the best practice obtained is the global LSTM model. That is, one LSTM model is used for all data sets and the entire study area. The results of these studies show that the global LSTM model performs better than the local model (Kratzert et al., 2019b; Fang et al., 2022). Moreover, the global LSTM model is able to achieve good results in ungauged basins (Kratzert et al., 2019a). In our study, we aim at streamflow probabilistic post-processing in 522 sub-basins. In the process of PLSTM to generate probabilistic outputs, for the robustness of the results, we first randomly~~

~~sample 10,000 times in each basin and at each time step, and then obtain the final probabilistic members after taking 100 quantiles. For 522 sub-basins, a total of 522×4×365×10000 = 7,621,200,000 samples are required for a 4-year test period. We used a single-card RTX3090 GPU with 24G of video memory for this study, but the amount of sampling required is much larger than the memory of our device. We therefore chose to train a local model for each sub-basin in this study. Future comparisons of the global and local models can be tested on devices with enough video memory, such as clusters or supercomputers containing multi-card GPUs. However, for post-processing in ungauged basins, Frame et al. (2021) give us the insight that the global LSTM model may give poorer post-processing results in these areas. This is due to the effect of basin area and flow regime. Therefore, for the objective of this study, post-processing uncorrected precipitation-driven streamflow simulations, the performance of the global model may be more influenced by the spatial distribution of biases.~~

~~5.4 Predictors or input features~~

~~In order to keep the model complexity and computational cost low, the predictor selected for this study is only one variable, the streamflow. However, more variables are available as predictors, including other meteorological variables, such as temperature and wind speed (Frame et al., 2021). These variables are also used to force hydrological models (Jiang et al., 2022). In addition, basin attributes are important predictors, especially in the global model. In previous studies, all of these variables have been shown to help the model to vary degrees (Jiang et al., 2022). For post-processing, there are also studies that use model state variables and other output variables as predictors for experiments (Frame et al., 2021). Basins-related attributes can provide us with local information, which is particularly helpful for simulations in ungauged areas. State variables or other output variables can give us information about the hydrological model, which also be considered as hybrid modeling. This increases the physical interpretability of the post-processing framework (Razavi, 2021; Tsai et al., 2021). However, biased precipitation-driven hydrologic models generate state variables and outputs that are often biased as well. Whether this is helpful for streamflow post-processing is unknown and needs to be further explored.~~

~~5.5 Predictors or input features~~

~~In this study, only a single hydrological model (DTVGM) is used to simulate streamflow obtained from different precipitation drivers to increase the diversity of post-processing experiments. Also, this excludes other two uncertainty sources, e.g., model structure and parameters. Therefore, the present study focuses on post-processing model comparisons for input uncertainties. In addition to input uncertainty, hydrologic model structure and parameter uncertainty are also important sources of uncertainty (Herrera et al., 2022; Mai et al., 2022). Future post-processing model comparisons can be performed using a multiple hydrological model approach to analyze model structure and model parameter uncertainties (Ghiggi et al., 2021; Troin et al., 2021; Mai et al., 2022).~~

~~5.6 Extreme events~~

~~Through comparative analysis and visualization, it can be found that both PLSTM and QRF models have some limitations in handling extreme events. Even, the QRF model performs a bit worse. This is because the QRF model is based on decision trees. The model prediction is performed by a historical analogy search. That is, the random forests model first finds the most similar samples in the training samples, and then the similar samples of the leaf nodes of multiple decision trees are averaged to obtain the final predictions (Li and Martin, 2017). There is no doubt that the limited sample, especially for extreme events, determines that it is not able to solve the prediction of extreme events very well. Not to mention that for post-processing extreme events that have never happened in history, the nature of QRF dictates that it is powerless. Fortunately, this can be improved by introducing extra parametric hybrid methods (e.g., a mix of RF and extreme-value distribution). Attempts that have occurred include a combination of QRF and extended generalized Pareto distributions (Taillardat et al., 2019). However, this class of hybrid approaches introduces additional complexity to the model and more hyperparameters that need to be calibrated. The PLSTM model is also limited by the sample size of extreme events, but it outperforms the QRF model in terms of these extreme events. It is a sign that the deep neural network is stronger than the decision tree class of traditional machine learning models. Compared to the historical analogy search of the QRF model, the LSTM model is able to make "true" predictions by neuronal computation based on predictors. And, the PLSTM model chosen in this study belongs directly to the mixture density networks. Their parameters are learned directly by neural network optimization (e.g., gradient descent algorithm). We believe this can be further improved by introducing more predictors and other distribution functions that are more specific to extreme events.~~

~~5~~6 Conclusions

In this study, ~~We conducted~~ a series of well-designed experiments to ~~comparing~~ compare the performance of two state-of-the-art models for streamflow probabilistic post-processing ~~was~~were conducted: a machine learning model (quantile regression forests~~, QRF~~) and a deep learning model (countable mixtures of asymmetric Laplacians long short-term memory~~probabilistic long short-term memory~~ network~~, PLSTM~~)~~ for streamflow probabilistic post-processing~~. Using observed precipitation and three different satellite precipitation products to drive the calibrated hydrological model, we generated a large-sample dataset of 522 sub-basins with paired streamflow reference and biased streamflow simulations. We evaluated the model performance from both probabilistic and deterministic perspectives, including reliability, sharpness, accuracy, and flow regime, through intuitive case studies. These experiments established a ~~bridge~~path for understanding the model differences in probabilistic modelling and post-processing, provided practical experience for model selection, and extracted insights for model improvement. It also serves as a reference for establishing benchmark tests for model evaluation, including dataset construction and metrics selection. Furthermore, streamflow post-processing provides dependable data support for a range of downstream tasks, such as flood risk analysis, reservoir scheduling, and water resource management. ~~By driving the calibrated hydrological model with observed precipitation and three satellite precipitation products respectively, we generated streamflow~~

~~reference and biased streamflow simulations, and used them to construct a standard dataset containing 522 sub-basins. Post-processing model performance is fully assessed through probabilistic and deterministic metrics.~~

~~In conclusion, decision-tree models based on historical search (including random forest but not limited to it) have limited ability to predict extreme values, but their low complexity and high parallelism makes them more efficient. Deep learning models (including PLSTM but not limited to it) fit the extreme values better by a deeper network. The performance will be stronger when more predictors are fed. But it comes at the cost of more computational resources. Model comparison improves our knowledge and understanding of the models. The use and development of different models requires the user to choose according to their needs and capabilities.~~

The empirical findings of this study ~~between~~ for the two post-processing models are summarized below.

(1) Based on the ~~The~~ probabilistic assessment~~, indicates that~~ the QRF and ~~PLSTM~~CMAL-LSTM models exhibit ~~perform~~ comparable performance~~y~~. However, t~~T~~heir model differences are ~~closely~~ correlated with~~related to~~ the flow accumulation area (FAA) of ~~the~~ sub-basin~~s and there is a scale effect~~. In cases where the catchment area of a sub-basin is small, the QRF model generates a narrower prediction interval, resulting in better CRPS scores compared to the CMAL-LSTM model in most sub-basins. Conversely, for larger sub-basins (over 60,000 km^2 in this study), the CMAL-LSTM model outperforms the QRF model due to its ability to learn autocorrelation skills of features and capture extreme values.~~The threshold condition is 60,000 km^2. When the FAA of the sub-basin is less than the threshold, the QRF model performs better than the PLSTM model in most cases. When the FAA of the sub-basin is larger than the threshold, the PLSTM model should be preferred.~~

(2) Based on the deterministic assessment, it can be concluded that the CMAL-LSTM model performs better than the QRF model in capturing high-flow process and flow duration curve. On the other hand, the QRF model tends to underestimate the high-flow process, resulting in worse NSE score across all sub-basins. Both models, however, have the issue of underestimating flood peaks due to sparse samples of extreme events.~~The deterministic assessment shows that the PLSTM model outperforms the QRF model. The PLSTM model captures high-flow process and flow duration curve better than the QRF model. The latter tends to underestimate the high-flow process. However, both models underestimate flood peaks due to the problem of sparse samples of extreme events.~~

(3) For the input uncertainties introduced by the different satellite precipitation products, both models are able to reduce their impact on the streamflow simulation. However, the performance of the post-processing models does not improve further in the multi-product experiments.~~However, the multi-feature experiments do not further improve the performance of the post-processing models.~~ Instead, the inclusion of heavily biased inputs leads to a deterioration in model performance. Opting for a single precipitation product that is best suited to the task at hand is a more prudent approach to safeguard model performance and minimize computational ~~expenditure~~cost, rather than using multiple precipitation products with varying degrees of quality.~~On the contrary, model performance degrades due to the mixing of highly biased inputs.~~

(4) Given the performance of post-processing models, the authors believe they have the potential to be applied to other sources of uncertainty that affect hydrological modelling, such as model structure and parameter uncertainty.

~~The results of both post-processing models and the constructed standard dataset of this study are made available through Zenodo repository (https://zenodo.org/record/7187505) (Zhang et al., 2022b). We expect more models to be compared by standard datasets and eventually enrich the model zoo of hydrological probabilistic post-processing.~~

Data and code availability. The GPM IMERG Final Run is free available at GES DISC (https://gpm.nasa.gov/node/3328). The PDIR data can be freely download from CHRS Data Portal (http://chrsdata.eng.uci.edu/). The GSMaP data is publicly available (at https://sharaku.eorc.jaxa.jp/GSMaP/index.htm). The CMA precipitation observation is provided by the National Meteorological Information ~~Center~~Centre of China Meteorological Administration. The soil types are free available at http://www.fao.org/soils-portal/soil-survey/soil-maps-and-databases/harmonized-world-soil-database-v12/en/. The land use data is free available from Chinese National Tibetan Plateau Third Pole Environment Data ~~Center~~Centre at http://data.tpdc.ac.cn/en/data/a75843b4-6591-4a69-a5e4-6f94099ddc2d/. The DEM data is free available at https://www.gscloud.cn/. The QRF model code is available at Github repository (https://github.com/jnelson18/pyquantrf) (Jnelson18, 2022). The ~~PLSTM~~CMAL-LSTM model code is available at Github repository (https://github.com/neuralhydrology/neuralhydrology) (Kratzert et al., 2022a). The dataset and results of this study are available at Zenodo repository (https://zenodo.org/record/7187505) (Zhang et al., 2022b).

Author contribution. Conceptualization, YZ, AY, PN, BA, SS, KH and YW; methodology, YZ and AY; software, YZ and AY; validation, YZ; data curation, YZ, AY, PN and BA; visualization, YZ; supervision, AY KH, and SS; project administration, AY. and SS; funding acquisition, AY and SS. original draft preparation, YZ; review and editing, YZ, AY, PN, BA, SS, KH and YW; All authors have read and agreed to the published version of the manuscript.

Competing interests. The authors declare that they have no conflict of interest.

Acknowledgements. This research is jointly supported by the Natural Science Foundation of China (No. 42171022, 51879009), the Second Tibetan Plateau Scientific Expedition and Research Program (No. 2019QZKK0405), the National Key Research and Development Program of China (No. 2018YFE0196000), the U.S. Department of Energy (DOE Prime Award DE-IA0000018).

References

Althoff, D., Rodrigues, L. N., and Bazame, H. C.: Uncertainty quantification for hydrological models based on neural networks: the dropout ensemble, Stochastic Environmental Research and Risk Assessment, 35(5), 1051-1067, https://doi.org/10.1007/s00477-021-01980-8, 2021.

Beven, K.: Changing ideas in hydrology—the case of physically-based models, Journal of Hydrology, 105(1-2), 157-172, https://doi.org/10.1016/0022-1694(90)90161-P, 1989.

Bogner, K., and Pappenberger, F.: Multiscale error analysis, correction, and predictive uncertainty estimation in a flood forecasting system, Water Resources Research, 47(7), e2010WR009137, https://doi.org/10.1029/2010WR009137, 2011.

Bormann, K. J., Evans, J. P., and McCabe, M. F.: Constraining snowmelt in a temperature-index model using simulated snow densities, Journal of Hydrology, 517, 652-667, https://doi.org/10.1016/j.jhydrol.2014.05.073, 2014.

Breiman, L.: Random forests, Machine Learning, 45(1), 5-32, https://doi.org/10.1023/a:1010933404324, 2001.

Bröcker, J.: Evaluating raw ensembles with the continuous ranked probability score, Quarterly Journal of the Royal Meteorological Society, 138(667), 1611-1617, https://doi.org/10.1002/qj.1891, 2012.

Chawanda, C. J., George, C., Thiery, W., Griensven, A. V., Tech, J., Arnold, J., and Srinivasan, R.: User-friendly workflows for catchment modelling: Towards reproducible SWAT+ model studies, Environmental Modelling and Software, 134, 104812, https://doi.org/10.1016/j.envsoft.2020.104812, 2020.

Chen, H., Yong, B., Shen, Y., Liu, J., Hong, Y., and Zhang, J.: Comparison analysis of six purely satellite-derived global precipitation estimates, Journal of Hydrology, 581, 124376, https://doi.org/10.1016/j.jhydrol.2019.124376, 2020.

Clark, M. P., Nijssen, B., Lundquist, J. D., Kavetski, D., Rupp, D. E., Woods, R. A., Freer, J. E., Gutmann, E. D., Wood, A. W., Brekke, L. D., Arnold, J. R., Gochis, D. J., and Rasmussen, R. M.: A unified approach for process-based hydrologic ~~modeling~~modelling: 1. ~~Modeling~~Modelling concept, Water Resources Research, 51(4), 2498-2514, https://doi.org/10.1002/2015WR017198, 2015.

Corzo Perez, G. A., Van Huijgevoort, M., Voß, F., and Van Lanen, H.: On the spatio-temporal analysis of hydrological droughts from global hydrological models, Hydrology and Earth System Sciences, 15(9), 2963-2978, https://doi.org/10.5194/hessd-8-619-2011, 2011.

Cunha, L. K., Mandapaka, P. V., Krajewski, W. F., Mantilla, R., and Bradley, A. A.: Impact of radar-rainfall error structure on estimated flood magnitude across scales: An investigation based on a parsimonious distributed hydrological model, Water Resources Research, 48(10), https://doi.org/10.1029/2012WR012138, 2012.

Dembélé, M., Hrachowitz, M., Savenije, H. H. G., Mariéthoz, G., and Schaefli, B.: Improving the Predictive Skill of a Distributed Hydrological Model by Calibration on Spatial Patterns With Multiple Satellite Data Sets, Water Resources Research, 56(1), https://doi.org/10.1029/2019WR026085, 2020.

Dong, J., Crow, W. T., and Reichle, R.: Improving Rain/No-Rain Detection Skill by Merging Precipitation Estimates from Different Sources, Journal of Hydrometeorology, 21(10), 2419-2429. https://doi.org/10.1175/JHM-D-20-0097.1, 2020.

Evin, G., Lafaysse, M., Taillardat, M., and Zamo, M.: Calibrated ensemble forecasts of the height of new snow using quantile regression forests and ensemble model output statistics, Nonlinear Processes in Geophysics, 28(3), 467-480, https://doi.org/10.5194/npg-28-467-2021, 2021.

Falck, A. S., Maggioni, V., Tomasella, J., Vila, D. A., and Diniz, F. L. R.: Propagation of satellite precipitation uncertainties through a distributed hydrologic model: A case study in the Tocantins–Araguaia basin in Brazil, Journal of Hydrology, 527, 943-957, https://doi.org/10.1016/j.jhydrol.2015.05.042, 2015.

Fang, K., and Shen, C.: Near-Real-Time Forecast of Satellite-Based Soil Moisture Using Long Short-Term Memory with an Adaptive Data Integration Kernel, Journal of Hydrometeorology, 21(3), 399-413, https://doi.org/10.1175/JHM-D-19-0169.1, 2020.

Fang, K., Kifer, D., Lawson, K., Feng, D., and Shen, C.: The data synergy effects of time-series deep learning models in hydrology, Water Resources Research, e2021WR029583. https://doi.org/10.1029/2021WR029583, 2022.

Fang, K., Shen, C., Kifer, D., and Yang, X.: Prolongation of SMAP to spatiotemporally seamless coverage of continental US using a deep learning neural network, Geophysical Research Letters, 44(21), 11-30, https://doi.org/10.1002/2017GL075619, 2017.

Frame, J. M., Kratzert, F., Raney, A., Rahman, M., Salas, F. R., and Nearing, G. S.: Post-Processing the National Water Model with Long Short-Term Memory Networks for Streamflow Predictions and Model Diagnostics, JAWRA Journal of the American Water Resources Association, 57(6), 885-905, https://doi.org/10.1111/1752-1688.12964, 2021.

Ghiggi, G., Humphrey, V., Seneviratne, S. I., and Gudmundsson, L.: G-RUN ENSEMBLE: A Multi-Forcing Observation-Based Global Runoff Reanalysis, Water Resources Research, 57(5), e2020WR028787, https://doi.org/10.1029/2020WR028787, 2021.

Gneiting, T., Balabdaoui, F., and Raftery, A. E.: Probabilistic forecasts, calibration and sharpness, Journal of the Royal Statistical Society: Series B (Statistical Methodology), 69(2), 243-268, https://doi.org/10.1111/j.1467-9868.2007.00587.x, 2007.

Gou, J., Miao, C., Duan, Q., Tang, Q., Di, Z., Liao, W., Wu, J., and Zhou, R.: Sensitivity Analysis-Based Automatic Parameter Calibration of the VIC Model for Streamflow Simulations Over China, Water Resources Research, 56(1), e2019WR025968, https://doi.org/10.1029/2019WR025968, 2020.

Gou, J., Miao, C., Samaniego, L., Xiao, M., Wu, J., and Guo, X.: CNRD v1.0: A High-Quality Natural Runoff Dataset for Hydrological and Climate Studies in China. Bulletin of the American Meteorological Society, 102(5), E929-E947. https://doi.org/10.1175/BAMS-D-20-0094.1, 2021.

Hartmann, H. C., Pagano, T. C., Sorooshian, S., and Bales, R.: Confidence builders: Evaluating seasonal climate forecasts from user perspectives, Bulletin of the American Meteorological Society, 83(5), 683-698, https://doi.org/10.1175/1520-0477(2002)083<0683:CBESCF>2.3.CO;2, 2002.

Herrera, P. A., Marazuela, M. A., and Hofmann, T.: Parameter estimation and uncertainty analysis in hydrological modelling, Wiley Interdisciplinary Reviews-Water, 9(1), e1569, https://doi.org/10.1002/wat2.1569, 2022.

Honti, M., Scheidegger, A., and Stamm, C.: The importance of hydrological uncertainty assessment methods in climate change impact studies, Hydrology and Earth System Sciences, 18(8), 3301-3317, https://doi.org/10.5194/hess-18-3301-2014, 2014.

Hori, T., Cho, J., and Watanabe, S.: End-to-end speech recognition with word-based RNN language models, 2018 IEEE Spoken Language Technology Workshop (SLT), 389-396, https://doi.org/10.1109/SLT.2018.8639693, 2018.

Hou, A. Y., Kakar, R. K., Neeck, S., AA, A., Kummerow, C. D., Kojima, M., Oki, R., Nakamura, K., and Iguchi, T.: The Global Precipitation Measurement Mission, Bulletin of the American Meteorological Society, 95(5), 701-722, https://doi.org/10.1175/BAMS-D-13-00164.1, 2013.

Huffman, G. J., Bolvin, D. T., Nelkin, E. J., and Tan, J.: Integrated Multi-satellitE Retrievals for GPM (IMERG) technical documentation, NASA/GSFC Code, 612(47), 2019, 2015.

Huffman, G.J., E.F. Stocker, D.T. Bolvin, E.J. Nelkin, Jackson T.: GPM IMERG Final Precipitation L3 1 day 0.1 degree x 0.1 degree V06, Edited by Andrey Savtchenko, Greenbelt, MD, Goddard Earth Sciences Data and Information Services Center (GES DISC), Accessed: [2021-7-30], https://doi.org/10.5067/GPM/IMERGDF/DAY/06, 2019.

Jajarmizadeh, M., Harun, S., and Salarpour, M.: A review on theoretical consideration and types of models in hydrology, Journal of Environmental Science and Technology, 5(5), 249-261, https://doi.org/10.3923/jest.2012.249.261, 2012.

Jiang, L., and Bauer-Gottwein, P.: How do GPM IMERG precipitation estimates perform as hydrological model forcing? Evaluation for 300 catchments across Mainland China, Journal of Hydrology, 572, 486-500, https://doi.org/10.1016/j.jhydrol.2019.03.042, 2019.

Jiang, S., Zheng, Y., Wang, C., and Babovic, V.: Uncovering Flooding Mechanisms Across the Contiguous United States Through Interpretive Deep Learning on Representative Catchments, Water Resources Research, 58(1), e2021WR030185, https://doi.org/10.1029/2021WR030185, 2022.

Jnelson18.: jnelson18/pyquantrf: DOI release (v0.0.3doi), Zenodo [code], https://doi.org/10.5281/zenodo.5815105, 2022.

Kasraei, B., Heung, B., Saurette, D. D., Schmidt, M. G., Bulmer, C. E., and Bethel, W.: Quantile regression as a generic approach for estimating uncertainty of digital soil maps produced from machine-learning, Environmental Modelling and Software, 144, 105139, https://doi.org/10.1016/j.envsoft.2021.105139, 2021.

Kaune, A., Chowdhury, F., Werner, M., and Bennett, J.: The benefit of using an ensemble of seasonal streamflow forecasts in water allocation decisions, Hydrology and Earth System Sciences, 24(7), 3851-3870, https://doi.org/10.5194/hess-24-3851-2020, 2020.

Khakbaz, B., Imam, B., Hsu, K., and Sorooshian, S.: From lumped to distributed via semi-distributed: Calibration strategies for semi-distributed hydrologic models, Journal of Hydrology, 418, 61-77. https://doi.org/10.1016/j.jhydrol.2009.02.021, 2012.

Kling, H., Fuchs, M., and Paulin, M.: Runoff conditions in the upper Danube basin under an ensemble of climate change scenarios, Journal of Hydrology, 424, 264-277, https://doi.org/10.1016/j.jhydrol.2012.01.011, 2012.

Klotz, D., Kratzert, F., Gauch, M., Keefe Sampson, A., Brandstetter, J., Klambauer, G., Hochreiter, S., and Nearing, G.: Uncertainty estimation with deep learning for rainfall–runoff modelling, Hydrology and Earth System Sciences, 26(6), 1673-1693, https://doi.org/10.5194/hess-26-1673-2022, 2022.

Kobold, M., and Sušelj, K.: Precipitation forecasts and their uncertainty as input into hydrological models, Hydrology and Earth System Sciences, 9(4), 322-332, https://doi.org/10.5194/hess-9-322-2005, 2005.

Kratzert, F., Klotz, D., Brenner, C., Schulz, K., and Herrnegger, M.: Rainfall–runoff modelling using Long Short-Term Memory (LSTM) networks, Hydrology and Earth System Sciences, 22(11), 6005-6022, https://doi.org/10.5194/hess-22-6005-2018, 2018.

Kratzert, F., Klotz, D., Herrnegger, M., Sampson, A. K., Hochreiter, S., and Nearing, G. S.: Toward Improved Predictions in Ungauged Basins: Exploiting the Power of Machine Learning, Water Resources Research, 55(12), 11344-11354, https://doi.org/10.1029/2019WR026065, 2019a.

Kratzert, F., Klotz, D., Hochreiter, S., and Nearing, G. S.: A note on leveraging synergy in multiple meteorological data sets with deep learning for rainfall–runoff modelling, Hydrology and Earth System Sciences, 25(5), 2685-2703, https://doi.org/10.5194/hess-25-2685-2021, 2021.

Kratzert, F., Klotz, D., Shalev, G., Klambauer, G., Hochreiter, S., and Nearing, G.: Towards learning universal, regional, and local hydrological behaviors via machine learning applied to large-sample datasets, Hydrology and Earth System Sciences, 23(12), 5089-5110, https://doi.org/10.5194/hess-23-5089-2019, 2019b.

Kratzert, F., Gauch, M., Nearing, G., and Klotz, D.: NeuralHydrology-A Python library for Deep Learning research in hydrology, Journal of Open Source Software, 7(71), 4050, https://doi.org/10.21105/joss.04050, 2022a

Kratzert, F., Nearing, G., Addor, N., Erickson, T., Gauch, M., Gilon, O., Gudmundsson, L., Hassidim, A., Klotz, D., and Nevo, S.: Caravan-A global community dataset for large-sample hydrology, EarthArXiv, [preprint], https://doi.org/10.31223/X50S70, 2022b.

Kubota, T., Aonashi, K., Ushio, T., Shige, S., Takayabu, Y. N., Kachi, M., Arai, Y., Tashima, T., Masaki, T., and Kawamoto, N.: Global Satellite Mapping of Precipitation (GSMaP) products in the GPM era, Satellite precipitation measurement, 1, 355-373, https://doi.org/10.1007/978-3-030-24568-9_20, 2020.

Kubota, T., Shige, S., Hashizume, H., Aonashi, K., Takahashi, N., Seto, S., Hirose, M., Takayabu, Y. N., Ushio, T., and Nakagawa, K.: Global precipitation map using satellite-borne microwave radiometers by the GSMaP project: Production and validation, IEEE Transactions On Geoscience and Remote Sensing, 45(7), 2259-2275, https://doi.org/10.1109/TGRS.2007.895337, 2007.

Lees, T., Buechel, M., Anderson, B., Slater, L., Reece, S., Coxon, G., and Dadson, S. J.: Benchmarking Data-Driven Rainfall-Runoff Models in Great Britain: A comparison of LSTM-based models with four lumped conceptual models, Hydrology and Earth System Sciences, 25(10), 5517–5534, https://doi.org/10.5194/hess-2021-127, 2021.

Li, A. H., and Martin, A.: Forest-type regression with general losses and robust forest, Proceedings of the 34th International Conference on Machine Learning, 70, 2091-2100, 2017.

Li, B., Friedman, J., Olshen, R., and Stone, C.: Classification and regression trees (CART), Biometrics, 40(3), 358-361, Retrieved from http://statweb.lsu.edu/faculty/li/IIT/tree1.pdf, 1984.

Li, D., Marshall, L., Liang, Z., and Sharma, A.: Hydrologic multi-model ensemble predictions using variational Bayesian deep learning, Journal of Hydrology, 604, 127221, https://doi.org/10.1016/j.jhydrol.2021.127221, 2022.

Li, D., Marshall, L., Liang, Z., Sharma, A., and Zhou, Y., Bayesian LSTM With Stochastic Variational Inference for Estimating Model Uncertainty in Process-Based Hydrological Models, Water Resources Research, 57(9), https://doi.org/10.1029/2021WR029772, 2021.

Li, M., Wang, Q. J., Bennett, J. C., and Robertson, D. E.: A strategy to overcome adverse effects of autoregressive updating of streamflow forecasts, Hydrology and Earth System Sciences, 19(1), 1-15, https://doi.org/10.5194/hess-19-1-2015, 2015.

Li, M., Wang, Q. J., Bennett, J. C., and Robertson, D. E.: Error reduction and representation in stages (ERRIS) in hydrological modelling for ensemble streamflow forecasting, Hydrology and Earth System Sciences, 20(9), 3561-3579, https://doi.org/10.5194/hess-20-3561-2016, 2016.

Li, W., Duan, Q., Miao, C., Ye, A., Gong, W., and Di, Z.: A review on statistical postprocessing methods for hydrometeorological ensemble forecasting, Wiley Interdisciplinary Reviews: Water, 4(6), e1246, https://doi.org/10.1002/wat2.1246, 2017.

Mai, J., Craig, J. R., Tolson, B. A., and Arsenault, R.: The sensitivity of simulated streamflow to individual hydrologic processes across North America, Nature Communications, 13(1), https://doi.org/10.1038/s41467-022-28010-7, 2022.

Mai, J., Shen, H., Tolson, B. A., Gaborit, É., Arsenault, R., Craig, J. R., Fortin, V., Fry, L. M., Gauch, M., Klotz, D., Kratzert, F., O'Brien, N., Princz, D. G., Rasiya Koya, S., Roy, T., Seglenieks, F., Shrestha, N. K., Temgoua, A. G. T., Vionnet, V., and Waddell, J. W.: The Great Lakes Runoff Intercomparison Project Phase 4: the Great Lakes (GRIP-GL), Hydrology and Earth System Sciences, 26(13), 3537-3572, https://doi.org/10.5194/hess-26-3537-2022, 2022.

Meinshausen, N., and Ridgeway, G.: Quantile regression forests, Journal of Machine Learning Research, 7(6), 983-999, https://www.jmlr.org/papers/volume7/meinshausen06a/meinshausen06a.pdf, 2006.

Miao, C., Gou, J., Fu, B., Tang, Q., Duan, Q., Chen, Z., Lei, H., Chen, J., Guo, J., and Borthwick, A. G.: High-quality reconstruction of China’s natural streamflow, Science Bulletin, 67(5), 547-556, https://doi.org/10.1016/j.scib.2021.09.022, 2022.

Nash, J. E., and Sutcliffe, J. V.: River flow forecasting through conceptual models part I—A discussion of principles, Journal of Hydrology, 10(3), 282-290, https://doi.org/10.1016/0022-1694(70)90255-6, 1970.

Nasreen, S., Součková, M., Vargas Godoy, M. R., Singh, U., Markonis, Y., Kumar, R., Rakovec, O., and Hanel, M.: A 500-year runoff reconstruction for European catchments, Earth System Science Data, 14, 4035–4056, https://doi.org/10.5194/essd-14-4035-2022, 2022.

Nearing, G. S., Tian, Y., Gupta, H. V., Clark, M. P., Harrison, K. W., and Weijs, S. V.: A philosophical basis for hydrological uncertainty, Hydrological sciences journal, 61(9), 1666-1678, https://doi.org/10.1080/02626667.2016.1183009, 2016.

Nguyen, P., Ombadi, M., Gorooh, V. A., Shearer, E. J., Sadeghi, M., Sorooshian, S., Hsu, K., Bolvin, D., and Ralph, M. F.: PERSIANN Dynamic Infrared–Rain Rate (PDIR-Now): A Near-Real-Time, Quasi-Global Satellite Precipitation Dataset, Journal of Hydrometeorology, 21(12), 2893-2906, https://doi.org/10.1175/JHM-D-20-0177.1, 2020a.

Nguyen, P., Shearer, E. J., Ombadi, M., Gorooh, V. A., Hsu, K., Sorooshian, S., Logan, W. S., and Ralph, M.: PERSIANN Dynamic Infrared–Rain Rate Model (PDIR) for High-Resolution, Real-Time Satellite Precipitation Estimation, Bulletin of the American Meteorological Society, 101(3), E286-E302, https://doi.org/10.1175/BAMS-D-19-0118.1, 2020b.

Pan, B., Anderson, G. J., Goncalves, A., Lucas, D. D., Bonfils, C. J., Lee, J., Tian, Y., and Ma, H. Y.: Learning to correct climate projection biases, Journal of Advances in ~~Modeling~~Modelling Earth Systems, 13(10), e2021MS002509, https://doi.org/10.1029/2021MS002509, 2021.

Parrish, M. A., Moradkhani, H., and DeChant, C. M.: Toward reduction of model uncertainty: Integration of Bayesian model averaging and data assimilation, Water Resources Research, 48(3), https://doi.org/10.1029/2011WR011116, 2012.

Razavi, S.: Deep learning, explained: Fundamentals, explainability, and bridgeability to process-based modelling, Environmental Modelling and Software, 144, 105159, https://doi.org/10.1016/j.envsoft.2021.105159, 2021.

Schaake, J. C., Hamill, T. M., Buizza, R., and Clark, M.: HEPEX: the hydrological ensemble prediction experiment, Bulletin of the American Meteorological Society, 88(10), 1541-1548, https://doi.org/10.1175/BAMS-88-10-1541, 2007.

Shen, C., and Lawson, K.: Applications of deep learning in hydrology, Deep Learning for the Earth Sciences: A Comprehensive Approach to Remote Sensing, Climate Science, and Geosciences, 283-297, https://doi.org/10.1002/9781119646181.ch19, 2021.

Shen, Y., Ruijsch, J., Lu, M., Sutanudjaja, E. H., and Karssenberg, D.: Random forests-based error-correction of streamflow from a large-scale hydrological model: Using model state variables to estimate error terms, Computers and Geosciences, 159, 105019, https://doi.org/10.1016/j.cageo.2021.105019, 2022.

Shen, Z., Yong, B., Gourley, J. J., and Qi, W.: Real-time bias adjustment for satellite-based precipitation estimates over Mainland China, Journal of Hydrology, 596, 126133, https://doi.org/10.1016/j.jhydrol.2021.126133, 2021.

Sit, M., Demiray, B. Z., Xiang, Z., Ewing, G. J., Sermet, Y., and Demir, I.: A comprehensive review of deep learning applications in hydrology and water resources, Water Science and Technology, 82(12), 2635-2670, https://doi.org/10.2166/wst.2020.369, 2020.

Sittner, W. T., Schauss, C. E., and Monro, J. C.: Continuous hydrograph synthesis with an API-type hydrologic model, Water Resources Research, 5(5), 1007-1022, https://doi.org/10.1029/WR005i005p01007, 1969.

Sivapalan, M.: From engineering hydrology to Earth system science: milestones in the transformation of hydrologic science, Hydrology and Earth System Sciences, 22(3), 1665-1693, https://doi.org/10.5194/hess-22-1665-2018, 2018.

Sordo-Ward, Á., Granados, I., Martín-Carrasco, F., and Garrote, L.: Impact of Hydrological Uncertainty on Water Management Decisions, Water Resources Management, 30(14), 5535-5551, https://doi.org/10.1007/s11269-016-1505-5, 2016.

Staudemeyer, R. C., and Morris, E. R.: Understanding LSTM-a tutorial into long short-term memory recurrent neural networks, arXiv [preprint], arXiv:1909.09586, 2019.

Sun, Q., Miao, C., Duan, Q., Ashouri, H., Sorooshian, S., and Hsu, K. L.: A Review of Global Precipitation Data Sets: Data Sources, Estimation, and Intercomparisons, Reviews of Geophysics, 56(1), 79-107, https://doi.org/10.1002/2017RG000574, 2018.

Taillardat, M., Fougères, A., Naveau, P., and Mestre, O.: Forest-Based and Semiparametric Methods for the Postprocessing of Rainfall Ensemble Forecasting, Weather and Forecasting, 34(3), 617-634, https://dio.org/10.1175/WAF-D-18-0149.1, 2019.

Taillardat, M., Mestre, O., Zamo, M., and Naveau, P.: Calibrated Ensemble Forecasts Using Quantile Regression Forests and Ensemble Model Output Statistics, Monthly Weather Review, 144(6), 2375-2393, https://doi.org/10.1175/MWR-D-15-0260.1, 2016.

Tan, M. L., Gassman, P. W., Yang, X., and Haywood, J.: A review of SWAT applications, performance and future needs for simulation of hydro-climatic extremes, Advances in Water Resources, 143, 103662, https://doi.org/10.1016/j.advwatres.2020.103662, 2020.

Tian, Y., Peters-Lidard, C. D., Eylander, J. B., Joyce, R. J., Huffman, G. J., Adler, R. F., Hsu, K., Turk, F. J., Garcia, M., and Zeng, J.: Component analysis of errors in satellite-based precipitation estimates, Journal of Geophysical Research, 114(D24), https://doi.org/10.1029/2009JD011949, 2009.

Troin, M., Arsenault, R., Wood, A. W., Brissette, F., and Martel, J. L.: Generating Ensemble Streamflow Forecasts: A Review of Methods and Approaches Over the Past 40 Years, Water Resources Research, 57(7), https://doi.org/10.1029/2020WR028392, 2021.

Tsai, W., Feng, D., Pan, M., Beck, H., Lawson, K., Yang, Y., Liu, J., and Shen, C.: From calibration to parameter learning: Harnessing the scaling effects of big data in geoscientific modelling, Nature Communications, 12(1), 1-13, https://doi.org/10.1038/s41467-021-26107-z, 2021.

Tyralis, H., and Papacharalampous, G.: Quantile-based hydrological modelling, Water, 13(23), 3420, https://doi.org/10.3390/w13233420, 2021.

Tyralis, H., Papacharalampous, G., Burnetas, A., and Langousis, A.: Hydrological post-processing using stacked generalization of quantile regression algorithms: Large-scale application over CONUS, Journal of Hydrology, 577, 123957, https://doi.org/10.1016/j.jhydrol.2019.123957, 2019.

Wang, Q. J., Robertson, D. E., and Chiew, F. H. S.: A Bayesian joint probability ~~modeling~~modelling approach for seasonal forecasting of streamflows at multiple sites, Water Resources Research, 45(5), W05407, https://doi.org/10.1029/2008WR007355, 2009.

Wu, J., Yen, H., Arnold, J. G., Yang, Y. C. E., Cai, X., White, M. J., Santhi, C., Miao, C., and Srinivasan, R.: Development of reservoir operation functions in SWAT+ for national environmental assessments, Journal of Hydrology, 583, 124556, https://doi.org/10.1016/j.jhydrol.2020.124556, 2020.

Xia, J.: Identification of a constrained nonlinear hydrological system described by Volterra Functional Series, Water Resources Research, 27(9), 2415-2420, https://doi.org/10.1029/91WR01364, 1991.

Xia, J., Wang, G., Tan, G., Ye, A., and Huang, G. H.: Development of distributed time-variant gain model for nonlinear hydrological systems, Science in China Series D: Earth Sciences, 48(6), 713-723, https://doi.org/10.1360/03yd0183, 2005.

Xu, L., Chen, N., Moradkhani, H., Zhang, X., and Hu, C.: Improving Global Monthly and Daily Precipitation Estimation by Fusing Gauge Observations, Remote Sensing, and Reanalysis Data Sets, Water Resources Research, 56(3), https://doi.org/10.1029/2019WR026444, 2020.

Yang, Q., Wang, Q. J., and Hakala, K.: Achieving effective calibration of precipitation forecasts over a continental scale, Journal of Hydrology: Regional Studies, 35, 100818, https://doi.org/10.1016/j.ejrh.2021.100818, 2021.

Ye, A., Duan, Q., Schaake, J., Xu, J., Deng, X., Di, Z., Miao, C., and Gong, W.: Post-processing of ensemble forecasts in low-flow period, Hydrological Processes, 29(10), 2438-2453, https://doi.org/10.1002/hyp.10374, 2015.

Ye, A., Duan, Q., Yuan, X., Wood, E. F., and Schaake, J.: Hydrologic post-processing of MOPEX streamflow simulations, Journal of Hydrology, 508, 147-156, https://doi.org/10.1016/j.jhydrol.2013.10.055, 2014.

Ye, A., Duan, Q., Zeng, H., Li, L., and Wang, C.: A distributed time-variant gain hydrological model based on remote sensing, Journal of Resources and Ecology, 1(3), 222-230, https://doi.org/10.3969/j.issn.1674-764x.2010.03.005, 2010.

Ye, A., Duan, Q., Zhan, C., Liu, Z., and Mao, Y.: Improving kinematic wave routing scheme in Community Land Model, Hydrology Research, 44(5), 886-903, https://doi.org/10.2166/nh.2012.145, 2013.

Yilmaz, K. K., Gupta, H. V., and Wagener, T.: A process-based diagnostic approach to model evaluation: Application to the NWS distributed hydrologic model, Water Resources Research, 44(9), W09417, https://doi.org/10.1029/2007WR006716, 2008.

Zhang, X., Liu, P., Cheng, L., Liu, Z., and Zhao, Y, A back-fitting algorithm to improve real-time flood forecasting, Journal of Hydrology, 562, 140-150, https://doi.org/10.1016/j.jhydrol.2018.04.051, 2018.

Zhang, Y., and Ye, A.: Machine Learning for Precipitation Forecasts Postprocessing: Multimodel Comparison and Experimental Investigation, Journal of Hydrometeorology, 22(11), 3065-3085, https://doi.org/10.1175/JHM-D-21-0096.1, 2021.

Zhang, Y., Ye, A., Nguyen, P., Analui, B., Sorooshian, S., and Hsu, K.: New insights into error decomposition for precipitation products, Geophysical Research Letters, 48(17), e2021GL094092, https://doi.org/10.1029/2021GL094092, 2021a.

Zhang, Y., Ye, A., Nguyen, P., Analui, B., Sorooshian, S., and Hsu, K.: Error Characteristics and Scale Dependence of Current Satellite Precipitation Estimates Products in Hydrological ~~Modeling~~Modelling, Remote Sensing, 13(16), 3061, https://doi.org/10.3390/rs13163061, 2021b.

Zhang, Y., Ye, A., Nguyen, P., Analui, B., Sorooshian, S., and Hsu, K.: QRF4P-NRT Probabilistic Post-processing of Near-real-time Satellite Precipitation Estimates using Quantile Regression Forests, Water Resources Research, 58(5), e2022WR032117, https://doi.org/10.1029/2022WR032117, 2022a.

Zhang, Y., Ye, A., Nguyen, P., Analui, B., Sorooshian, S., and Hsu, K.: Dataset and results for "Comparing machine learning and deep learning models for probabilistic post-processing of satellite precipitation-driven streamflow simulation" [Data set]. Zenodo. https://doi.org/10.5281/zenodo.7187505, 2022b.

Zhao, L., Duan, Q., Schaake, J., Ye, A., and Xia, J.: A hydrologic post-processor for ensemble streamflow predictions, Advances in geosciences, 29(29), 51-59, https://doi.org/10.5194/adgeo-29-51-2011, 2011.

Zhao, P., Wang, Q. J., Wu, W., and Yang, Q.: Extending a joint probability ~~modeling~~modelling approach for post-processing ensemble precipitation forecasts from numerical weather prediction models, Journal of Hydrology, 605, 127285, https://doi.org/10.1016/j.jhydrol.2021.127285, 2022.

Zhou, X., Polcher, J., and Dumas, P.: Representing Human Water Management in a Land Surface Model Using a Supply/Demand Approach, Water Resources Research, 57(4), https://doi.org/10.1029/2020WR028133, 2021.

Zhu, S., Luo, X., Yuan, X., and Xu, Z.: An improved long short-term memory network for streamflow forecasting in the upper Yangtze River, Stochastic Environmental Research and Risk Assessment, 34(9), 1313-1329, https://doi.org/10.1007/s00477-020-01766-4, 2020.

Zounemat-Kermani, M., Batelaan, O., Fadaee, M., and Hinkelmann, R: Ensemble machine learning paradigms in hydrology: A review, Journal of Hydrology, 598, 126266, https://doi.org/10.1016/j.jhydrol.2021.126266, 2021.